UC Berkeley
UC Berkeley Electronic Theses and Dissertations

Title

Energy Homeostasis in Cellobiose Utilizing Saccharomyces cerevisiae

Permalink

https://escholarship.org/uc/item/0kb8c7rs

Author

Chomvong, Kulika

Publication Date

2016

Peer reviewed|Thesis/dissertation

Energy Homeostasis in Cellobiose Utilizing *Saccharomyces cerevisiae*

By

Kulika Chomvong

A dissertation submitted in partial satisfaction of the

requirements for the degree of

Doctor of Philosophy

in

Microbiology

in the

Graduate Division

of the

University of California, Berkeley

Committee in charge:

Professor Jamie H.D. Cate, Co-Chair
Professor N. Louise Glass, Co-Chair
Professor Arash Komeili
Professor Chris R. Somerville

Fall 2016

Energy Homeostasis in Cellobiose Utilizing *Saccharomyces cerevisiae*

Abstract

Energy Homeostasis in Cellobiose Utilizing *Saccharomyces cerevisiae*

by

Kulika Chomvong

Doctor of Philosophy in Microbiology

University of California, Berkeley

Professor Jamie H. D. Cate, Co-Chair

Professor N. Louise Glass, Co-Chair

Plant biomass is a promising renewable starting material for chemical and fuel derivations. Complete consumption of sugar components in the plant cell wall is essential for a cost effective process design. The yeast *Saccharomyces cerevisiae* can be engineered to co-consume cellobiose and xylose, a scheme that allows simultaneous consumption of sugar content from cellulose and hemicellulose polysaccharides, decreasing overall process time. As the reactions are expected to occur in anaerobic conditions given the large-scale nature of the process, cellobiose phosphorylase (CBP), an enzyme that catalyzes intracellular cellobiose breakdown in anaerobic bacteria was studied and showed energetic benefits in anaerobic conditions. However, xylose was identified as a mixed-inhibitor and a substrate forming a byproduct of the CBP reaction. Protein engineering of CBP partially relieved the negative impact of xylose. A single distal mutation on CBP altered its susceptibility to xylose, potentially by modifying spatial conformation of CBP. In parallel, a novel xylose synthetic pathway involving xylulose-1-phosphate was tested, in an attempt to increase the xylose consumption rate, decrease cellular xylose and its negative impact on CBP. However, the existing xylose utilization pathway outperformed the synthetic pathway, likely because exogenous gene integration interfered with the existing regulatory network. Finally, cellobiose consumption was used as a minimal 2-gene synthetic biology pathway to explore cell physiology. This pathway induced drastic changes in cellular metabolites, allowing for the identification of novel regulation controlling ATP levels in cells. Uncoupling extracellular glucose sensors Snf3/Rgt2 from carbon utilization revealed a novel role of Snf3/Rgt2 in ATP regulation at the transcriptional level, potentially via the master regulator Gcn4. This regulation acted independently of proton pumping by Pma1, which is a known to be a major source of ATP consumption in yeast cells, but whose regulation remains to be determined. Together, these two pathways set an upper bound on ATP concentrations needed for optimal fermentation.

Dedication

I dedicate this dissertation to my parents, for their endless love and confidence.

Acknowledgements

Table of Contents

iii

Introduction

The use of plant biomass as a starting material for derivation of chemicals, fuels or food requires complete consumption of plant cell wall materials. The plant cell wall is mainly comprised of the polysaccharides cellulose and hemicellulose. One proposed scheme to simultaneously consume sugars derived from the two types of polysaccharide chains is a cellobiose-xylose consumption system [1]. Cellulose can be hydrolyzed to cellobiose, a glucose dimer linked by a ß-1,4 glycosidic bond. Hydrolysis of hemicellulose, though more complex in terms of monomer composition, yields a pentose sugar, xylose, as a main product. Co-consumption of cellobiose and xylose circumvents glucose repression effects observed when glucose is provided with other carbon sources [2], resulting in undesirable sequential sugar utilization (Fig. i-1).

The simultaneous consumption of cellobiose and xylose was successfully demonstrated in the yeast *Saccharomyces cerevisiae* [1]. Cellobiose is transported into the cell by a cellodextrin transporter (CDT-1) and hydrolyzed inside the cell by intracellular ß-glucosidase (GH1-1), both derived from the plant cell wall-consuming fungus, *Neurospora crassa* [3]. Xylose can be utilized either by an oxidoreductive pathway, comprising xylose reductase and xylitol dehydrogenase, that converts xylose to xylulose [4, 5]. Alternatively, xylose can be utilized by xylose isomerase, which converts xylose directly to xylulose [6]. Glucose and xylulose are then metabolized using glycolysis and the pentose phosphate pathway, respectively.

Given its industrial scale-up potential and the nature of *S. cerevisiae*, the system is expected to operate under anaerobic conditions. Cellobiose phosphorylase (CBP) derived from anaerobic bacteria is expected to have energetic benefits over GH1-1. CBP cleaves cellobiose with inorganic phosphate to glucose and glucose 1-phosphate (G1P) [7]. Since G1P conversion to glucose 6-phosphate does not require additional ATP, overall cellobiose consumption was shown to be superior to the system using GH1-1 under anaerobic condition [8].

As cellobiose utilization has to be operated in the presence of xylose, the effect of xylose on cellobiose utilization by CBP was investigated (Chapter 1). Xylose was identified as a mixed-inhibitor and a substrate for the reverse reaction of CBP producing an undesirable byproduct, 4-O-β-D-glucopyranosyl-D-xylose (GX). To overcome the negative impact of xylose on CBP, protein engineering of CBP by chromosomal library selection was performed and the mutation with improved phenotype analyzed (Chapter 2). In parallel, a novel synthetic xylose utilization pathway proceeding through xylulose-1-phosphate was designed and examined, in an attempt to improve xylose utilization rates and thus decrease the xylose inhibitory effects on the cellobiose phosphorolytic reaction (Chapter 3). Although designed to be linear and modular for ease of integration, the pathway performance was suboptimal, potentially because exogenous components interfered with the intricate regulatory network, built-in for survival of yeast in its native environment. Chapter 4 detailed an example of dramatic metabolic and cellular regulatory changes observed in a minimal synthetic organism with only two exogenous genes for the cellobiose pathway. This platform led to discovery of novel connections between carbon sensing and energy homeostasis evident under perceived starvation conditions.

Chapter 1. Undesirable side-reaction of the energy efficient cellobiose phosphorolytic pathway

1.1 Overview

Cellobiose and xylose co-fermentation holds promise for efficiently producing biofuels from plant biomass. Cellobiose phosphorylase (CBP), an intracellular enzyme generally found in anaerobic bacteria, cleaves cellobiose to glucose and glucose-1-phosphate, providing energetic advantages under the anaerobic conditions required for large-scale biofuel production. However, the efficiency of CBP to cleave cellobiose in the presence of xylose is unknown. This study investigated the effect of xylose on anaerobic CBP-mediated cellobiose fermentation by *Saccharomyces cerevisiae*.

Yeast capable of fermenting cellobiose by the CBP pathway consumed cellobiose and produced ethanol at rates 61% and 42% slower, respectively, in the presence of xylose than in its absence. The system generated significant amounts of the byproduct 4-O-β-d-glucopyranosyl-d-xylose (GX), produced by CBP from glucose-1-phosphate and xylose. *In vitro* competition assays identified xylose as a mixed-inhibitor for cellobiose phosphorylase activity. The negative effects of xylose were effectively relieved by efficient cellobiose and xylose co-utilization. GX was also shown to be a substrate for cleavage by an intracellular β-glucosidase.

Xylose exerted negative impacts on CBP-mediated cellobiose fermentation by acting as a substrate for GX byproduct formation and a mixed-inhibitor for cellobiose phosphorylase activity. Future efforts will require efficient xylose utilization, GX cleavage by a β-glucosidase, and/or a CBP with improved substrate specificity to overcome the negative impacts of xylose on CBP in cellobiose and xylose co-fermentation.

1.2 Introduction

Cellulosic biofuels could make significant contributions to meet the ever-rising demand for energy. To economically produce fuels from cellulosic biomass, sugars derived from cellulose as well as hemicellulose must be utilized completely [9-11]. The co-fermentation of cellobiose derived from cellulose and xylose derived from hemicellulose allows these sugars to be consumed simultaneously [1], and may enable continuous biofuel production [12]. In this system, cellobiose and xylose are transported into engineered *S. cerevisiae* using a cellodextrin transporter (that is, CDT-1 from *Neurospora crassa*) and endogenous hexose transporters, respectively [1, 3]. Intracellular cellobiose is then hydrolyzed into two molecules of glucose by an intracellular β-glucosidase (NCU00130; GH1-1) [3]. At the same time, xylose is

consumed by an oxidoreductive pathway, comprising xylose reductase and xylitol dehydrogenase, that converts xylose to xylulose [4, 5]. Alternatively, xylose can be utilized by xylose isomerase, which converts xylose directly to xylulose [6]. Glucose and xylulose are then metabolized using glycolysis and the pentose phosphate pathway, respectively, resulting in ethanol production [1].

A pathway potentially better suited to the anaerobic environment of large-scale biofuels production substitutes cellobiose phosphorolysis for the hydrolytic reaction of β-glucosidase [8, 13]. This pathway comprises cellobiose phosphorylase (CBP), which cleaves intracellular cellobiose into glucose and glucose-1-phosphate (G1P) [7]. The phosphorolytic pathway requires one less ATP for each molecule of cellobiose to be metabolized by glycolysis. This is because glucose generated by hydrolysis of cellobiose requires two ATP molecules for hexokinase generation of glucose-6-phosphate (G6P) [14], whereas CBP uses inorganic phosphate in place of one of the ATP molecules to produce G1P. G1P can then be converted to G6P without the need for ATP by the enzyme phosphoglucomutase [15]. Under anaerobic conditions, in which glycolysis generates only two ATP molecules per glucose, increased ATP can result in increased biomass at the expense of ethanol product yield [16]. However, the phosphorolytic pathway can be engineered to perform better than the hydrolytic pathway in terms of product yield in stressful conditions like those expected in lignocellulosic hydrolysates [8].

Although the cellobiose phosphorolytic pathway has potential advantages, its efficiency, hereafter defined as incomplete or low rate of consumption, in the context of cellobiose and xylose co-fermentation is not known. Previously, cellobiose phosphorolytic pathways were combined with xylose isomerase pathways to construct anaerobic cellobiose and xylose co-fermentation systems in *Saccharomyces cerevisiae* and in *Escherichia coli* [17, 18]. However, they are inefficient in terms of sugar consumption and ethanol production rates [17], or the systems remain to be fully optimized [18]. CBP from *Ruminococcus albus* NE1 (RaCBP) uses xylose as a substrate for the reverse of the phosphorolytic reaction [19]. We therefore hypothesized that the inefficiency in cellobiose and xylose co-fermentation previously observed was due to xylose interference with cellobiose consumption via CBP. The presence of xylose is unavoidable because it is a major component of hemicellulose, which has to be utilized for economical biofuels production [9-11]. We therefore tested the effect of xylose on CBP cellobiose fermentation, as well as two potential approaches to alleviate inefficient CBP-mediated cellobiose fermentation in the presence of xylose.

1.3 Results

1.3.1 Inefficient cellobiose fermentation in the presence of xylose

A codon-optimized CBP gene from *Saccharophagus degradans* (SdCBP) [8] and a mutant cellodextrin transporter encoding *N. crassa* CDT-1 (F213L) [8] were cloned into the 2 μ plasmid pRS426 under the control of constitutive P_{PGK1} promoters (hereafter

called pCS plasmid). *S. cerevisiae* strain D452-2 transformed with this plasmid was used for anaerobic fermentations (Table 1-1). The fermentations were carried out with 80 g/L of cellobiose as a carbon source, either with or without 40 g/L of xylose present. The engineered strain was capable of fermenting cellobiose to ethanol in both conditions (Fig. 1-1A,B). However, in the presence of xylose, the rates of cellobiose consumption and ethanol production decreased by 61% and 42%, respectively (Fig. 1-1A,B, Table 1-2). As a result, approximately 20 g/L of cellobiose remained in the fermentation broth after 72 hours in the presence of xylose (Fig. 1-1A), whereas all of the cellobiose was consumed within 36 hours in the absence of xylose (Fig. 1-1A). These results indicated that the presence of xylose had a severe negative impact on cellobiose fermentation mediated by CBP.

Interestingly, in the fermentation supplied with 40 g/L of xylose, the xylose concentration showed an initial decrease followed by a slight recovery after 36 hours (Fig. 1-1C). Xylitol was also produced with a titer of approximately 9 g/L at 72 hours (Fig. 1-1D). These results suggest that approximately half of the xylose transported into the cell was reduced to xylitol but the rest remained unaccounted for.

1.3.2 *In vitro* and *in vivo* production of glucopyranosyl-xylose

To determine the fate of xylose that was unaccounted for by xylitol production, xylose and G1P were used as substrates for the reverse reaction catalyzed by purified SdCBP. Chromatograms of the reaction analyzed by ion chromatography showed a decrease in xylose and G1P concentration along with the appearance of a new peak (1-2A). Analysis of the reaction by mass spectrometry (MS) identified the molecular mass of the product to be 312 g/mol, consistent with that of 4-O-β-D-glucopyranosyl-D-xylose (GX) (Fig. 1-2B,C). Tandem mass spectrometry (MS-MS) further indicated that the product comprised one hexose unit and one pentose unit (Fig. 1-2D). These results suggested that the *in vitro* reverse reaction of SdCBP produced a GX dimer when xylose and G1P were provided as substrates.

Using GX synthesized *in vitro* as a standard, GX was detected in the fermentation broth when cellobiose and xylose were supplied to yeast engineered with the CBP cellobiose consumption pathway (Fig. 1-1E). Interestingly, the concentration of GX initially increased but started to decrease after 36 hours, with its highest concentration reaching approximately 30 g/L (Fig. 1-1E). Extracellular concentrations of xylitol and GX combined accounted for 88% to 100% of the imported xylose. Thus, yeast utilizing cellobiose by the CBP consumption pathway formed GX from intracellular xylose and G1P, in addition to converting some of the imported xylose to xylitol.

1.3.3 Competition assays identified xylose as a mixed-inhibitor

To investigate the inhibitory effect of xylose on SdCBP activity, the catalytic properties of SdCBP were determined in the presence of varying xylose concentrations (Fig. 1-3), at the time points preceding the production of GX. Initial rates of cellobiose

phosphorolysis were calculated from the amount of G1P produced at different cellobiose concentrations (Fig. 1-3A). As the concentration of xylose increased, the apparent maximal rate ($V_{max,app}$) linearly decreased while the apparent substrate concentration at which the reaction rate is half of $V_{max,app}$ ($K_{M,app}$) linearly increased (Fig. 1-3A,B). This result indicated that the apparent affinity of CBP for cellobiose and its maximal phosphorolytic rate for cellobiose were inversely proportional to the xylose concentration, identifying xylose as a mixed-inhibitor for the cellobiose phosphorolysis reaction (Fig. 1-3B). The negative impact of xylose on SdCBP phosphorolytic activity may therefore contribute to the decrease in cellobiose consumption rate observed phenotypically in the above fermentations (Fig. 1-1A), in addition to the production of GX.

1.3.4 Reduced glucopyranosyl-xylose formation in an efficient xylose utilizing strain, SR8-a

Strain SR8-a is an engineered *S. cerevisiae* strain capable of rapid xylose fermentation [20]. We wondered whether rapid xylose utilization, which would maintain a lower intracellular concentration of xylose, could mitigate formation of GX by CBP. Strain SR8-a (xylose utilizing strain developed by metabolic and evolutionary engineering; Table 1-1) and strain D452-2 used above, which lacks a xylose-utilization pathway, were transformed with the pCS plasmid and fermentations were carried out with 80 g/L of cellobiose as a carbon source, with or without 40 g/L of xylose present. In the absence of xylose, the cellobiose consumption and ethanol production profiles of the engineered D452-2 and SR8-a strains were equivalent. Notably, in the presence of xylose, the cellobiose consumption rate of the SR8-a strain was two-fold higher than that of the D452-2 strain (Fig. 1-4A, Table 1-2). The SR8-a strain completely consumed cellobiose in 40 hours and xylose in 24 hours (Fig. 1-4A,C). In the SR8-a background, GX was produced at a lower concentration, at a slower rate, and started to decrease after 16 hours, in comparison to 48 hours in the D452-2 strain (Fig. 1-4E). In addition, the engineered SR8-a strain produced less xylitol and more ethanol than the D452-2 strain (Fig. 1-4B,D). This result suggested that efficient xylose utilization reduced the formation of GX and increased the CBP-mediated cellobiose consumption rate in the presence of xylose.

The cellobiose consumption rate of the SR8-a strain supplemented with xylose was not as rapid as that of the D452-2 strain with no xylose present, showing a 22% decrease (Fig. 1-1A, Fig. 1-4A, Table 1-2). However, the negative effect of xylose on cellobiose consumption was alleviated in comparison to the 61% decrease in cellobiose consumption rate with the D452-2 strain in the presence of xylose (Fig. 1-1A).

1.3.5 Cleavage of glucopyranosyl-xylose by intracellular β-glucosidase and β-xylosidase

4

Given that the GX formed by CBP in the reverse phosphorolytic reaction should have a β-1,4 linkage, we wondered whether GX might serve as a substrate for either an intracellular β-xylosidase (NCU01900) or the intracellular β-glucosidase (NCU00130; GH1-1) from *N. crassa*. Although the amount of GX did not change significantly when the β-xylosidase or no enzyme was used (Fig. 1-5), the β-glucosidase GH1-1 completely hydrolyzed GX, as indicated by the disappearance of the GX peak (Fig. 1-5). Signals of the hydrolysis products, namely glucose and xylose, overlapped but the increase was detected (Fig. 1-5). Further enzymatic analysis of β-glucosidase GH1-1 activity revealed that its maximal rate for GX cleavage was three times lower and its K_M for GX was seven-fold higher than that for cellobiose (Table 1-3). These results showed that the β-glucosidase GH1-1, but not the β-xylosidase NCU01900, was capable of cleaving GX to glucose and xylose. However, cellobiose may compete with GX hydrolysis in the context of *in vivo* cellobiose consumption.

1.4 Discussion

In this study, we identified GX production as a competing off-pathway product of cellobiose and xylose co-fermentation when cellobiose is consumed using a CBP-mediated pathway. The production of GX results in a decreased efficiency of cellobiose fermentation (Fig. 1-1), especially in the absence of a xylose-consumption pathway. The decrease in extracellular xylose concentration (Fig. 1-1C) indicates that xylose is transported into the cell, likely via endogenous hexose transporters. Though lacking a xylose utilization pathway, the engineered yeast strain D452-2 expressing the pCS plasmid is expected to convert some xylose to xylitol by means of endogenous aldose reductase (Gre3) activity [20], consistent with the fact that xylitol was detected in the fermentation medium (Fig. 1-1D). We further verified that much of the remaining xylose loss in the intracellular pool was due to its conversion to GX by the reverse phosphorolysis reaction catalyzed by CBP between G1P and xylose. Interestingly, we found that the extracellular concentration of GX eventually starts to decrease, and at the same time that of xylose begins to recover (Fig. 1-1C,E).

We propose that, in the presence of xylose, cellobiose is first transported into yeast cells via cellodextrin transporter mutant CDT-1 (F213L) and cleaved by CBP to generate glucose and G1P (Fig. 1-6). At the same time, xylose is transported into the cell via hexose transporters. With xylose and G1P present inside the cell, CBP catalyzes the reverse phosphorolysis reaction, producing GX, which can be exported by the cellodextrin transporter (Fig. 1-6). The model explains the initial decrease in xylose concentration and increase in GX concentration in the media (Fig. 1-1C,E). CDT-1, a proton symporter [21], can reversibly transport substrates [1] because of the thermodynamic driving forces of high intracellular substrate (that is, GX) concentrations competing with high extracellular proton concentrations. At later stages of the fermentation, GX in the media is transported back into the cell via the cellodextrin transporter, along with the rest of the cellobiose (Fig. 1-6). GX is then cleaved by SdCBP to generate G1P and xylose. Some xylose released is then exported back into the media via endogenous hexose transporters. The second part of the model explains

5

the decrease in GX concentration and the increase in xylose concentration in the media (Fig. 1-1C,E).

Formation and cleavage of GX as observed here is unfavorable to cellobiose fermentation. GX exhausts resources that could have been dedicated to cellobiose consumption, namely the use of CDT-1 to export and import GX and SdCBP to form and cleave GX. This is especially deleterious because GX processes occur simultaneously with cellobiose consumption (Fig.s 1-1A,E and 6). Furthermore, GX formation requires G1P as one of the substrates (Fig. 1-2A). G1P is thus diverted from glycolysis, where in the absence of xylose it would be converted to G6P by phosphoglucomutase. GX formation would thereby decrease the rate of ethanol production because some of G1P produced from cellobiose via CBP is wasted in the formation of GX. These considerations suggest that GX formation likely results in a decrease in cellobiose import by CDT-1, slows cleavage of cellobiose, and reduces the rate of ethanol production. Extracellular concentrations of cellobiose and ethanol also support this model (Fig. 1-1A,B).

The reported catalytic efficiency ($k_{cat,app}/K_{M,app}$) of RaCBP for xylose in the reverse phosphorolysis reaction is only 1% of that for glucose [18]. However, with SdCBP, a substantial amount of GX formation is observed (Fig. 1-1E). This may be explained by differences between the two CBPs, or by the high concentrations of intracellular xylose and low concentrations of intracellular glucose present in our experiments. When the xylose utilization pathway is absent, high intracellular xylose concentrations are expected. Although we did not measure the intracellular concentration of xylose directly, it is expected to be similar to the extracellular concentration due to the fact that xylose is imported by hexose transporters, which are facilitators [22, 23]. Thus, the imported xylose not accounted for by xylitol production (Fig. 1-1C,D), would result in an intracellular concentration of xylose above the reported $K_{M,app}$ of RaCBP for xylose (25 mM) [19]. By contrast, the intracellular concentration of glucose is expected to be small because glucose can be efficiently converted to G6P and consumed by glycolysis. The maximal reported free intracellular glucose concentration is 2 to 3 mM [24], slightly above the $K_{M,app}$ of RaCBP on glucose (1.5 mM) [19]. Furthermore, the CBP reverse reaction is thermodynamically favorable, with a $\Delta G°$ = −3.6 kJ mol^{-1} for cellobiose formation [8, 25]. Thus, the amount of GX formation we observed was consistent with the known thermodynamic and kinetic properties of the enzymes used in the CBP-mediated cellobiose consumption pathway, especially due to the drive from a high intracellular xylose concentration.

By using *in vitro* competition assays, we identified xylose as a mixed inhibitor of CBP for the cellobiose phosphorolytic reaction (Fig. 1-3A,B). The synthesis of GX from xylose and G1P, albeit slow [26], shows that xylose can bind to the CBP enzyme active site (Fig. 1-2). This helps to explain the decrease in the apparent affinity for cellobiose in the presence of xylose (increase in $K_{M,app}$). The decrease in maximal phosphorolytic rate of cellobiose ($V_{max, app}$) in the presence of xylose suggests that xylose also inhibits cellobiose phosphorolytic activity in some other way, unrelated to xylose competition with cellobiose for the enzyme active site. CBP is an asymmetric homodimer [26, 27], and its active site pocket is formed at the interface of an $(\alpha/\alpha)_6$-barrel domain and a helical extension from the N-terminal domain of the adjacent subunit (Fig. 1-7) [27].

Notably, in a crystal structure of *Cellulomonas uda* CBP in complex with cellobiose [PDB: 3S4A] [28], the reducing end of the cellobiose molecule is in contact with the extension from the adjacent subunit (Fig. 1-7). Xylose likely binds at this position, because its structure is similar to that of glucose, enabling the formation of GX from xylose and G1P. Thus, as xylose binds to and/or releases from the reducing end of the active site in one subunit, it may come into contact with the N-terminal domain of the other subunit. The interaction may alter CBP enzymatic activity, preventing cellobiose phosphorylation in the adjacent unit or resulting in decreased product dissociation from the adjacent active site.

By carrying out cellobiose and xylose co-fermentation using an efficient xylose-utilizing strain, SR8-a [29], we were able to increase the cellobiose consumption rate and decrease GX titer (Fig. 1-4A,B), likely by keeping the steady-state intracellular xylose concentration low. The low concentrations of xylose present inside the cell would improve the apparent kinetic properties of cellobiose phosphorylation, resulting in a faster cellobiose consumption rate (Fig. 1-3). Furthermore, with less intracellular xylose present, less substrate is available for GX formation. Thus, smaller amounts of GX are made, exported out of the cell and re-imported, reserving the capacity of the cellodextrin transporter and CBP for cellobiose phosphorolysis (Fig. 1-6). Finally, less GX formation allows G1P to more efficiently enter into glycolysis by its conversion to G6P, thereby increasing the ethanol production rate. Thus, an efficient xylose utilization pathway can be used to alleviate cellobiose fermentation inefficiencies due to the use of CBP.

For bacteria with CBP, ORFs encoding xylose isomerase are found to co-exist, suggesting that cellobiose and xylose co-fermentation by anaerobic bacteria may be common, for example in *S. degradans*, *Cellvibrio gilvus*, *Ruminococcus sp.* and *Clostridium phytofermentans.* Although co-fermentation has not been shown with these organisms, they may have evolved means of avoiding the production of GX. Previous efforts to construct an anaerobic cellobiose and xylose co-fermentation system in *S. cerevisiae* using CBP and xylose isomerase from *Ruminococcus flavefaciens* were only partly successful [17]. This may be due to the inefficient xylose isomerase conversion step, resulting in high intracellular concentrations of xylose that negatively impact CBP-mediated cellobiose consumption.

We also explored whether CBP-mediated cellobiose conversion in the presence of xylose could be augmented by the use of a hydrolytic enzyme to cleave GX after its formation. We found that the intracellular β-glucosidase GH1-1 from *N. crassa* was capable of GX hydrolysis to glucose and xylose (Fig. 1-5). Thus, low levels of GH1-1 co-expressed with CBP might be used to reduce GX and its associated burdens on the cellobiose consumption pathway (Fig. 1-6). However, cellobiose was preferred as a substrate for GH1-1 in comparison to GX (Table 1-3) and the catalytic efficiency of GH1-1 for cellobiose is higher than that of CBP for cellobiose [8]. Hence, co-expression of GH1-1 with CBP would likely result in most of the cellobiose being hydrolyzed to glucose instead of following the phosphorolytic pathway. This effect would defeat the purpose of using CBP for its energetic advantage, because G1P generation would be replaced by glucose production. To circumvent this challenge, the intracellular β-glucosidase would need to have an increased substrate specificity for GX and lower activity for cellobiose. Protein engineering of an intracellular β-glucosidase with these

properties may be feasible, because xylose is smaller than glucose. Thus, the enzyme active site of β-glucosidase could be engineered to be more bulky, allowing the binding of GX while eliminating that of cellobiose. Successes in similar protein engineering challenges have been reported [30-32].

Alternatively, CBP could be engineered to reduce or eliminate GX production. This approach is advantageous because it addresses the GX complications directly. In contrast to the use of engineered GH1-1 for GX cleavage, this approach allows the system to fully harvest the energetic advantages of the phosphorolytic pathway. However, CBP protein engineering may be challenging because xylose is a mixed-inhibitor of CBP activity (Fig. 1-3), and therefore may require random mutagenesis, multiple site saturation mutagenesis or evolutionary engineering approaches to achieve the necessary cellobiose specificity [30, 33, 34].

1.5 Materials and Methods

Plasmid construction

Plasmids constructed and used in this study are listed in Table 1-1. Plasmids containing a codon-optimized CBP gene from *S. degradans* (SdCBP) [GenBank: 90020965] [8] and cellodextrin transporter mutant from *N. crassa cdt-1* (F213L) [8] were used as templates for combining *cdt-1* (F213L) and SdCBP expression cassettes in pRS426 (pCS). SdCBP was cloned into *E. coli* expression plasmid pET302 with an N-terminal His_6 tag to create pET-Sd. The In-Fusion HD Cloning Kit (Clontech, Mountain View, CA, USA) was used for all plasmid construction.

Yeast strains and media

S. cerevisiae background strains used in this study were D452-2 (*MATα leu*2 *his*3 *ura*3 *can*1) and SR8-a (*ura*3) (Table 1-1). Plasmids were transformed into these strains using a standard lithium acetate yeast transformation protocol [35]. Transformants were selected on synthetic defined medium plates, which contained DOBA (MP Biomedicals, Santa Ana, CA, USA) mixed with two-fold appropriate CSM dropout mixture.

Fermentations

Single colonies from synthetic defined plates were selected and re-streaked. Re-streaked colonies were inoculated in optimal minimal medium (oMM) supplemented with 20 g/L of cellobiose to prepare seed cultures. The oMM contained 1.7 g/L YNB Y1251 (Sigma, Saint Louis, MO, USA), two-fold appropriate CSM dropout mixture, 10 g/L $(NH_4)_2SO_4$, 1 g/L $MgSO_4{\cdot}7H_2O$, 6 g/L KH_2PO_4, 100 mg/L adenine hemisulfate, 10 mg/L inositol, 100 mg/L glutamic acid, 20 mg/L lysine, 375 mg/L serine and 0.1 mM 2-(*N*-morpholino) ethanesulfonic acid (MES) pH 6.0. Seed cultures were harvested at mid- to late-exponential phase and washed twice with sterile water. Washed seed cultures were inoculated at an initial optical density at 600 nm of 20 in 200 mL serum flasks containing 50 mL of media. The flasks were closed with butyl rubber stoppers, sealed with aluminum crimps, and purged with nitrogen gas to obtain strict anaerobic fermentations.

The fermentation media contained oMM supplemented with 80 g/L cellobiose, with or without 40 g/L xylose. The flasks were incubated at 30°C, 220 rpm. Extracellular concentrations of cellobiose, xylose, xylitol and ethanol were determined by high performance liquid chromatography on a Prominence HPLC (Shimadzu, Kyoto, Japan) equipped with Rezex RFQ-FastAcid H 10 × 7.8 mm column. The column was eluted with 0.01 N of H_2SO_4 at a flow rate of 1 mL/min, 55°C. Quantification of GX was performed using an ICS-3000 Ion Chromatography System (Dionex, Sunnyvale, CA, USA) equipped with a CarboPac® PA200 carbohydrate column. The column was eluted with a NaOAc gradient in 100 mM NaOH at a flow rate of 0.4 mL/min, 30°C.

SdCBP protein purification

pET-Sd (pET302-NT/His$_6$-SdCBP) was transformed into the BL21 (DE3) *E. coli* strain and induced by isopropyl β-D-1-thiogalactopyranoside at a final concentration of 0.2 mM. *E. coli* cells were lysed and protein purified by His·Bind Resin (Novagen, Darmstadt, Germany) according to supplied protocols. Purified SdCBP was stored in 20 mM MES, pH 6.0 and quantified using a NanoDrop 1000 spectrophotometer, assuming an extinction coefficient of 1.79×10^5 M^{-1} cm^{-1}, 280 nm.

In vitro synthesis and purification of glucopyranosyl-xylose

We incubated 10 mM xylose and 10 mM G1P with and without 20 nM purified SdCBP in 20 mM MES, pH 6.0 at 37°C for 12 hours. The reaction was stopped by dilution with 0.1 M NaOH at a ratio of 1:200. Signals of components in the solutions were detected using an ICS-3000 Ion Chromatography System (Dionex) with the same conditions described above.

The synthesized GX was purified by ÄKTA Purifier (GE Healthcare Life Sciences, Munich, Germany) equipped with a Supelclean^{TM} ENVI-Carb^{TM} column. The column was eluted with a gradient of acetonitrile at a flow rate of 3.0 mL/min at room temperature. Purified fractions were verified using an ICS-3000 Ion Chromatography System (Dionex) with the same conditions described above.

Mass spectrometry and tandem mass spectrometry

MS of the GX in the *in vitro* synthesis solution was performed on an LTQ XL ion trap instrument (Thermo Fisher Scientific, San Jose, CA, USA) with an electrospray ionization source operated in negative mode. The sample was introduced into the mass spectrometer by direct injection into a flow of 50% water/0.1% formic acid and 50% acetonitrile/0.1% formic acid set at a flow rate of 0.2 mL/min. The MS settings were capillary temperature 350°C, ion spray voltage 4 kV, sheath gas flow 60 (arbitrary units), auxiliary gas flow 10 (arbitrary units), sweep gas flow 5 (arbitrary units). The scan rate for full scan and MS/MS product ion scan was m/z 95 to m/z 500. The compound at m/z 357 was isolated with a m/z 2 isolation width (±1 Da) and fragmented with a normalized collision-induced dissociation energy setting of 35%. The activation time and the activation Q were 30 ms and 0.250, respectively. The mass measurement accuracy was < 3 ppm root mean square.

Competition assay and kinetic parameters

We incubated 10 nM of purified SdCBP, 5 mM of inorganic phosphate and varying cellobiose concentrations at 30°C in 20 mM MES, pH 6.0 with 0, 2.5 or 5 mM xylose. All experiments were carried out in duplicate. G1P concentrations were detected continuously using a G1P Colorimetry Assay Kit (Sigma-Aldrich), according to the provided protocol. Initial rates at each cellobiose concentration were calculated from the rate of G1P production. Apparent kinetic parameters were determined by non-linear regression.

In vitro glucopyranosyl-xylose hydrolytic activity assay

GX synthesized as described above was used at a concentration of 1 mM. The substrate was incubated with 0.5 µM of purified β-xylosidase (NCU01900) or β-glucosidase (NCU00130) in 1× PBS, pH 7.4 at 30°C for 2 hours. β-xylosidase (NCU01900) [35] and β-glucosidase (NCU00130) were expressed and purified as described [6]. To stop the reactions, they were diluted with 0.1 M NaOH. Signals of components in the solutions were detected using an ICS-3000 Ion Chromatography System (Dionex) with the same conditions described above.

For kinetic parameter comparisons, 20 nM of purified GH1-1 and varying concentrations of cellobiose and purified GX were incubated at 30°C in 1× PBS, pH 7.4. All reactions were carried out in duplicate. The reactions were stopped at 0, 5, 10 and 15 minutes by addition of 0.1 M NaOH. Initial rates at each cellobiose and GX concentration were calculated from the rate of glucose production. The ICS-3000 Ion Chromatography System (Dionex) equipped with CarboPac^{TM} PA20 column was eluted with 3 mM KOH at a flow rate of 0.4 mL/min, 30°C, for glucose and xylose separation and to determine glucose concentrations in the reactions. Apparent kinetic parameters were determined by non-linear regression.

Chapter 2. Protein engineering of cellobiose phosphorylase for reduced xylose inhibition and byproduct formation

2.1 Overview

Cellobiose phosphorylase (CBP) is capable of cleaving cellobiose to glucose and glucose 1-phosphate. However, xylose, a pentose sugar that generally co-exists with cellodextrin in the plant biomass, acts as a mixed-inhibitor and a substrate for the reverse reaction in place of glucose (Chapter 1). In theory, preventing xylose from binding to the active site could relieve its inhibitory effects. However, xylose is smaller than glucose, lacking only a single methoxy group. Xylose thus poses a spatial challenge for this protein engineering problem, since simple steric occlusion cannot be used to block its binding to the active site without also preventing glucose binding. Using CRISPR-based chromosomal library selection, we identified a distal mutation in CBP responsible for improved cellobiose consumption and improved kinetic parameters in the presence of xylose. *In silico* analysis suggests this mutation may help stabilize the cellobiose phosphorylase dimer complex and avert xylose binding at the active site.

2.2 Introduction

Enzymes are the crucial workhorses for most chemical conversions in biology. Their precise activity and specificity are fine-tuned through evolution of the polypeptide chain as part of a complex regulatory network in living organisms, ensuring survival in challenging environments. Given their efficiency, many enzymes produced biologically have been used in industrial settings to catalyze chemical reactions in a scale much larger than their native environment. However, the conditions in which they operate likely do not match those of the cells, for example involving different temperatures, pH values, and other chemicals. Exposure to novel conditions may directly affect the enzyme efficiency and even render them inactive.

Cellobiose phosphorylase (CBP) is used by many organisms as a means to consume cellobiose released from plant cell walls as a carbon source, often in anaerobic conditions. CBP is an energy efficient enzyme capable of hydrolyzing cellobiose to glucose and glucose 1-phosphate in the presence of inorganic phosphate [7, 8]. Its activity is greatly compromised in the presence of xylose. Xylose acts as its mixed-inhibitor, reducing CBP's apparent affinity for cellobiose and reducing its apparent maximal rate [36]. In addition, production of 4-O-ß-D-glucopyranosyl-D-xylose (GX) is observed *in vivo* when xylose is present during cellobiose consumption [26, 36] (Fig. 1-6). Given that CBP is a common phosphorolytic enzyme in anaerobic bacteria, these bacteria may have evolved separate mechanisms to bypass the xylose inhibition problem. However, when CBP is taken from its native host and expressed in the industrially relevant organism *Saccharomyces cerevisiae*, it lost the ability to bypass xylose inhibition. Since xylose and cellobiose typically coexist in the starting material of

plant biomass of interest for the production of renewable energy and chemicals [9, 11], it is essential to relieve xylose inhibition of CBP for it to be used industrially.

In this study, through CRISPR chromosomal library selection [37], we identified a single mutation in CBP which helped alleviate inhibition by xylose. This mutation, located distal from the enzyme active site, provides a rare opportunity to determine how protein conformations can prevent small molecule binding yet allow a bigger molecule to occupy the same pocket within the enzyme.

2.3 Results

2.3.1 Selection of mutated cellobiose phosphorylase from a chromosomal library

A chromosomal CBP library was created using error-prone PCR and the CRISPRm system [37]. Mutated cbp was assembled at the $URA3$ locus ($ura3::P_{PGK1}$-cbp-T_{ADH1}) into a S288C diploid strain expressing an improved cellodextrin transporter ($lyp1::P_{TDH3}$-$cdt1$ $F213L$-T_{CYC1}) [8]. The library was pooled and subjected to selection in liquid media containing 1% cellobiose and with 2% xylose as competitor. High concentrations of xylose in the cellobiose media would be expected to act as a selection pressure, favoring cbp mutants capable of overcoming mixed inhibition by xylose and/or reducing GX synthesis by CBP [36].

After growth for 3 days, yeasts were plated on 1% cellobiose 2% xylose minimal media plates to isolate improved yeast clones. Of 10 large colonies picked from the selection, strain CX9 showed improved aerobic growth in 1% cellobiose plus 2% xylose (Fig. 2-1A). The cbp allele in the CX9 strain (cbp_{CX9}) had 7 mutations—Y47H, K256M, E270D, I384L, N488D, N578S and Y631F—located throughout the protein sequence (Fig. 2-1B). To validate that the improved phenotype was not a consequence of background mutations, cbp_{CX9} was reintroduced into the initial strain. In aerobic conditions, the strain expressing cbp_{CX9} showed improved growth and cellobiose consumption in comparison to the strain expressing wild-type CBP (Fig. 2-1C).

To identify the mutation(s) responsible for the improved phenotype, two approaches were conducted in parallel. First, combinatorial chimeras of wild-type CBP and cbp_{CX9} were constructed and compared. All strains whose cbp region 1 (Y47H, K256M and E270D) was derived from cbp_{CX9} showed improved cellobiose consumption rates comparable to that of the full-length cbp_{CX9} (Fig. 2-2A). Second, each mutation in cbp_{CX9} was individually reverted to its original sequence. When residue 47 was mutated back to tyrosine, the cellobiose consumption phenotype reverted to that of wild-type CBP even in the presence of the other six mutations (Fig. 2-2B). Introduction of Y47H into wild-type CBP resulted in an improved cellobiose consumption profile, similar to that of cbp_{CX9} (Fig. 2-3A). These results indicated that Y47H was necessary and sufficient to replicate nearly all of the improved phenotype of cbp_{CX9}.

2.3.2 *In vivo* analysis of CBP mutants

To better understand the physiological impact of the mutation, the extracellular xylose and GX levels of the *cbp* mutants were analyzed. When provided with cellobiose and xylose, strains expressing the cellobiose phosphorolytic pathway are known to import xylose even in the absence of a xylose utilization pathway [36]. The xylose acts as a substrate along with glucose 1-phosphate in the reverse of the CBP reaction, producing the GX dimer, which is secreted back into the media [36]. While the cellobiose consumption profile of *cbp* Y47H was similar to that of *cbp*$_{CX9}$, its extracellular xylose and GX concentrations were intermediate between those of strains expressing wild-type CBP or *cbp*$_{CX9}$ (Fig. 2-3). The *cbp* mutants had higher extracellular xylose concentrations consistent with the lower secreted GX concentrations at all time points. These results suggested that xylose did not interact with *cbp* mutants as well, decreasing GX formation, thereby improving the overall cellobiose consumption in the presence of xylose. However, the difference between the two *cbp* mutants, evident through the xylose and GX concentrations, suggests that mutations apart from Y47H in CBP also contribute to the improvement of the *cbp*$_{CX9}$ strain.

2.3.3 *In vitro* characterization of CBP mutants

To study the effects of the *cbp* mutants *in vitro,* xylose competition and GX synthesis assays were performed using purified *cbp* proteins (Fig. 2-4). Xylose acts as a mixed inhibitor of the cellobiose phosphorolytic forward reaction [36], resulting in a decrease in V$_{max,app}$ and an increase in K$_{m,app}$. For the *cbp* mutants, the decrease in V$_{max,app}$ in the presence of xylose was attenuated by 60-70%. However, a substantial rescue of the increase in K$_{m,app}$ in the presence of xylose was only observed in *cbp*$_{CX9}$ (40%)*.* The increase in K$_{m,app}$ of *cbp* Y47H remained elevated, comparable to that of wild-type CBP (Fig. 2-4 A-D). These results suggest that, unlike *cbp*$_{CX9}$, Y47H only relieved xylose inhibition at the level of V$_{max,app}$, but not K$_{m,app}$. The difference in their response to xylose in terms of K$_{m,app}$ might explain the intermediate phenotype of strains expressing *cbp* Y47H in the presence of xylose.

To test the effect of *cbp* mutations on the reverse reaction with xylose, end-point GX synthesis assays were performed (Fig. 2-4E,F). The amount of GX synthesized was normalized by the amount of cellobiose synthesized by the same enzyme variant, with either xylose or glucose provided as one of the substrates, respectively. Wild type CBP synthesized 5 times more GX than the *cbp* mutants, suggesting that the mutations decrease the ability of CBP to carry out the reverse reaction with xylose as a substrate, consistent with the lower GX concentrations observed in the media in growth assays.

2.3.4 Conserved improved phenotypes in a CBP homolog

Tyrosine 47 is highly conserved among CBP homologs (Fig. 2-5A). To test the generality of the *cbp* Y74H enzymatic properties and phenotypes, the Y47 position in CBP from *Cellulomonas gilvus* (CgCBP, 63% identity) was mutated to histidine for *in vivo* and *in vitro* analysis. In the presence of xylose, cellobiose consumption of yeast expressing Cg*cbp* Y47H improved in comparison to the strain expressing wild-type

Cg*cbp* (Fig. 2-5B). Extracellular xylose generated by the strain expressing Cg*cbp* Y47H was also higher than that of the wild-type Cg*cbp* strain, corresponding to the lower amount of GX secreted (Fig. 2-5C, D). In the xylose competition assay, xylose had no effect on $V_{max,app}$ and $K_{m,app}$ of Cg*cbp* Y47H, while wild-type CgCBP exhibited the expected decrease in $V_{max,app}$ and increase in $K_{m,app}$ (Fig. 2-5E, F). In the end-point GX synthesis assay, wild-type CgCBP synthesized 2.6 times more GX than the Cg*cbp* Y47H (Fig. 2-5G, H). Together, these results suggest that the improved phenotypes associated with the Y47H mutation might be conserved generally among CBP homologs.

2.3.5 *In silico* analysis of Y47H mutation in CBP

To understand the effect of the Y47H mutation on the structure of CBP, the crystal structure of *Cellulomonas uda* in complex with cellobiose (PDB:3S4A) [28] was used for modeling the Y47H mutation. The mutation was distal to CBP active site (Fig. 2-6A) and one of the possible rotamers of histidine replacing tyrosine at position 47 showed minimal van der Waals overlap with surrounding protein side chains (Fig. 2-6B). A surface view of the structure reveals cellobiose to be buried inside CBP as expected, with the Y47H mutation situated on the surface of the structure (Fig. 2-6C). Electrostatic calculations revealed that the position of Y47H is at the edge of a positively-charged elongated pocket, surrounded by negatively-charged residues, formed between two CBP units (Fig. 2-6D). A similar electrostatic distribution exists when using the crystal structure of CgCBP in complex with glucose and SO_4 (PDB:2CQS) [38] for the analysis.

2.4 Discussion

Xylose is a known mixed-inhibitor of the cellobiose phosphorylase (CBP) enzyme [36]. Xylose inhibition of CBP is problematic because cellobiose and xylose generally co-exist as components of plant biomass during its deconstruction. Thus, improving CBP to be tolerant of the presence of xylose is critical for its industrial use. However, this particular protein-engineering problem is quite challenging. The fact that CBP produces GX from glucose 1-phosphate and xylose by the reverse reaction [36] directly implies that xylose is capable of binding to the CBP active site. It likely binds to the same pocket as the glucose product from the forward CBP reaction [19]. To relieve xylose inhibition, the enzyme would need to be modified so that xylose can no longer bind to the active site, while still allowing glucose to be released from the enzyme complex. Since glucose is released before glucose 1-phosphate [39], it is crucial that xylose not bind to the glucose pocket before glucose 1-phosphate is released, as the reverse reaction of GX formation has a favorable Gibbs free energy [8, 12]. Considering how xylose is identical to glucose apart from the removal of a single methoxy group, using spatial constrains to prevent xylose binding would be unlikely to also allow glucose binding.

Using a chromosomal library selection [37], we successfully identified a single mutation in CBP responsible for reduced xylose inhibition. The mutation of the

conserved tyrosine at position 47 to histidine improved cellobiose consumption rate of yeast in the presence of xylose. This phenotype was accompanied by reduced xylose import and reduced GX production. Y47H is distal to the CBP active site, raising questions as to how it influences xylose binding. Studies have revealed that distal mutations can greatly contribute to enzyme kinetics as they may change protein conformation and that they are part of the protein functional residue network [40, 41]. The position of Y47H at the edge of a positively-charged stretch formed between two CBP monomers may contribute to the improved apparent kinetics and reduced GX formation. Mutation from a moderately polar tyrosine to a positively-charged histidine on the complex surface likely enhances salt bridge formation with nearby negatively-charged residues, possibly stabilizing the dimer complex. Improved cellobiose production by CBP Y47H in the reverse reaction, in the presence of xylose, supports this hypothesis. We speculate that the Y47H mutation could stabilize the two monomers in a closed configuration that partially blocks xylose entrance to the active site. It could also induce conformational changes that reduce xylose allosteric inhibition of CBP. Further structural studies of the CBP Y47H compared to wildtype CBP by X-ray crystallography or nuclear magnetic resonance spectroscopy are essential for identifying the conformational changes caused by the Y47H mutation. These studies could inform future protein engineering and the rational design of substrate specificity, in cases that require preventing a smaller molecule binding to a site that normally binds a larger molecule.

2.5 Materials and Methods

Yeast strains, selection and anaerobic fermentation

A *S. cerevisiae* S288C diploid strain was used for chromosomal library selection using the CRISPRm system [37]. First, cellodextrin transporter CDT-1 with a F213L mutation [8] was introduced at the *lyp1* locus (*lyp1::P$_{TDH3}$-cdt1 F213L-T$_{CYC1}$*). Then, codon optimized cellobiose phosphorylase from *Saccharophagus degradans* was subjected to mutation using GeneMorph II Random Mutagenesis Kit (Agilent Technologies) and introduced at the *URA3* locus (*ura3::P$_{PGK1}$-cbp-T$_{ADH1}$*). The library was pooled and selected in liquid oMM media [42] containing 2% xylose and 1% cellobiose. The selection culture was plated on minimal media plates containing 2% xylose and 1% cellobiose to screen for larger-than-average colonies.

Cellobiose consumption phenotypes of different CBP mutants were determined using *S. cerevisiae* D452-2 (MATα *leu2 his3 ura3 can1*), expressing pRS316- *P$_{TDH3}$-cdt1 F213L-T$_{CYC1}$* and pRS315- *P$_{PGK1}$-cbp-T$_{ADH1}$*. The strains were selected and maintained on oMM media supplied with appropriate CSM dropout mixtures. The In-Fusion HD Cloning Kit (Clontech) was used for all plasmid construction.

The phenotypes were also evaluated under anaerobic conditions using oMM media provided with 8% cellobiose and 4% xylose with a starting OD$_{600}$ of 20. The cultures were purged with nitrogen gas and sealed to maintain strict anaerobic conditions. Extracellular concentrations of cellobiose, xylose and GX were determined

15

by a Prominece HPLC (Shimadzu) and an ICS-3000 Ion Chromatography System (Dionex), as described [36].

Protein purification

Cellobiose phosphorylases fused with an N-terminal His-tag were expressed in *E. coli* strain BL21 (DE3), induced by IPTG as described [36] and purified by HisTrap HP column (GE Healthcare) on the AKTA Explore FPLC system (GE Healthcare) according to the supplied protocol.

Competition assay and kinetic parameters

10 nM of purified CBP was incubated with 5 mM inorganic phosphate and varying cellobiose concentrations at 30 °C in 20 mM MES, pH 6.0 with 0 or 10 mM xylose. G1P concentrations were continuously monitored as a readout using a G1P Colorimetry Assay Kit (Sigma-Aldrich). The G1P production rate was used for apparent K_m and V_{max} calculations by non-linear regression.

4-O-ß-D-glucopyranosyl-D-xylose (GX) synthesis assay

200 nM of purified CBP was incubated with 10 mM G1P and 10 mM xylose or glucose in 20 mM MES, pH 6.0 at 30 °C for 1 hour. The reactions were stopped by adding 0.1 M NaOH, and concentrations of either GX or cellobiose were analyzed on the ICS-3000 Ion Chromatography System (Dionex), as described [3].

CBP Homology and Modeling

SdCBP structure was predicted using Phyre2 [43]. SdCBP homology to other CBP enzymes was determined using the phmmer algorithm (EMBL-EBI) [44], aligned using MUSCLE (EMBL-EBI) [45] and the sequence map was created using WebLogo (Berkeley) [46]. Crystal structures of CBP in complexes with cellobiose [28] or glucose and sulfate [38] were used to model the Y47H mutation. Visualization, surface calculations and electrostatic calculations were carried out using PyMOL (Schrödinger) [47].

Chapter 3. Alternative xylose utilization pathway design

3.1 Overview

The efficient use of hemicellulose in the plant cell wall is critical for the economic conversion of plant biomass to renewable fuels and chemicals. Previously, the yeast *Saccharomyces cerevisiae* has been engineered to convert the hemicellulose-derived pentose sugars xylose and arabinose to D-xylulose-5-phosphate for conversion via the pentose phosphate pathway (PPP). However, efficient pentose utilization requires PPP optimization and may interfere with its roles in NADPH and pentose production. High concentration of extracellular xylose also has a negative impact on cellobiose phosphorolytic pathway as described in Chapter 1-2. Here, we developed an alternative xylose utilization pathway that largely bypasses the PPP. In the new pathway, D-xylulose is converted to D-xylulose-1-phosphate, a novel metabolite to *S. cerevisiae*, which is then cleaved to glycolaldehyde and dihydroxyacetone phosphate. This synthetic pathway served as a platform for the biosynthesis of ethanol and ethylene glycol. The use of D-xylulose-1-phosphate as an entry point for xylose metabolism opens the way for optimizing chemical conversion of pentose sugars in *S. cerevisiae* in a modular fashion.

3.2 Introduction

Utilization of pentose sugars in hemicellulose is essential for economical biofuel and renewable chemical production from plant cell wall derived biomass [48, 49]. Although highly efficient at fermenting glucose, most *Saccharomyces cerevisiae* strains cannot utilize xylose and arabinose [50]. To broaden its substrate spectrum, heterologous enzymes from bacteria and fungi have been successfully engineered into *S. cerevisiae* to enable xylose and arabinose consumption [50-52]. These pathways deliver xylose and arabinose to the endogenous pentose phosphate pathway (PPP) via D-xylulose-5-phosphate (X5P). It has been found that to improve pentose utilization efficiency, expression of the endogenous PPP enzymes must be manipulated [53, 54]. This may be because the PPP in *S. cerevisiae* is primarily dedicated to NADPH regeneration and ribose 5-phosphate synthesis [55, 56], not for xylose and arabinose utilization. A systematic approach to identify the limiting steps for pentose utilization via the PPP requires careful investigation of the regulation of many enzymes and metabolites in the PPP and in glycolysis. One proposed alternative involves the addition of a heterologous phosphoketolase pathway, producing ethanol via conversion of X5P to glyceraldehyde-3-phosphate and acetyl-phosphate [57]. However, the proposed

system still relies on and produces X5P, a key intermediate metabolite in the PPP [57]. Here, we explored an alternative 3-step pentose utilization pathway, designed to bypass the endogenous PPP.

The alternative xylose utilization pathway in *S. cerevisiae* is comprised of 3 main steps (Fig. 3-1). First, D-xylose is converted to D-xylulose by xylose isomerase (XI) or the two enzymes xylose reductase (XR) and xylitol dehydrogenase (XDH) [4-6]. D-xylulose is then phosphorylated to D-xylulose-1-phosphate (X1P) by an ATP-dependent ketohexokinase (KHK) [58, 59]. The third step is catalyzed by endogenous fructose-1,6-bisphosphate aldolase (*FBA1*), which can cleave X1P to glycolaldehyde and dihydroxyacetone phosphate (DHAP) [58]. These three steps would deliver three carbons from xylose to glycolysis using DHAP as an intermediate. The second product from the third step, glycolaldehyde, is normally toxic to yeast [60], but could be converted to ethylene glycol (EG) by endogenous NADH-dependent alcohol dehydrogenase (*ADH1*) and/or NADPH-dependent 3-methylbutanl/methylglyoxal reductase (*GRE2*). The *in vivo* activities of these enzymes on glycolaldehyde in *S. cerevisiae* have been demonstrated [61, 62]. The alternative pathway thus should enable xylose utilization in *S. cerevisiae*. A synthetic utilization of xylose via X1P has been demonstrated in *Escherichia coli* [63, 64].

We reasoned that the proposed three-step xylose utilization pathway would likely require further engineering to alleviate potential inefficiencies. Endogenous xylulokinase (*XKS1*), which is responsible for phosphorylating D-xylulose to X5P, might direct most of the D-xylulose flux from xylose to the PPP. *XKS1* might therefore need to be disrupted so that the flux of D-xylulose is directed to the new synthetic pathway. In addition, the pathway as envisioned generates 1 net ATP and an excess of NAD^+ and/or $NADP^+$. Thus, the pathway may need to be supplied with additional ATP and reducing power to produce a functional and balanced system.

Here, we tested whether the new pathway functions in *S. cerevisiae*, allowing xylose utilization via an intermediate metabolite, X1P, typically not present in traditional pentose utilization.

3.3 Results

3.3.1 Construction of the synthetic xylose utilization pathway in *S. cerevisiae*

As a first test of the synthetic xylose utilization pathway (Fig. 3-1), we used the XI from *Bacteroides stercoris* HJ-15 for the conversion of D-xylose to D-xylulose. We hypothesized that rat liver KHK might be used to catalyze the second step of the pathway–the conversion of D-xylulose to D-xylulose-1-phosphate (X1P)–due to its similarity to ketohexokinase from human liver (80% amino acid identity), which catalyzes this reaction [58], and the fact that rat liver KHK can phosphorylate fructose in *S. cerevisiae* cell lysates [59]. Finally, we relied on the endogenous fructose 1,6-bisphosphate aldolase (*FBA1*) to cleave X1P to glycolaldehyde and dihydroxyacetone phosphate (DHAP), as a partially purified aldolase from human liver could cleave X1P *in vitro* [58].

Exogenous components of the synthetic pathway (Fig. 3-1)–xylose isomerase (XI) from *B. stercoris* HJ-15 and ketohexokinase (RnKHK) from rat liver–were introduced into *S. cerevisiae* strain D452-2 and a D452-2 strain with xylulokinase deleted (D452-2 *xks1*Δ::KanMX) to eliminate xylulose conversion to X5P. To test xylose consumption by these strains, fermentation experiments with 40 g/L of xylose were carried out under strict anaerobic conditions. Xylose was consumed when XI and RnKHK were expressed in the backgrounds with and without *xks1*Δ (Fig. 3-2B). However, xylose consumption in the *xks1*Δ background did not start until after approximately 6 days while that in the strain with functional *XKS1* started immediately (Fig. 3-2B). In total, the amount of xylose consumed after 10 days in the *xks1*Δ background was approximately 2-fold lower than that with functional *XKS1* (Fig. 3-2B). Notably, EG production was detected only when XI and RnKHK were expressed in the *xks1*Δ background (Fig. 3-2E). These results suggest that *XKS1* deletion was necessary for driving metabolic flux through D-xylulose-1-phosphate to produce ethylene glycol. Nevertheless, the decrease in xylose consumption in the *xks1*Δ background implied that components downstream of the xylose isomerase step were potential bottlenecks of the pathway. Concentrations of xylitol and glycerol, which are byproducts of xylose metabolism, were lower in the *xks1*Δ background, consistent with a lower carbon flux passing through the pathway (Fig. 3-2 C,D). We also attempted to substitute XR and XDH for XI to convert xylose to xylulose. However, the resulting strain used xylose poorly and did not produce EG (Fig. 3-2.) and thus was not pursued further.

3.3.2 Overexpression of the endogenous components in the synthetic pathway

In addition to the two exogenous components shown to be necessary for EG biosynthesis, three endogenous enzymes involved in the synthetic pathway— *FBA1, GRE2* and *ADH1* (Fig. 3-1)—were individually overexpressed in the *xks1*Δ XI-RnKHK strains. *FBA1* overexpression (OE) showed 33% and 56% increases in total amount of xylose consumed and EG titer, respectively (Fig. 3-3). *FBA1* overexpression resulted in immediate xylose consumption in contrast to the approximately 6-day lag phase observed in the starting strain (Fig. 3-3B). The positive impacts of *GRE2* and *ADH1* overexpression, while observable, were not as prominent as that of *FBA1* overexpression (Fig. 3-3). No further improvements were observed when *GRE2* and/or *ADH1* were overexpressed along with *FBA1* (Fig. 3-3B). Production of xylitol, glycerol and ethanol positively correlated with the amount of xylose consumed (Fig. 3-3C,D,F). These results suggested that the pathway was primarily limited by the aldolase activity of Fba1, responsible for converting D-xylulose-1-phosphate to glycolaldehyde and DHAP, and not the final reduction of glycolaldehyde to ethylene glycol by Gre2p and/or Adh1.

3.3.3 Cellobiose co-utilization enhanced the synthetic xylose consumption pathway

Previous experiments demonstrated that a cellodextrin consumption pathway (CD), comprised of a cellodextrin transporter and intracellular β-glucosidase from

Neurospora crassa [3]*, could be used for the co-consumption of cellobiose and xylose [1]. We reasoned that co-consumption of cellobiose might increase the ATP levels and NAD(P)H reducing equivalents available for the alternative xylose consumption pathway. In the co-utilization system, intracellular ATP and NADH were 42% and 104% higher than that provided with xylose as the sole carbon source (Fig. 3-4A), as predicted. When cellobiose and xylose were co-utilized, ethylene glycol titers increased by 30% and 160% in strains expressing endogenous levels of *FBA1* or overexpressing *FBA1* (strains *xks1Δ* XI-RnKHK-CD and *xks1Δ* XI-RnKHK-*FBA1*-CD), respectively (Fig. 3-4B). Co-utilization of cellobiose resulted in improved xylose consumption, increased xylitol production, increased glycerol production and improved cell viability (OD600) in comparison to when xylose was provided as a sole carbon source (Fig. 3-5). Compared to cellobiose consumption as the sole carbon source, a 15% decrease in glycerol titer was observed (Fig. 3-5). These results show that cellobiose co-utilization enhanced xylose consumption via the synthetic pathway, by supplying the system with excess ATP and NADH. Furthermore, they revealed that cellobiose co-utilization and *FBA1* overexpression had a synergistic effect on the efficiency of the xylose consumption pathway.

We further investigated whether supplying additional NADH in the absence of cellobiose could increase ethylene glycol production. The engineered yeast (*xks1Δ* XI-RnKHK-*FBA1*) were provided with xylose in anaerobic fermentations in the presence of formate, which is the substrate for endogenous NADH-generating formate dehydrogenase (Fdh1) similar to NADH-generating butanediol dehydrogenase (Bdh1) [65]. The activities of Fdh1 were verified in crude cell lysates, which were incubated with NAD^+ and formate (Fig. 3-6). When the strains were provided with 25 mM formate, a decrease in formate concentration was detected. In the presence of formate, improved xylose consumption, decreased EG, xylitol and glycerol productions were detected while ethanol production remained unchanged (Fig. 3-6). These results imply that an attempt to provide excess NADH alone may help improve xylose consumption but is not sufficient to improve carbon conversion by the synthetic xylose utilization pathway.

3.3.4 Leakage in the modular design of the synthetic pathway

The three-step xylose utilization pathway for ethylene glycol biosynthesis is designed to bypass the central PPP (Fig. 3-1). Product titers and the intracellular metabolites of the strain expressing the alternative synthetic pathway (*xks1Δ* XI-RnKHK-*FBA1*-CD strain) were compared to those of the traditional xylose utilization pathway (XI strain). For the synthetic pathway, the ethanol and EG titers were approximately 1.4 g/L and 0.48 g/L, respectively, resulting in a product molar ratio of 4:1 (ethanol:EG) (Fig. 3-A). As expected, metabolic profiling showed that X1P was only detected when the alternative pathway was expressed (Fig. 3-7B). Notably, unique metabolites in the PPP—namely xylulose-5-phosphate (X5P), ribose-5-phosphate (R5P) and sedoheptulose-7-phosphate (S7P)—were observed at significant levels (Fig. 3-7B), even though the new pathway was designed to bypass the PPP. While relative levels of X5P and R5P in the strain expressing the traditional pathway (XI strain) were

110% and 48% higher, S7P was 77% higher in the strain expressing the alternative pathway (Fig. 3-7B).

In the *xks1Δ* background, there are three possible routes to X5P, R5P and S7P production via the PPP. First, reverse reactions involving fructose-6-phosphate (F6P), glyceraldehyde-3-phosphate (GADP), and erythrose-4-phosphate (E4P) (Fig. 3-1) could result in X5P, R5P and S7P production. The steady-state flux distribution in the engineered strain could lead to buildups of X5P, R5P and S7P.

Second, it is possible that unannotated activities in *S. cerevisiae* are responsible for the conversion of X1P to X5P. To investigate the effect of a large buildup of X1P in the system, a strain expressing a 6xHis-tagged Fba1 was lysed and the Fba1 purified using a HisTrap column. The flowthrough of the lysate lacking Fba1 was incubated with X1P overnight. A decrease in X1P levels was observed in comparison to when no lysate was provided (Fig. 3-8). However, the expected product, X5P was not observed at the detection limit of the experiment. Further mass spectrometry analysis was unable to identify the production of compounds with a molecular mass identical to that of X5P or xylulose. The resulting products could not be determined, potentially because of its rapid downstream reaction or the limitation of the mass spectrometry protocols. We also tested three endogenous proteins that might be responsible for X1P conversion to X5P—namely Pgm1, Pgm2 and Prm15. The purified enzymes were active in the conversion of glucose-1-phosphate to glucose-6-phosphate (Fig. 3-9) [66]. However, only purified Prm15 resulted in a decrease in X1P levels (Fig. 3-8). As with the crude lysates, mass spectrometry methods did not detect xylulose, X5P or compounds with similar masses to pentose monophosphates. In addition, tests of strains with individual deletions of *PGM1*, *PGM2*, or *PRM15* did not affect EG production titers, rates, or ethanol:ethylene glycol titer ratios appreciably (Fig. 3-8).

The third possible route for X5P, R5P and S7P production is from gluconeogenesis intermediates. Gluconeogenesis produces 6-carbon compounds from 3-carbon compounds under carbon starvation [2]. Beginning with 6-phosphogluconate, 6-carbon compounds can be converted to ribulose-5-phosphate and ribose 5-phosphate (R5P), X5P and S7P, respectively. To better understand the effect of upper glycolytic intermediates and the X1P synthetic pathway, cellobiose was supplied to the system in addition to xylose. The levels of X1P, X5P, R5P and S7P decreased in comparison to when xylose was provided as a sole carbon source (Fig. 3-7). This finding supports the hypothesis that PPP intermediates present in the X1P system may be a result of upper glycolytic intermediates produced by gluconeogenesis.

3.4 Discussion

Although the PPP is the canonical route for pentose sugar utilization in microbes [67], the PPP in *S. cerevisiae* has not evolved to efficiently consume these sugars. We therefore devised an alternative route for xylose consumption. In our present design, three carbons in xylose can be directed to glycolysis in three linear steps, while the remaining two carbons can be converted to ethylene glycol, with a total loss of 1 carbon via CO_2 for every molecule of xylose consumed (20% carbon loss). In contrast, the traditional pathway requires 3 molecules of xylose to produce 5 molecules of ethanol

21

accompanied by a loss of 5 CO_2 (33.3% carbon loss) [68]. Thus when fully optimized, the alternative pathway in theory should be advantageous over the traditional pathway in terms of theoretical carbon loss. In this study, the theoretical carbon loss calculation was not present because the leakage problem detected in the synthetic pathway likely disrupted the stereochemistry of the reactions. Producing excess NAD^+, this synthetic pathway could be coupled with NAD^+ deficient metabolic pathways; for example, a cellobiose utilization pathway and 2,3-butandiol production pathways [69], to achieve an overall redox balance. Furthermore, the modular nature of this pathway may prove advantageous for understanding pentose utilization in *S. cerevisiae*. Here, we used ethylene glycol production from the alternative xylose utilization pathway as a phenotypic indicator of its metabolic efficiency, for two reasons. First, native *S. cerevisiae* strains do not synthesize EG. Thus, EG can be used as a readout for the efficiency of the alternative pentose utilization pathway. Second, EG is currently produced from ethylene derived from nonrenewable petrochemical resources [70]. The biosynthetic routes to EG from xylose were demonstrated in *Escherichia coli* via xylonate and 2-dehydro-3-deoxy-D-pentonate [71] and D-ribulose 1-phosphate [72, 73]. With a rising global demand for EG, a biosynthetic pathway in *S. cerevisiae*–the preferred microbe for industrial fermentations–would prove beneficial for large-scale bioprocessing.

We found that *xks1Δ* was necessary for EG production. This is likely necessary at present, because the expression levels of enzymes within the synthetic pathway are suboptimal or unbalanced. By deleting the endogenous xylulokinase (*XKS1*), the major route for xylulose utilization via X5P and the PPP was removed, thereby forcing the intracellular xylulose to go through the alternative synthetic pathway. In comparison to the PPP, xylose consumption through the X1P pathway was slower. This result implies that enzymes in the pathway downstream of xylose isomerase function suboptimally. Taking advantage of the 3-step linear fashion of the synthetic pathway, we found that overexpression of the downstream aldolase *FBA1* increased the ethylene glycol titer and accelerated xylose consumption, whereas overexpression of *GRE2* and/or *ADH1* resulted in limited improvements. This may be due to the fact that cleavage of X1P to DHAP and glycolaldehyde by Fba1 is thermodynamically unfavorable [74]. However, the negligible benefit of *GRE2* and/or *ADH1* overexpression was unexpected because glycolaldehyde is toxic to *S. cerevisiae* cells [60]. Therefore, in the present implementation, the enzymatic steps following xylulose formation but prior to glycolaldehyde production—namely ketohexokinase and aldolase—are likely to be the limiting steps in the new pathway.

Given that ketohexokinase requires ATP to phosphorylate xylulose early in the pathway, the system may face an ATP deficiency similar to the case of unbalanced glycolysis [75]. To test this model, a cellobiose utilization pathway was introduced to increase ATP equivalents available for xylose conversion without competing for xylose transport. Cellobiose fermentation is expected to provide the system with 3-4 ATPs for every molecule of cellobiose consumed [8], while only one net ATP was expected from the synthetic pathway per one molecule of xylose. When cellobiose was provided, the intracellular ATP and NADH increased by 42% and 104%, respectively, and the EG titer nearly tripled. Its synergistic effect with *FBA1* overexpression also suggested that both

ketohexokinase and aldolase are independent limiting steps of the pathway. In addition to providing excess ATP, cellobiose fermentation may also help with co-factor recycling. Its fermentation usually generates glycerol, potentially due to an excess of NADH that overflows from the acetaldehyde oxidation branch [1]. Since the synthetic xylose consumption pathway is NADH deficient, excess NADH from cellobiose fermentation may help keep the system balanced. This hypothesis is supported by a 15% decrease in glycerol titer observed in the cellobiose-xylose mixture in comparison to when cellobiose was provided as a sole carbon source. However, when formate was provided to the synthetic xylose utilization system, generating NADH by endogenous formate dehydrogenase (Fdh1) [65], xylose consumption improved while EG production worsened. The small decrease in formate concentration implied limited activity of Fdh1. Increasing Fdh1 expression may provide more cellular NADH and may change the observed phenotypes. Taken together with the results when cellobiose was co-consumed, the NADH deficiency inherent in the pathway likely became more relevant when the system was not ATP limited.

The synthetic pathway is predicted to be fully modular and separate from the PPP. However, the high ratio of ethanol to EG (4:1 as opposed to the expected 1:1) suggested a leakage of the synthetic system into the PPP. Steady-state distributions suggested that unknown *S. cerevisiae* enzymes might be responsible for the leakage. However, our inability to find such an enzyme to date suggests that the leakage occurred through gluconeogenesis followed by production of PPP intermediates from 6-carbon compounds. Further biochemical studies of crude lysate fractions coupled with protein mass spectrometry should help identify the cause of X1P leakage.

The present results provide evidence that an alternative pentose utilization pathway in *S. cerevisiae* can partially bypass the X5P entry point and the PPP. This study showed the first evidence of X1P *in vivo* production, to the best of our knowledge. The synthetic pathway is simple and linear with three enzymatic steps to convert xylose to an intermediate for glycolysis. We envision that molecular and systems-level understanding of this new synthetic pathway could spur its broader application in alternative sugar utilization strategies.

3.5 Materials and Methods

Strains and Plasmids

S. cerevisiae D452-2 (*MATα, leu2, his3, ura3,* and *can1*) was used for the synthetic pathway construction. Plasmids and strains used in this work are described in Table 3-1. The codon-optimized sequence for RnKHK is given at the end of the SI Materials and Methods. The In-Fusion HD Cloning Kit (Clontech) was used for all plasmid construction. Plasmids were transformed into the yeast strains using a standard lithium acetate yeast transformation protocol [76]. Transformants were selected on synthetic defined (SD) medium plates, which contained DOBA (MP Biomedicals, Santa Ana, CA) mixed with 2-fold appropriate CSM dropout mixture.

Fermentation experiments

Single colonies from SD plates were selected and re-streaked. Re-streaked colonies were inoculated in Optimal Minimal Medium (oMM) [77] supplemented with 20 g/L of glucose to prepare seed cultures. For strains transformed with the plasmid encoding the cellobiose utilizing pathway (pCD), 20 g/L of cellobiose was provided in place of glucose. Seed cultures were harvested at mid- to late-exponential phase and washed twice with sterile water. Washed seed cultures were inoculate at an initial OD600 of 10-20 in 150 mL serum flasks containing 40 mL of media. The flasks were closed with butyl rubber stoppers, sealed with aluminum crimps, and purged with nitrogen gas to obtain strict anaerobic fermentations. The fermentation media contained oMM and 0.1 M 2-(N-morpholino)ethanesulfonic acid (MES), pH 6.0 supplemented with 40 g/L xylose, and/or 80 g/L cellobiose. The flasks were incubated at 30 °C, 220 rpm. All fermentations were performed with two biological replicates.

Analytical Methods

Extracellular concentrations of xylose, cellobiose, xylitol, glycerol, ethylene glycol and ethanol were determined by high performance liquid chromatography on a Prominence HPLC (Shimadzu) equipped with Aminex HPX-87H 300x7.8 mm column. The column was eluted with 0.01 N of H_2SO_4 at a flow rate of 0.5 mL/min, 30 °C.

Intracellular metabolites at the exponential phase of ethylene glycol production (t = 4 days) were quenched in 180 µL of 40:40:20 acetonitrile:methanol:water. Following the addition of 10 nmols of d3 serine (as an internal standard), the mixtures were vortexed and centrifuged at 13,000 rpm for 10 minutes. The supernatants were injected onto an Agilent 6460 QQQ LC-MS/MS and the chromatography was achieved by normal phase separation with a Luna NH_2 column (Phenomenex) starting with 100% acetonitrile with a gradient to 100% 95:5 water acetonitrile. 0.1% formic acid or 0.2% ammonium hydroxide with 50 mM ammonium acetate was added to assist with ionization in positive and negative ionization mode, respectively. Data were quantified by integrating the area under the curve of each metabolite multiple reaction monitoring transition, compared to internal standard. Five biological replicates were used for each sample analyzed.

X1P, X5P and S7P were separated using a 1200 Series liquid chromatography instrument (Agilent Technologies, Santa Clara, CA). A 1 µL aliquot of the sample was injected onto an Agilent Eclipse XDB-C18 (2.1 mm i.d., 150 mm length, 3.5 µm particle size) column with a Zorbax SB-C8 (2.1 mm i.d., 12.5 mm length, 5 µm particle size) guard column and eluted at 25 °C and a flow rate of 0.2 mL/min with the following gradient (modification from [78]): 15 min isocratic 100% buffer A (10 mM tributylamine/15 mM acetic acid), then in 15 min with a linear gradient to 60% buffer B (methanol), 2 min isocratic 60% B, then 10 min equilibration with 100% buffer A. The eluent from the column was introduced into a mass spectrometer for 25 minutes after the first 10 minutes. Mass spectrometry (MS) was performed on an LTQ XL ion trap instrument (Thermo Fisher Scientific, San Jose, CA) with an ESI source operated in negative ion mode. The MS settings were capillary temperature 350 °C, ion spray voltage 4.5 kV, sheath gas flow: 60 (arbitrary units), auxiliary gas flow 10 (arbitrary units), sweep gas flow 5 (arbitrary units). For MS/MS product ion scan, the scan range was m/z 80 to m/z 300. The compounds X1P, X5P and R5P at m/z 229.1 and S7P at

m/z 289.1 were isolated with an m/z 2 isolation width and fragmented with a normalized collision-induced dissociation energy setting of 35% and with an activation time of 30 ms and an activation Q of 0.250. The detection limits for X1P and X5P based on this method were approximately 1-5 µM, depending on the experiment.

Xylulose phosphate synthesis

D-xylulose-1-phosphate (X1P) and D-xylulose-5-phosphate (X5P) were synthesized using purified rat liver ketohexokinase (RnKHK) and *E.coli* xylulokinase (xylB), respectively. The N-terminally His$_6$-tagged RnKHK (pNT/His-RnKHK) was expressed in D452-2 *xks1Δ* and purified using HisTrap^{TM} HP (GE Healthcare Life Sciences) according to the provided protocol. *E.coli* xylulokinase was cloned into pET302 N-terminal his-tag construct (pET-xylB) expressed in BL21 Star (DE3), induced with 0.2 mM IPTG and purified using HisTrap^{TM} HP column. The reactions comprised of 1 mM D-xylulose and 1 mM ATP, catalyzed by 1 µM purified enzyme in 1X PBS buffer, were incubated at 30°C and 37°C overnight for the purified RnKHK and xylB, respectively. Formation of the products was verified by mass spectrometry according to the protocol previously described.

Mutase purifications and activity assays

PGM1, PGM2 and *PRM15* were cloned from *S. cerevisiae* D452-2 genomic DNA into plasmid pRS423 to create N-terminal His$_6$-tag fusion constructs. The constructs were transformed and expressed in strain D452-2 in oMM media supplied with 20 g/L glucose. The cells were lysed and purified using HisTrap^{TM} HP (GE Healthcare Life Sciences) according to standard protocols. Purified enzymes or crude cell lysates were incubated with 1 mM X1P synthesized as previously described in 1X phosphate buffered saline (PBS), pH 7.4 at 30°C. The reactions were stopped by addition of 0.1 M NaOH solution.

Chapter 4. Metabolite profiling study of cellobiose utilizing *S. cerevisiae*

4.1 Overview

Despite a modular linear design, introduction of the synthetic xylose utilization pathway (Chapter 3) was less than optimal. It is likely because organisms evolve intricate regulatory network suitable for their environment overtime, such that integration of exogenous components could interrupt the network and result in an imbalanced state. In this chapter, minimal synthetic biological system was used as a platform to study network interference.

Glycolysis is central to energy metabolism in most organisms, and is highly regulated to enable optimal growth. In the yeast *Saccharomyces cerevisiae*, feedback mechanisms that control flux through glycolysis span transcriptional control to metabolite levels in the cell. Using a cellobiose consumption pathway, we decoupled glucose sensing from carbon utilization, revealing new modular layers of control that induce ATP consumption to drive rapid carbon fermentation. Proton pumping and regulation of amino acid biosynthesis mediated by extracellular glucose sensors independently contributed to maintenance of energy homeostasis. Controlling the upper bound of cellular ATP levels may be a general mechanism used to regulate energy levels in cells, via a regulatory network that can be uncoupled from ATP concentrations under perceived starvation conditions.

4.2 Introduction

Most microorganisms favor glucose as their primary carbon source, as reflected in their genetic programs hard-wired for this preference. Central to carbon metabolism is glycolysis, which is finely tuned to the dynamic state of the cell due to the fact that glycolysis first consumes ATP before generating additional ATP equivalents. To avoid catastrophic depletion of ATP, yeast has evolved a transient ATP hydrolysis futile cycle coupled to gluconeogenesis [75]. Glycolysis in yeast is also tightly coupled to glucose transport into the cell, entailing three extracellular glucose sensing mechanisms and at least one intracellular glucose signaling pathway [79].

Synthetic biology and metabolic engineering of yeast holds promise to convert this microorganism into a "cell factory" to produce a wide range of chemicals derived from renewable resources or those unattainable through traditional chemical routes. However, many applications require tapping into metabolites involved in central carbon metabolism, a daunting challenge as living cells have numerous layers of feedback regulation that fine-tune growth to changing environments. Cellular regulation evolved intricate networks to maintain and ensure cell survival. For example the yeast *Saccharomyces cerevisiae* has evolved to rapidly consume high concentrations of glucose through fermentation, while repressing the expression of other carbon consumption pathways, an effect termed glucose repression. When perturbed genetically, regulatory networks such as those in glucose repression often generate undesirable or unexpected phenotypes.

For yeast to be useful in producing large volumes of biofuels or renewable chemicals, it will be important to expand its carbon utilization to include multiple sugars in the plant cell wall. One promising approach that helps overcome glucose repression and allows simultaneous utilization of different sugars is a cellobiose consumption pathway [1]. Cellobiose is a disaccharide with two units of glucose linked by a ß-1,4 glycosidic bond. The cellobiose pathway, comprised of a minimal additional pathway in yeast—a cellodextrin transporter (CDT-1) and intracellular ß-glucosidase [3]–avoids glucose repression by importing carbon in the form of cellobiose instead of glucose. The cellodextrin transporter allows cellobiose to enter the cell where it is hydrolyzed to glucose and consumed via the native glycolytic consumption pathway. By moving glucose production into the cell, the *N. crassa*-derived cellobiose consumption pathway is nearly the minimal synthetic biological module imaginable in *S. cerevisiae*, comprised of just two genes. Nevertheless, in *S. cerevisiae* the cellobiose consumption pathway is inferior to consumption of extracellular glucose in terms of rate and results in a prolonged lag phase [42]. Previous efforts to understand the impact of cellobiose consumption on the physiology of *S. cerevisiae* using transcriptional profiling revealed that cellobiose improperly regulates mitochondrial activity and amino acid biosynthesis, both of which are tightly coupled to the transition from respiration to fermentation [42].

Since glycolytic enzymes are regulated mostly at the post-transcriptional level [80], we probed cellobiose consumption in *S. cerevisiae* at the metabolite level. We found that key metabolites in glycolysis are highly imbalanced, leading to low flux through glycolysis and slow fermentation. We also found that excess ATP levels drive the imbalance, and identified a new regulatory role of glucose sensors in cellular ATP homeostasis.

4.3 Results

S. cerevisiae cells ferment cellobiose more slowly than glucose and often exhibit a prolonged lag phase when transitioning to consumption of this disaccharide [42]. We hypothesized that cellobiose consumption results in an ATP deficit in glycolysis relative to glucose, due to the fact that the cellodextrin transporter (CDT-1) in the cellobiose utilizing pathway is a proton symporter, requiring ATP hydrolysis for cellobiose uptake [21]. Moreover, under anaerobic conditions, ATP production is limited to substrate-level phosphorylation, further restricting ATP availability. We measured the steady-state concentrations of ATP and other metabolites in central carbon metabolism in yeast fermenting cellobiose compared to glucose. Of the 48 compounds analyzed, the abundance of 25 compounds was significantly different (p-value < 0.01) between cellobiose and glucose-fed samples (Fig. 4-1A). Surprisingly, ATP levels increased by 6-fold in the cellobiose grown cells (Fig. 4-1B). The relative abundance of compounds in glycolysis—fructose 6-phosphate (F6P), glucose 6-phosphate (G6P), glucose and pyruvate—increased by 444-, 81-, 7- and 3-fold, respectively, while that of phosphoenolpyruvate decreased by 2-fold (Fig. 4-1B).

4.3.1 Phosphofructokinase-1 inhibition by excess ATP

Given the dramatic buildup of glucose, G6P and F6P intermediates prior to the phosphofructokinase (*PFK1*) reaction in glycolysis (Fig. 4-2A), we reasoned that Pfk1 might be the bottleneck of cellobiose consumption. Pfk1 catalyzes the phosphorylation of F6P, using one ATP and yielding fructose 1,6-bisphosphate (F1,6BP) as a product. As the second committed step in glycolysis, Pfk1 is heavily regulated—with ATP acting as an allosteric inhibitor and AMP and fructose 2,6-bisphosphate serving as activators [81-83].

To test whether allosteric inhibition of Pfk1 by ATP limited cellobiose fermentation, a mutation in Pfk1 that makes the enzyme ATP-insensitive (P722L in the Pfk1 beta subunit [84]) was introduced into the chromosomally encoded *PFK1* gene (mutation here termed *pfk1m*) in the cellobiose utilizing strain. This mutation was previously shown to reduce ATP inhibition but also AMP and fructose 2,6-bisphosphate activation of Pfk1 [84]. Consistent with allosteric inhibition of Pfk1 by ATP, the cellobiose consumption efficiency (E_c) of the *pfk1m* strain increased by 33% in comparison to the strain with wild-type Pfk1 (Fig. 4-2B). Furthermore, the relative abundance of G6P and F1,6BP decreased by 47% and 34%, respectively, while that of ATP remained relatively unchanged (Fig. 4-2C). These results suggested that the 6-fold increase in cellular ATP concentrations allosterically inhibited Pfk1, resulting in accumulation of glucose, G6P and F6P, which eventually slowed down cellobiose consumption.

4.3.2 Limited activity of plasma membrane ATPase

Although the *pfk1m* strain partially increased the rate of cellobiose fermentation, the levels of cellular ATP remained elevated relative to glucose fermentation. It is unlikely that ATP production was the cause of the difference, as fermentation is limited to substrate-level phosphorylation under anaerobic conditions regardless of carbon source. We therefore tested whether the activity of one of the major ATP sinks in yeast, the plasma membrane ATPase (Pma1) was responsible for the ATP buildup. Pma1 hydrolyzes 25-40% of cellular ATP in yeast [85] and is heavily regulated by glucose levels [86].

A constitutively active mutant form of *PMA1* (*pma1-Δ916*, here abbreviated *pt*) [87] was introduced into the endogenous *PMA1* locus in the cellobiose utilizing strain. This mutation results in high Pma1 ATPase activity even under carbon starvation conditions [87]. We observed a 66% decrease in cellular ATP levels in the *pt* strain in comparison to the wild-type control (WT, or cellobiose pathway only) (Fig. 4-2C). Phenotypically, the E_c of the mutant strain was 4 times that of the control (Fig. 4-2A). In addition, the concentrations of G6P and F1,6BP decreased by 58% and 93%, respectively, relative to strains expressing wild-type *PMA1*. Notably, these concentrations dropped more than when the ATP-insensitive *PFK1* mutant was introduced (Fig. 4-2C). These results suggest that increased Pma1 ATPase activity improved cellobiose fermentation, likely by alleviating ATP accumulation that allosterically inhibited Pfk1 in glycolysis.

With decreased intracellular ATP concentrations in the *pma1-Δ916* strain, ATP inhibition at the Pfk1 step is unlikely to limit glycolysis. Consistent with this hypothesis, the cellobiose consumption profile of a *pfk1m-pt* double mutant was identical to that of the *pt* strain (Fig. 4-2A). Surprisingly, the levels of G6P, F1,6BP and ATP in the double mutant strain were higher than in the *pt* strain (Fig. 4-2C). In fact, their levels were similar to those in the *pfk1m* strain (Fig. 4-2C). This may be because *pfk1m* has reduced activation by AMP and fructose 2,6-bisphosphate, in addition to reduced inhibition by high ATP concentrations [84]. Taken together, these data suggest that the effect of reduced Pfk1 allosteric activation may only be evident in the absence of Pfk1 inhibition by ATP.

4.3.3 Carbon starvation-like state of the plasma membrane ATPase

We wondered whether the limited Pma1 activity in cellobiose-fed cells is due to the absence of extracellular glucose in the media. Transcriptionally, the presence of glucose increases *PMA1* mRNA levels by 2-4 times via the regulation by Rap1, Gcr1 and Sir2 [88-90]. Consistent with the requirement for extracellular glucose sensing, previous RNA sequencing experiments revealed a 40% decrease in *PMA1* transcript levels when cellobiose was provided in place of glucose [42]. However, although transcriptional regulation of *PMA1* is important, it is slower than post-transcriptional regulation and results in smaller changes [86, 91]. In the presence of glucose, phosphorylation of Ser-899 and Ser-911/Thr-912 in Pma1 decreases its K_m for ATP and increases its V_{max}, respectively [86, 92, 93]. Given the excess amount of ATP observed in cellobiose utilizing conditions (Fig. 4-1), we hypothesized that V_{max}-determining phosphorylation states of Ser-911 and Thr-912 might play a major role in establishing the efficiency of cellobiose fermentation.

Combinatorial mutations of Ser-911/Thr-912 to alanine and aspartic acid were introduced into the endogenous *PMA1* gene to prevent or mimic phosphorylation, respectively. We were unable to obtain strains with *pma1* S911A T912A and *pma1* S911A T912D, potentially because the combinations were lethal. All mutant strains whose Pma1 S911 position was mutated to aspartic acid consumed cellobiose more efficiently in comparison to when the S911 position remained unchanged (Fig. 4-3A). By contrast, mutating Pma1 T912 to aspartic acid did not show a correlation with the cellobiose consumption phenotype. These results suggest that phosphorylation of Pma1 at S911 was lacking when cellobiose was provided as a sole carbon source.

According to the above mutational analysis, the Pma1 phosphorylation state of cellobiose-fed cells was similar to that in carbon starvation conditions (Fig. 4-3B) [93]. Based on the relatively high level of intracellular glucose present in the cellobiose-grown cells (Fig. 4-1), extracellular glucose is likely to be essential for full activation of Pma1 through S911 phosphorylation, as high intracellular glucose concentrations (Fig. 4-1) or glucose metabolism [94] was unable to satisfy this role.

4.3.4 Positive effects of extracellular glucose sensor deletions

29

Snf3, Rgt2 and Gpr1 are the three known sensors of extracellular glucose in *S. cerevisiae*. Snf3 and Rgt2 mainly regulate glucose transport while Gpr1 controls cell physiology via an interaction with Gpa2 to activate protein kinase A and cAMP synthesis [94]. To mimic the presence of extracellular glucose, constitutively active mutations (*snf3* R229K, *rgt2* R231K and *gpa2* R273A) were introduced into the endogenous loci to probe the role of each glucose-sensing pathway [95, 96]. The cellobiose consumption efficiency of all the three mutant strains decreased by ~25% (Fig. 4-4). We then inverted the genetic modifications by deleting *SNF3, RGT2* and/or *GPA2*. Surprisingly, the triple glucose-sensing deletion strain (*snf3Δrgt2Δgpa2Δ, or srgΔ*) showed a 275% increase in cellobiose consumption efficiency (E_c)(Fig. 4-5A).

Combinatorial deletions revealed that the Gpr1 pathway did not contribute to improved cellobiose fermentation, but the combined *SNF3* and *RGT2* deletions (*srΔ*) were necessary and sufficient to replicate the E_c of the triple deletion strain (Fig. 4-4 and Fig. 4-5). Consistent with the observed E_c values, the intracellular ATP levels of *srgΔ* and *srΔ* decreased by 41% and 18% respectively, while those in the individual-deletion strains *snf3Δ* and *rgt2Δ* remained unchanged (Fig. 4-5A). These results reveal a negative correlation between E_c and cellular ATP levels (Fig. 4-5B) and that Snf3 and Rgt2 acted together to regulate cellular ATP levels, in addition to regulating glucose transport.

4.3.5 Snf3/Rgt2 regulation of cellular ATP levels

To examine whether Snf3/Rgt2 regulated the cellular ATP level in cellobiose fermentations via Pma1, a *snf3Δ rgt2Δ pma1-Δ916* strain (*srΔ-pt*) was constructed. Notably, the E_c of the *srΔ-pt* strain increased more than 4 times in comparison to the wild-type control (Fig. 4-5A, C). The improvement was additive, within the range of the ΔE_c summation of *srΔ* and *pma1-Δ916* strains relative to wild type cells (Fig. 4-5C). Although ATP levels decreased in a nearly linear fashion as a function of E_c (Fig. 4-5B), it is not presently possible to ascertain whether the *srΔ* and *pma1-Δ916* mutations act entirely independently due to limitations in measurement accuracy (Fig. 4-5C).

To further determine the relationship between Snf3/Rgt2 and Pma1, the biochemical properties of Pma1 from different strains consuming cellobiose were analyzed. Western blots showed lower Pma1 protein levels in *srΔ* and *srΔ-pt* in comparison to the wild-type and *pt* strains (Fig. 4-6A). The difference in Pma1 abundance when comparing wild-type and *pt* strains was negligible, but was similarly decreased in both the *srΔ* and *srΔ-pt* strains (Fig. 4-6A). These results suggest that deletion of Snf3/Rgt2 slightly decreased Pma1 protein abundance.

Next, we examined overall Pma1 ATPase activity (Fig. 4-6B). Consistent with the constitutively active nature of the *pt* mutation, the activities of Pma1 in the *pt* and *srΔ-pt* strains were higher than those observed in the WT or *srΔ* strains, respectively. Notably, the ATPase activitiy of Pma1 in *srΔ* was comparable to the WT strain suggesting that Snf3 and Rgt2 in combination do not regulate Pma1 transcriptionally or post-translationally in a straightforward manner.

4.3.6 Transcriptional impact of Snf3/Rgt2 Deletion

Given the lower cellular ATP concentration (Fig. 4-5A) but nearly unchanged Pma1 ATPase activity in the *sr*Δ strain relative to WT (Fig. 4-6B), Snf3/Rgt2 likely regulate ATP homeostasis through an additional mechanism other than Pma1. A systems-level analysis of yeast transcriptomes from the WT, *s*Δ, *r*Δ, and *sr*Δ strains identified 137 genes that were differentially expressed and unique to *sr*Δ (p-value < 0.001 and absolute fold change > 2 for *sr*Δ compared pairwise with WT, *s*Δ and *r*Δ). Notably, 14 genes (10.2%) encoding ATP binding proteins and those involved in ATP catabolic processes were upregulated. The 137 genes were further categorized into five clusters, revealing upregulation of genes involved in amino acid biosynthesis, fatty acid biosynthesis and iron homeostasis, and downregulation of those in phospholipid biosynthesis, phospholipid metabolism, mitochondrial structure, negative regulation of gluconeogenesis and translation initiation factor eIF1 (SUI1). A more comprehensive analysis of genes involved in amino acid biosynthesis revealed a high correlation with upregulation of Gcn4, the central transcriptional activator of genes in this pathway (Fig. 4-7) [97, 98].

4.4 Discussion

To identify the effects of a minimal alteration to carbon metabolism in yeast, we chose a cellobiose-consumption pathway composed of two genes and analyzed its cellular metabolite profiles in comparison to cells provided with glucose, yeast's preferred carbon source. More than half of the metabolites changed abundance significantly when cellobiose was provided in place of glucose. The slow-fermentation phenotype of cellobiose consumption resulted from a surprising accumulation of cellular ATP, rather than ATP depletion as originally expected [21]. The high ATP levels resulted in a bottleneck in upper glycolysis at the step of Pfk1, as revealed by the buildup of G6P and F6P in *S. cerevisiae* fermenting cellobiose. Furthermore, the Pfk1 bottleneck was relieved in cells expressing an ATP-insensitive *PFK1* allele, resulting in improved cellobiose fermentation. These results contrast with previous studies that identified ATP depletion and the buildup of fructose-1,6-bisphosphate–the metabolite immediately downstream of Pfk1–as a weak link in glycolysis [75].

Although ATP is central to a cell's energy currency, too much ATP is not necessary beneficial [99, 100]. In fact, we observed a negative correlation between cellular ATP levels and cellobiose consumption efficiency (Fig. 4-5B). A similar correlation has been reported for glucose as a carbon source, suggesting metabolic uncoupling of energy homeostasis in yeast cells [101]. We propose that intracellular glucose concentrations–generated by cellobiose hydrolysis in our experiments–and glucose metabolism [94] are insufficient to trigger glucose activation of key metabolic pathways and enzyme activity, further exacerbated the uncoupling. For example, we found that the ATP-dependent proton pump Pma1 existed in a carbon-starvation like state during cellobiose fermentation, and was partially responsible for the aberrant accumulation of ATP. These results suggest that neither intracellular glucose nor

glucose metabolism are sufficient to fully activate Pma1. Future experiments will be required to reveal why ATP was not consumed by other cellular processes triggered under starvation [102].

We also found that the well-studied glucose sensors Snf3/Rgt2 exhibited a novel role in cellular ATP homeostasis through an unknown mechanism independent of the major plasma membrane ATPase Pma1. Deletion of extracellular glucose sensors (Snf3/Rgt2) increased cellobiose consumption efficiency and restored ATP levels. It is known that deletion of *SNF3* and *RGT2* slow down glucose consumption [103], due to the inability of these strains to degrade Mth1/Std1, which block the promoter regions of hexose transporters required for optimal glucose import [104-107]. Unlike glucose, cellobiose does not signal Mth1 degradation even with intact Snf3/Rgt2 [107]. Thus, genes downstream of Mth1 regulation, including hexose transporters, are not expected to be responsible for the improved E_c and decreased cellular ATP levels observed in *sr∆*. Based on transcriptome profiling, the lack of Snf3 and Rgt2 increases ATP-requiring cellular activities through regulatory nodes other than Mth1. Consistent with this model, no growth defect is observed in a *mth1∆* strain growing on glucose, suggesting that Snf3/Rgt2 has additional regulatory nodes other than Mth1 [103].

Regulation of ATP levels by the combined action of Snf3 and Rgt2 seems to involve transcriptional activation of amino acid biosynthetic pathways (Fig. 4-7), although Snf3 and Rgt2 are glucose sensors [94]. In yeast, general amino acid control (GAAC) requires transcription factor Gcn4, which directly activates the amino acid biosynthetic pathways, as well as pathways for vitamins associated with amino acid synthesis in conditions of amino acid starvation or stress [97, 98]. Notably, the transcription profile of the *sr∆* strain compared to WT reveals that pathways directly regulated by Gcn4 are induced during cellobiose fermentation, indicating that Gcn4 is activated in these conditions (Fig. 4-7). Interestingly, we found that patterns of transcription activation of wild-type *GCN4* relative to *gcn4∆* strains correlate highly with *sr∆* relative to WT in cellobiose fermentations (correlations of 0.52 with [97] and 0.68 with [98],respectively) (Fig. 4-7).

The present results indicate that Snf3 and Rgt2 might repress Gcn4 levels in the absence of glucose. These results come as a surprise, as previous experiments showed glucose limitation induced *GCN4* mRNA translation as a starvation response [108]. Glucose limitation was shown to activate *GCN4* mRNA translation by stimulating Gcn2 kinase activity [108], which is responsible for phosphorylating translation initiation factor eIF2 and depleting active ternary complexes of eIF2 with initiator tRNA and GTP [109]. By contrast, a chemical genetics approach identified the kinase Snf1, the yeast homologue of human AMP-activated protein kinase (AMPK), as a repressor of *GCN4* mRNA translation in conditions with a non-glucose sugar and abundant amino acid availability [110], conditions more in line with those used here. In the present experiments, *GCN4* mRNA levels remain unchanged in *sr∆* relative to WT, indicating that Gcn4 repression by Snf3 and Rgt2 also likely occurs translationally [109].

One possible additional mechanism of activation of *GCN4* mRNA translation could be depletion of translation initiation factor 1 (eIF1, encoded by *SUI1*). In the *sr∆* strain, levels of *SUI1* mRNA decreased nearly 2.6-fold. Consistent with a direct role for eIF1, previous results demonstrated that activation of *GCN4* translation decreases with

increased functional eIF1 levels [109, 111]. Notably, *SUI1* transcript levels were also lower in *GCN4* cells when compared to *gcn4Δ* strains under starvation conditions [98]. Future experiments will be required to demonstrate a direct link between eIF1 levels and *GCN4* mRNA translation activation.

The present systems-level study of a minimal synthetic biology pathway for cellobiose consumption revealed the dramatic impact of decoupling extracellular and intracellular glucose sensing, resulting in an overabundance of ATP in cells. The inability of *S. cerevisiae* to catabolize ATP for cellular processes in the presence of intracellular glucose and glucose metabolism but in the absence of extracellular glucose resulted in slow fermentation. Thus, ATP levels must be kept in a relatively narrow range for optimal fermentation and to allow robust startup of glycolysis, yet yeast seems to lack a direct mechanism to monitor ATP concentrations. For example, a dynamic model showed that a small concentration difference of inorganic phosphate, a product of ATP hydrolysis, could alter the cell destiny from a stable glycolytic steady state to an imbalanced dead-end state [75]. Here, we found that the extracellular glucose sensing by Snf3/Rgt2 required for optimal glucose fermentation [79] can be uncoupled from the role of these receptors in regulating ATP homeostasis under carbon starvation conditions. It will be important in the future to map the fully regulatory pathways of ATP homeostasis leading from Snf3/Rgt2 and, independently, terminating in Pma1, along with the mechanisms connecting carbon utilization to the translation of the master transcriptional regulator Gcn4.

4.5 Materials and Methods

Yeast strains, media and anaerobic fermentation

The *S. cerevisiae* background strain used in this study was S288C *ura3::P$_{PGK1}$-cdt-1 N209S/F262Y-T$_{ADH1}$ lyp1::P$_{TDH3}$-gh1-1 (codon optimized)-T$_{CYC1}$* derived by chromosomal DNA library selection [37]. The strain was subjected to further modifications using the CRISPRm system [37].

Seed cultures for cellobiose fermentation experiments were grown in 20 g/L glucose modified optimal minimal media (oMM) [42] and harvested at mid-log phase. All cellobiose fermentation experiments were conducted under strict anaerobic conditions, in 80 g/L cellobiose oMM media at an initial OD$_{600}$ of 20, using 10 mL serum flasks containing 5 mL fermentation in 2-5 biological replicates. The flasks were incubated at 30°C, 220 rpm. The cellobiose consumption efficiency (E$_c$) was defined as the inverse of the area under the curve of extracellular cellobiose concentration over time.

Analytical analysis of yeast metabolites

Extracellular cellobiose concentrations were determined by high performance liquid chromatography on a Prominence HPLC (Shimadzu, Kyoto, Japan) equipped with Rezex RFQ-FastAcid H 10 x 7.8 mm column. The column was eluted with 0.01 N of H$_2$SO$_4$ at a flow rate of 1 mL/min, 55°C.

For the metabolite profiling comparison between glucose and cellobiose, equal amounts of yeast cells at mid-exponential phase of anaerobic sugar consumption (10

g/L cellobiose or glucose) were harvested (final pellet OD_{600} equivalent to 5). The samples were quenched in 180 µL of 40:40:20 acetonitrile:methanol:water. Following the addition of 10 nmols of d3 serine (as an internal standard), the mixtures were vortexed and centrifuged at 13,000 rpm for 10 minutes. The supernatants were injected onto an Agilent 6460 QQQ LC-MS/MS and the chromatography was achieved by normal phase separation with a Luna NH_2 column (Phenomenex) starting with 100% acetonitrile with a gradient to 100% 95:5 water acetonitrile. 0.1% formic acid or 0.2% ammonium hydroxide with 50 mM ammonium acetate was added to assist with ionization in positive and negative ionization mode, respectively. Five biological replicates were used for each sample analyzed.

For targeted intracellular metabolite comparisons, yeast cells equivalent to 20 OD_{600} units were harvested and filtered through a 0.8 µm nylon membrane, prewashed with 3 mL water, followed by another 3 mL water wash after cell filtration. The membranes were placed in 1.5 mL extraction solution (0.1 M formic acid, 15.3 M acetonitrile) flash-frozen in liquid nitrogen, and stored at -80°C. Before analysis, the extracts were vortexed for 15 minutes and centrifuged to collect the supernatants at 4°C. Glucose 6-phosphate and fructose 1,6-bisphosphate were separated and identified using a 1200 Series liquid chromatography instrument (Agilent Technologies, Santa Clara, CA). 1 µL of each sample was injected onto an Agilent Eclipse XDB-C18 (2.1 mm i.d., 150 mm length, 3.5 µm particle size) column with a Zorbax SB-C8 (2.1 mm i.d., 12.5 mm length, 5 µm particle size) guard column and eluted at 25 °C and a flow rate of 0.2 mL/min with the following gradient (modification from [78]): 15 min isocratic 100% buffer A (10 mM tributylamine/15 mM acetic acid), then in 15 min with a linear gradient to 60% buffer B (methanol), 2 min isocratic 60% B, then 10 min equilibration with 100% buffer A. The eluent from the column was introduced into a mass spectrometer for 25 minutes after the first 10 minutes. Mass spectrometry (MS) was performed on an LTQ XL ion trap instrument (Thermo Fisher Scientific, San Jose, CA) with an ESI source operated in negative ion mode. The MS settings were capillary temperature 350 °C, ion spray voltage 4.5 kV, sheath gas flow: 60 (arbitrary units), auxiliary gas flow 10 (arbitrary units), sweep gas flow 5 (arbitrary units). For the MS/MS product ion scan, the scan range was m/z 80 to m/z 300. The compounds G6P at m/z 259.1 and F16BP at m/z 339.1 were isolated with an m/z 2 isolation width and fragmented with a normalized collision-induced dissociation energy setting of 35% and with an activation time of 30 ms and an activation Q of 0.250.

Plasma membrane isolation
Strains were subjected to cellobiose fermentation under anaerobic conditions. Yeast cells with an OD_{600} equivalent to 40 were harvested at mid-log phase and flash frozen in liquid nitrogen. Membrane fractions were extracted based on the protocol published in [112].

Western blots
20 µg of the isolated membrane fractions were used for western blots. 1:200 anti-Pma1 (yN-20) (Santa Cruz Biotechnology) and 1:5000 donkey anti-goat IgG-HRP (Santa Cruz Biotechnology) were used to detect the presence of untagged Pma1.

Pma1 ATPase activity assay

The ATPase assay described in [113] was modified as follows. 30 µg of the isolated membrane fraction was incubated in assay buffer (50 mM MES pH 5.7, 10 mM $MgSO_4$, 50 mM KCl, 5 mM NaN_3, 50 mM KNO_3) with and without 3 mM orthovanadate for 25 minutes at 30 °C. 1.8 mM ATP was added to start the 100 uL reactions. The reactions were incubated at 30 °C for 15 minutes, then the membranes were isolated from the reactions by centrifugation at 13,000x g for 10 minutes at 4°C. The released inorganic phosphate was measured in the supernatant using the ATPase/GTPase Activity Assay Kit (Sigma-Aldrich) based on the manufacturer's protocol. The raw Pma1 ATPase activities were calculated by subtracting the concentration of released inorganic phosphate in reactions provided with orthovanadate from those without.

RNA Sequencing

Total RNA was extracted from yeast cells equivalent to 40 OD_{600} units harvested at mid exponential phase by the RiboPure Yeast kit (Thermo Fisher Scientific). Multiplexed libraries were then derived from the total RNA using TruSeq RNA Library Preparation Kits v2 (Illumina Sequencing). The quality of the library was evaluated by Agilent Bioanalyzer 2000 (Functional Genomics Laboratory, UC Berkeley) and sequenced with Illumina HiSeq2500 RAPID platform (Vincent J. Coates Genomic Sequencing Laboratory, UC Berkeley). The reads were assembled and analyzed in CLC Genomics Workbench 9 (Denmark). RPKM (Reads Per Kilobase of exon model per Million mapped reads) was chosen as the expression value output, which was further normalized by the total expression values in a sample.

Yeast cell-based cellobiose uptake assay

The cell-based cellobiose uptake assay was modified from [35]. Yeast strains were grown to mid-exponential phase in 2% oMM glucose, washed with assay buffer (5 mM MES, 100 mM NaCl, pH 6.0) three times and resuspended to a final OD_{600} of 10. Equal volumes of the cell suspension and 200 µM cellobiose were mixed to start the reactions, which were incubated at 30°C with continuous shaking for 15 minutes. The reactions were stopped by adding 150 µL of supernatants to 150 µL 0.1 M NaOH. The concentrations of the remaining cellobiose were measured using an ICS-3000 Ion Chromatography System (Dionex, Sunnyvale, CA, USA) equipped with a CarboPac® PA200 carbohydrate column. The column was eluted with a NaOAc gradient in 100 mM NaOH at a flow rate of 0.4 mL/min, 30°C.

Conclusions

The application of biologically engineered organisms and the molecular and systems-level understanding of their physiology are interconnected. In this dissertation, cellobiose-xylose co-consumption systems were examined in detail, revolving around the concept of cellular energy. The study started off at the molecular and biochemistry levels, and expanded to understanding the systems-level phenomena of the engineered yeasts.

In chapter 1, xylose was shown to have negative impacts on cellobiose fermentation mediated by CBP in *S. cerevisiae*. Xylose served as a substrate along with G1P in a favorable reverse reaction to form the byproduct GX dimer. GX was likely exported out of cells and imported back by the exogenous cellodextrin transporter before being cleaved by CBP. This exhausted resources that could have been reserved for cellobiose fermentation. Additionally, xylose was identified as a mixed-inhibitor of CBP activity, possibly due to the arrangement of the enzyme active sites in the CBP homodimer.

As xylose generally co-exists with cellobiose in the plant biomass, protein engineering of CBP was conducted to alter CBP specificity and reduce xylose inhibitory effects. In Chapter 2, using CRISPR-based chromosomal library selection, a distal mutation in CBP was identified. The single mutation, Y47H in *S. degradans* CBP, was necessary and sufficient to improve cellobiose consumption rate in the presence of xylose. *In vitro* characterization showed that the mutation decreased xylose inhibition by improving affinity and maximal rate kinetic parameters. The mutation also decreased GX synthesis in the reverse reaction. Similar *in vivo* and *in vitro* findings were observed when another CBP homolog was mutated to histidine at the conserved Y47 residue. *In silico* analysis identified the position of Y47H to be at the edge of a positively-charged elongated surface, surrounded by negatively-charged residues, that forms part of the interface between two CBP units. The mutation might enhance salt bridge formation, thereby stabilizing the enzyme complex, or impacting conformational changes that reduce xylose inhibition of CBP.

An alternative xylose utilization pathway involving xylulose-1-phosphate was developed in parallel (Chapter 3), in an attempt to increase xylose consumption rates, decrease intracellular xylose concentrations and thus relieve the negative impact it has on CBP. The established xylose utilization pathway relies on the PPP via X5P. However, efficient pentose utilization requires PPP optimization and may interfere with its role in NADPH and pentose production. The synthetic pathway that largely bypassed the PPP was designed and tested. Xylulose was converted in X1P, a novel metabolite to yeast, and directed to glycolysis in three linear steps. Despite the advantages the synthetic pathway seemed to have, its performance was inferior to that of the traditional pathway involving PPP. A metabolic intermediate leakage problem through unknown endogenous enzymes and/or gluconeogenesis leading to PPP was detected, likely because the synthetic pathway disrupted the cell regulatory network.

An example of a dramatic regulatory network disruption was shown in a minimal synthetic organism with only two exogenous genes for cellobiose consumption (Chapter 4). The less energy efficient breakdown of cellobiose by intracellular beta-glucosidase

36

(GH1-1) was used in place of CBP. Excess amounts of ATP was observed, in contrast to the previous hypothesis that cellobiose consumption using CDT-1 and GH1-1 may deplete cellular ATP. By decoupling glucose sensing from carbon utilization, we identified new modular layers of control that induce ATP consumption to drive rapid carbon fermentation, independent to the major plasma membrane ATPase activity. A novel role of two known glucose sensors, Snf3 and Rgt2, on cellular ATP regulation, via Gcn4 regulated amino acid biosynthesis was revealed from this systems-level study of cellobiose consumption system.

The motivation behind studying the use of CBP in place of GH1-1 was to decrease ATP consumption due to the use of CDT-1, a proton symporter. The excess ATP observed in cellobiose utilization suggested that the potential for CBP has not been fully unveiled, as the ATP that it saved likely could not be hydrolyzed and that systems-level mimicking of a non-starvation state could improve CBP even further. The findings revealed the power of coupling molecular and biochemical studies with systems-level analysis to unravel the intricate networks in living cells, which can be disrupted even in a minimal synthetic biological system.

References

1. Ha S-J, Galazka JM, Kim SR, et al (2011) Engineered Saccharomyces cerevisiae capable of simultaneous cellobiose and xylose fermentation. Proc Natl Acad Sci USA 108:504–509. doi: 10.1073/pnas.1010456108

2. Carlson M (1999) Glucose repression in yeast. Curr Opin Microbiol 2:202–207. doi: 10.1016/S1369-5274(99)80035-6

3. Galazka JM, Tian C, Beeson WT, et al (2010) Cellodextrin transport in yeast for improved biofuel production. Science 330:84–86. doi: 10.1126/science.1192838

4. Tantirungkij M, Nakashima N, Seki T, Yoshida T (1993) Construction of xylose-assimilating *Saccharomyces cerevisiae*. J Ferm Bioeng 83–88.

5. Kötter P, Ciriacy M (1993) Xylose fermentation by *Saccharomyces cerevisiae*. Appl Microbiol Biotechnol 776–783.

6. Kuyper M, Winkler AA, van Dijken JP, Pronk JT (2004) Minimal metabolic engineering of Saccharomyces cerevisiae for efficient anaerobic xylose fermentation: a proof of principle. FEMS Yeast Res 4:655–664. doi: 10.1016/j.femsyr.2004.01.003

7. Alexander JK (1961) Characteristics of cellobiose phosphorylase. J Bacteriol 81:903–910.

8. Ha S-J, Galazka JM, Joong Oh E, et al (2013) Energetic benefits and rapid cellobiose fermentation by Saccharomyces cerevisiae expressing cellobiose phosphorylase and mutant cellodextrin transporters. Metab Eng 15:134–143. doi: 10.1016/j.ymben.2012.11.005

9. Carroll A, Somerville C (2009) Cellulosic biofuels. Annu Rev Plant Biol 60:165–182. doi: 10.1146/annurev.arplant.043008.092125

10. Hinman ND, Wright JD, Hoagland W, Wyman CE (1989) Xylose fermentation-an economic analysis. Appl Biochem Biotechnol 20/21:391–401.

11. Galbe M, Zacchi G (2002) A review of the production of ethanol from softwood. Appl Microbiol Biotechnol 59:618–628. doi: 10.1007/s00253-002-1058-9

12. Li S, Du J, Sun J, et al (2010) Overcoming glucose repression in mixed sugar fermentation by co-expressing a cellobiose transporter and a β-glucosidase in Saccharomyces cerevisiae. J Ferm Bioeng 6:2129–2132. doi: 10.1039/C0MB00063A

13. Lou J, Dawson KA, Strobel HJ (1996) Role of phosphorolytic cleavage in

cellobiose and cellodextrin metabolism by the ruminal bacterium Prevotella ruminicola. Appl Environ Microbiol 62:1770–1773.

14. Goldberg RN (1975) Thermodynamics of hexokinase-catalyzed reactions. Biophys Chem 3:192–205.

15. Bro C, Knudsen S, Regenberg B, et al (2005) Improvement of galactose uptake in Saccharomyces cerevisiae through overexpression of phosphoglucomutase: example of transcript analysis as a tool in inverse metabolic engineering. Appl Environ Microbiol 71:6465–6472. doi: 10.1128/AEM.71.11.6465-6472.2005

16. de Kok S, Kozak BU, Pronk JT, van Maris AJA (2012) Energy coupling in Saccharomyces cerevisiae: selected opportunities for metabolic engineering. FEMS Yeast Res 12:387–397. doi: 10.1111/j.1567-1364.2012.00799.x

17. Aeling KA, Salmon KA, Laplaza JM, et al (2012) Co-fermentation of xylose and cellobiose by an engineered Saccharomyces cerevisiae. J Ind Microbiol Biotechnol 39:1597–1604. doi: 10.1007/s10295-012-1169-y

18. Rutter C, Chen R (2014) Improved cellobiose utilization in E. coli by including both hydrolysis and phosphorolysis mechanisms. Biotechnol Lett 36:301–307. doi: 10.1007/s10529-013-1355-7

19. Hamura K, Saburi W, Abe S, et al (2012) Enzymatic characteristics of cellobiose phosphorylase from Ruminococcus albus NE1 and kinetic mechanism of unusual substrate inhibition in reverse phosphorolysis. Biosci Biotechnol Biochem 76:812–818. doi: 10.1271/bbb.110954

20. Träff KL, Otero Cordero RR, van Zyl WH, Hahn-Hägerdal B (2001) Deletion of the GRE3 aldose reductase gene and its influence on xylose metabolism in recombinant strains of Saccharomyces cerevisiae expressing the xylA and XKS1 genes. Appl Environ Microbiol 67:5668–5674. doi: 10.1128/AEM.67.12.5668-5674.2001

21. Kim H, Lee W-H, Galazka JM, et al (2014) Analysis of cellodextrin transporters from Neurospora crassa in Saccharomyces cerevisiae for cellobiose fermentation. Appl Microbiol Biotechnol 98:1087–1094. doi: 10.1007/s00253-013-5339-2

22. Hamacher T, Becker J, Gárdonyi M, et al (2002) Characterization of the xylose-transporting properties of yeast hexose transporters and their influence on xylose utilization. Microbiology (Reading, Engl) 148:2783–2788. doi: 10.1099/00221287-148-9-2783

23. Ozcan S, Johnston M (1999) Function and regulation of yeast hexose transporters. Microbiol Mol Biol Rev 63:554–569.

24.   Teusink B, Diderich JA, Westerhoff HV, et al (1998) Intracellular glucose concentration in derepressed yeast cells consuming glucose is high enough to reduce the glucose transport rate by 50%. J Bacteriol 180:556–562.

25.   Alexander JK (1961) Characteristics of cellobiose phosphorylase. J Bacteriol 903–910.

26.   Kitaoka M, Taniguchi H, Sasaki T (1990) Production of glucosyl-xylose using Cellvibrio gilvus cells and its properties. Appl Microbiol Biotechnol 34:178–182. doi: 10.1007/BF00166776

27.   Bianchetti CM, Elsen NL, Fox BG, Phillips GN (2011) Structure of cellobiose phosphorylase from Clostridium thermocellum in complex with phosphate. Acta Crystallogr Sect F Struct Biol Cryst Commun 67:1345–1349. doi: 10.1107/S1744309111032660

28.   Van Hoorebeke A, Stout J, Kyndt J, et al (2010) Crystallization and X-ray diffraction studies of cellobiose phosphorylase from Cellulomonas uda. Acta Crystallogr Sect F Struct Biol Cryst Commun 66:346–351. doi: 10.1107/S1744309110002642

29.   Kim SR, Skerker JM, Kang W, et al (2013) Rational and evolutionary engineering approaches uncover a small set of genetic changes efficient for rapid xylose fermentation in Saccharomyces cerevisiae. PLoS ONE 8:e57048. doi: 10.1371/journal.pone.0057048

30.   Antikainen NM, Martin SF (2005) Altering protein specificity: techniques and applications. Bioorganic & Medicinal Chemistry 13:2701–2716. doi: 10.1016/j.bmc.2005.01.059

31.   DeSantis G, Liu J, Clark DP, et al (2003) Structure-based mutagenesis approaches toward expanding the substrate specificity of D-2-deoxyribose-5-phosphate aldolase. Bioorganic & Medicinal Chemistry 11:43–52.

32.   Cronin CN (1998) Redesign of choline acetyltransferase specificity by protein engineering. J Biol Chem 273:24465–24469.

33.   Wang J, Zhang S, Tan H, Zhao ZK (2007) PCR-based strategy for construction of multi-site-saturation mutagenic expression library. J Microbiol Methods 71:225–230. doi: 10.1016/j.mimet.2007.09.001

34.   Chica RA, Doucet N, Pelletier JN (2005) Semi-rational approaches to engineering enzyme activity: combining the benefits of directed evolution and rational design. Curr Opin Biotechnol 16:378–384. doi: 10.1016/j.copbio.2005.06.004

35.   Li X, Yu VY, Lin Y, et al (2015) Expanding xylose metabolism in yeast for plant

cell wall conversion to biofuels. Elife. doi: 10.7554/eLife.05896

36.   Chomvong K, Kordić V, Li X, et al (2014) Overcoming inefficient cellobiose fermentation by cellobiose phosphorylase in the presence of xylose. Biotechnology for Biofuels 7:85. doi: 10.1186/1754-6834-7-85

37.   Ryan OW, Skerker JM, Maurer MJ, et al (2014) Selection of chromosomal DNA libraries using a multiplex CRISPR system. Elife. doi: 10.7554/eLife.03703

38.   Hidaka M, Kitaoka M, Hayashi K, et al (2006) Structural dissection of the reaction mechanism of cellobiose phosphorylase. Biochem J 398:37–43. doi: 10.1042/BJ20060274

39.   Kitaoka M, Sasaki T, Taniguchi H (1992) Phosphorolytic Reaction of Cellvibrio gilvus Cellobiose Phosphorylase. Biosci Biotechnol Biochem 56:652–655. doi: 10.1271/bbb.56.652

40.   Lockless SW, Ranganathan R (1999) Evolutionarily conserved pathways of energetic connectivity in protein families. Science 286:295–299.

41.   Rod TH, Radkiewicz JL, Brooks CL (2003) Correlated motion and the effect of distal mutations in dihydrofolate reductase. Proceedings of the National Academy of Sciences 100:6980–6985. doi: 10.1073/pnas.1230801100

42.   Lin Y, Chomvong K, Acosta-Sampson L, et al (2014) Leveraging transcription factors to speed cellobiose fermentation by Saccharomyces cerevisiae. Biotechnology for Biofuels 7:126. doi: 10.1186/s13068-014-0126-6

43.   Kelley LA, Mezulis S, Yates CM, et al (2015) The Phyre2 web portal for protein modeling, prediction and analysis. Nat Protoc 10:845–858. doi: 10.1038/nprot.2015.053

44.   Finn RD, Clements J, Arndt W, et al (2015) HMMER web server: 2015 update. Nucleic Acids Res 43:W30–8. doi: 10.1093/nar/gkv397

45.   Edgar RC (2004) MUSCLE: multiple sequence alignment with high accuracy and high throughput. Nucleic Acids Res 32:1792–1797. doi: 10.1093/nar/gkh340

46.   Crooks GE, Hon G, Chandonia J-M, Brenner SE (2004) WebLogo: a sequence logo generator. Genome Res 14:1188–1190. doi: 10.1101/gr.849004

47.   DeLano WL (2002) PyMOL molecular graphics system.

48.   Ragauskas AJ, Williams CK, Davison BH, et al (2006) The path forward for biofuels and biomaterials. Science 311:484–489. doi: 10.1126/science.1114736

49.   Stephanopoulos G (2007) Challenges in engineering microbes for biofuels

production. Science 315:801–804. doi: 10.1126/science.1139612

50.   Fernandes S, Murray P (2010) Metabolic engineering for improved microbial pentose fermentation. Bioeng Bugs 1:424–428. doi: 10.4161/bbug.1.6.12724

51.   Hahn-Hägerdal B, Karhumaa K, Jeppsson M, Gorwa-Grauslund MF (2007) Metabolic engineering for pentose utilization in Saccharomyces cerevisiae. Adv Biochem Eng Biotechnol 108:147–177. doi: 10.1007/10_2007_062

52.   Matsushika A, Inoue H, Kodaki T, Sawayama S (2009) Ethanol production from xylose in engineered Saccharomyces cerevisiae strains: current state and perspectives. Appl Microbiol Biotechnol 84:37–53. doi: 10.1007/s00253-009-2101-x

53.   Johansson B, Hahn-Hägerdal B (2002) The non-oxidative pentose phosphate pathway controls the fermentation rate of xylulose but not of xylose in Saccharomyces cerevisiae TMB3001. FEMS Yeast Res 2:277–282.

54.   Jeppsson M, Johansson B, Hahn-Hägerdal B, Gorwa-Grauslund MF (2002) Reduced oxidative pentose phosphate pathway flux in recombinant xylose-utilizing Saccharomyces cerevisiae strains improves the ethanol yield from xylose. Appl Environ Microbiol 68:1604–1609. doi: 10.1128/AEM.68.4.1604-1609.2002

55.   Wamelink MMC, Struys EA, Jakobs C (2008) The biochemistry, metabolism and inherited defects of the pentose phosphate pathway: a review. J Inherit Metab Dis 31:703–717. doi: 10.1007/s10545-008-1015-6

56.   Ralser M, Wamelink MM, Kowald A, et al (2007) Dynamic rerouting of the carbohydrate flux is key to counteracting oxidative stress. J Biol 6:10. doi: 10.1186/jbiol61

57.   Sonderegger M, Schümperli M, Sauer U (2004) Metabolic engineering of a phosphoketolase pathway for pentose catabolism in Saccharomyces cerevisiae. Appl Environ Microbiol 70:2892–2897. doi: 10.1128/AEM.70.5.2892-2897.2004

58.   Bais R, James HM, Rofe AM, Conyers RA (1985) The purification and properties of human liver ketohexokinase. A role for ketohexokinase and fructose-bisphosphate aldolase in the metabolic production of oxalate from xylitol. Biochem J 230:53–60.

59.   Donaldson IA, Doyle TC, Matas N (1993) Expression of rat liver ketohexokinase in yeast results in fructose intolerance. Biochem J 291 (Pt 1):179–186.

60.   Jayakody LN, Hayashi N, Kitagaki H (2011) Identification of glycolaldehyde as the key inhibitor of bioethanol fermentation by yeast and genome-wide analysis of its toxicity. Biotechnol Lett 33:285–292. doi: 10.1007/s10529-010-0437-z

61.   Jayakody LN, Horie K, Hayashi N, Kitagaki H (2012) Improvement of tolerance of Saccharomyces cerevisiae to hot-compressed water-treated cellulose by expression of ADH1. Appl Microbiol Biotechnol 94:273–283. doi: 10.1007/s00253-012-3918-2

62.   Jayakody LN, Horie K, Hayashi N, Kitagaki H (2013) Engineering redox cofactor utilization for detoxification of glycolaldehyde, a key inhibitor of bioethanol production, in yeast Saccharomyces cerevisiae. Appl Microbiol Biotechnol 97:6589–6600. doi: 10.1007/s00253-013-4997-4

63.   Cam Y, Alkim C, Trichez D, et al (2015) Engineering of a Synthetic Metabolic Pathway for the Assimilation of (d)-Xylose into Value-Added Chemicals. ACS Synth Biol. doi: 10.1021/acssynbio.5b00103

64.   Alkim C, Cam Y, Trichez D, et al (2015) Optimization of ethylene glycol production from (D)-xylose via a synthetic pathway implemented in Escherichia coli. Microb Cell Fact 14:127. doi: 10.1186/s12934-015-0312-7

65.   Geertman J-MA, van Dijken JP, Pronk JT (2006) Engineering NADH metabolism in Saccharomyces cerevisiae: formate as an electron donor for glycerol production by anaerobic, glucose-limited chemostat cultures. FEMS Yeast Res 6:1193–1203. doi: 10.1111/j.1567-1364.2006.00124.x

66.   Walther T, Baylac A, Alkim C, et al (2012) The PGM3 gene encodes the major phosphoribomutase in the yeast Saccharomyces cerevisiae. FEBS Lett 586:4114–4118. doi: 10.1016/j.febslet.2012.09.042

67.   Mishra P, Singh A (1993) Microbial pentose utilization. Adv Appl Microbiol 39:91–152.

68.   McMillan JD (1993) Xylose fermentation to ethanol: a review. National Renewable Energy Laboratory

69.   Kim S-J, Seo S-O, Jin Y-S, Seo J-H (2013) Production of 2,3-butanediol by engineered Saccharomyces cerevisiae. Bioresour Technol 146:274–281. doi: 10.1016/j.biortech.2013.07.081

70.   Yue H, Zhao Y, Ma X, Gong J (2012) Ethylene glycol: properties, synthesis, and applications. Chemical Society Reviews 41:4218. doi: 10.1039/c2cs15359a

71.   Liu H, Ramos KRM, Valdehuesa KNG, et al (2013) Biosynthesis of ethylene glycol in Escherichia coli. Appl Microbiol Biotechnol 97:3409–3417. doi: 10.1007/s00253-012-4618-7

72.   Pereira B, Zhang H, De Mey M, et al (2016) Engineering a novel biosynthetic pathway in Escherichia coli for production of renewable ethylene glycol. Biotechnol Bioeng 113:376–383. doi: 10.1002/bit.25717

73.   Pereira B, Li Z-J, De Mey M, et al (2016) Efficient utilization of pentoses for bioproduction of the renewable two-carbon compounds ethylene glycol and glycolate. Metab Eng 34:80–87. doi: 10.1016/j.ymben.2015.12.004

74.   Flamholz A, Noor E, Bar-Even A, Milo R (2012) eQuilibrator--the biochemical thermodynamics calculator. Nucleic Acids Res 40:D770–5. doi: 10.1093/nar/gkr874

75.   van Heerden JH, Wortel MT, Bruggeman FJ, et al (2014) Lost in Transition: Start-Up of Glycolysis Yields Subpopulations of Nongrowing Cells. Science 343:1245114–1245114. doi: 10.1126/science.1245114

76.   Gietz RD, Woods RA (2002) Transformation of yeast by lithium acetate/single-stranded carrier DNA/polyethylene glycol method. Meth Enzymol 350:87–96.

77.   Hanscho M, Ruckerbauer DE, Chauhan N, et al (2012) Nutritional requirements of the BY series of Saccharomyces cerevisiae strains for optimum growth. FEMS Yeast Res 12:796–808. doi: 10.1111/j.1567-1364.2012.00830.x

78.   Luo B, Groenke K, Takors R, et al (2007) Simultaneous determination of multiple intracellular metabolites in glycolysis, pentose phosphate pathway and tricarboxylic acid cycle by liquid chromatography-mass spectrometry. J Chromatogr A 1147:153–164. doi: 10.1016/j.chroma.2007.02.034

79.   Youk H, van Oudenaarden A (2009) Growth landscape formed by perception and import of glucose in yeast. Nature 462:875–879. doi: 10.1038/nature08653

80.   Daran-Lapujade P, Rossell S, van Gulik WM, et al (2007) The fluxes through glycolytic enzymes in Saccharomyces cerevisiae are predominantly regulated at posttranscriptional levels. Proceedings of the National Academy of Sciences 104:15753–15758. doi: 10.1073/pnas.0707476104

81.   Bañuelos M, Gancedo C, Gancedo JM (1977) Activation by phosphate of yeast phosphofructokinase. J Biol Chem 252:6394–6398.

82.   Avigad G (1981) Stimulation of yeast phosphofructokinase activity by fructose 2,6-bisphosphate. Biochem Biophys Res Commun 102:985–991.

83.   Nissler K, Otto A, Schellenberger W, Hofmann E (1983) Similarity of activation of yeast phosphofructokinase by AMP and fructose-2,6-bisphosphate. Biochem Biophys Res Commun 111:294–300.

84.   Rodicio R, Strauss A, Heinisch JJ (2000) Single point mutations in either gene encoding the subunits of the heterooctameric yeast phosphofructokinase abolish allosteric inhibition by ATP. J Biol Chem 275:40952–40960.

85.   Gradmann D, Hansen UP, Long WS, et al (1978) Current-voltage relationships

for the plasma membrane and its principal electrogenic pump in Neurospora crassa: I. Steady-state conditions. J Membr Biol 39:333–367.

86.   Serrano R (1983) In vivo glucose activation of the yeast plasma membrane ATPase. FEBS Lett 156:11–14.

87.   Mason AB, Allen KE, Slayman CW (2014) C-terminal truncations of the Saccharomyces cerevisiae PMA1 H+-ATPase have major impacts on protein conformation, trafficking, quality control, and function. Eukaryotic Cell 13:43–52. doi: 10.1128/EC.00201-13

88.   Rao R, Drummond-Barbosa D, Slayman CW (1993) Transcriptional regulation by glucose of the yeast PMA1 gene encoding the plasma membrane H(+)-ATPase. Yeast 9:1075–1084. doi: 10.1002/yea.320091006

89.   García-Arranz M, Maldonado AM, Mazón MJ, Portillo F (1994) Transcriptional control of yeast plasma membrane H(+)-ATPase by glucose. Cloning and characterization of a new gene involved in this regulation. J Biol Chem 269:18076–18082.

90.   Kang WK, Kim YH, Kang HA, et al (2015) Sir2 phosphorylation through cAMP-PKA and CK2 signaling inhibits the lifespan extension activity of Sir2 in yeast. Elife. doi: 10.7554/eLife.09709

91.   Eraso P, Mazón MJ, Portillo F (2006) Yeast protein kinase Ptk2 localizes at the plasma membrane and phosphorylates in vitro the C-terminal peptide of the H+-ATPase. Biochimica et Biophysica Acta (BBA) - Biomembranes 1758:164–170. doi: 10.1016/j.bbamem.2006.01.010

92.   Portillo F, Eraso P, Serrano R (1991) Analysis of the regulatory domain of yeast plasma membrane H+-ATPase by directed mutagenesis and intragenic suppression. FEBS Lett 287:71–74.

93.   Lecchi S, Nelson CJ, Allen KE, et al (2007) Tandem phosphorylation of Ser-911 and Thr-912 at the C terminus of yeast plasma membrane H+-ATPase leads to glucose-dependent activation. J Biol Chem 282:35471–35481. doi: 10.1074/jbc.M706094200

94.   Rolland F, Winderickx J, Thevelein JM (2002) Glucose-sensing and -signalling mechanisms in yeast. FEMS Yeast Res 2:183–201.

95.   Ozcan S, Dover J, Rosenwald AG, et al (1996) Two glucose transporters in Saccharomyces cerevisiae are glucose. Proceedings of the National Academy of Sciences 93:12428–12432.

96.   Xue Y, Batlle M, Hirsch JP (1998) GPR1 encodes a putative G protein-coupled receptor that associates with the Gpa2p Galpha subunit and functions in a Ras-

independent pathway. EMBO J 17:1996–2007. doi: 10.1093/emboj/17.7.1996

97.   Moxley JF, Jewett MC, Antoniewicz MR, et al (2009) Linking high-resolution metabolic flux phenotypes and transcriptional regulation in yeast modulated by the global regulator Gcn4p. Proc Natl Acad Sci USA 106:6477–6482. doi: 10.1073/pnas.0811091106

98.   Natarajan K, Meyer MR, Jackson BM, et al (2001) Transcriptional profiling shows that Gcn4p is a master regulator of gene expression during amino acid starvation in yeast. Mol Cell Biol 21:4347–4368. doi: 10.1128/MCB.21.13.4347-4368.2001

99.   Pontes MH, Sevostyanova A, Groisman EA (2015) When Too Much ATP Is Bad for Protein Synthesis. J Mol Biol 427:2586–2594. doi: 10.1016/j.jmb.2015.06.021

100.   Browne SE (2013) When too much ATP is a bad thing: a pivotal role for P2X7 receptors in motor neuron degeneration. J Neurochem 126:301–304. doi: 10.1111/jnc.12321

101.   Larsson C, Nilsson A, Blomberg A, Gustafsson L (1997) Glycolytic Flux Is Conditionally Correlated with ATP Concentration in. J Bacteriol 179:7243–7250.

102.   Thomsson E, Larsson C, Albers E, et al (2003) Carbon starvation can induce energy deprivation and loss of fermentative capacity in Saccharomyces cerevisiae. Appl Environ Microbiol 69:3251–3257. doi: 10.1128/AEM.69.6.3251-3257.2003

103.   Choi K-M, Kwon Y-Y, Lee C-K (2015) Disruption of Snf3/Rgt2 glucose sensors decreases lifespan and caloric restriction effectiveness through Mth1/Std1 by adjusting mitochondrial efficiency in yeast. FEBS Lett 589:349–357. doi: 10.1016/j.febslet.2014.12.020

104.   Moriya H, Johnston M (2004) Glucose sensing and signaling in Saccharomyces cerevisiae through the Rgt2 glucose sensor and casein kinase I. Proceedings of the National Academy of Sciences 101:1572–1577. doi: 10.1073/pnas.0305901101

105.   Flick KM, Spielewoy N, Kalashnikova TI, et al (2003) Grr1-dependent inactivation of Mth1 mediates glucose-induced dissociation of Rgt1 from HXT gene promoters. Molecular Biology of the Cell 14:3230–3241. doi: 10.1091/mbc.E03-03-0135

106.   Lakshmanan J, Mosley AL, Ozcan S (2003) Repression of transcription by Rgt1 in the absence of glucose requires Std1 and Mth1. Curr Genet 44:19–25. doi: 10.1007/s00294-003-0423-2

107.   Jouandot D, Roy A, Kim J-H (2011) Functional dissection of the glucose

signaling pathways that regulate the yeast glucose transporter gene (HXT) repressor Rgt1. J Cell Biochem 112:3268–3275. doi: 10.1002/jcb.23253

108. Yang R, Wek SA, Wek RC (2000) Glucose limitation induces GCN4 translation by activation of Gcn2 protein kinase. Mol Cell Biol 20:2706–2717.

109. Hinnebusch AG (1997) Translational regulation of yeast GCN4. A window on factors that control initiator-trna binding to the ribosome. J Biol Chem 272:21661–21664.

110. Shirra MK, McCartney RR, Zhang C, et al (2008) A chemical genomics study identifies Snf1 as a repressor of GCN4 translation. J Biol Chem 283:35889–35898. doi: 10.1074/jbc.M805325200

111. Herrmannová A, Daujotyte D, Yang J-C, et al (2012) Structural analysis of an eIF3 subcomplex reveals conserved interactions required for a stable and proper translation pre-initiation complex assembly. Nucleic Acids Res 40:2294–2311. doi: 10.1093/nar/gkr765

112. Kaiser CA, Chen EJ, Losko S (2002) Subcellular fractionation of secretory organelles. Meth Enzymol 351:325–338.

113. Viegas CA, Sá-Correia I (1991) Activation of plasma membrane ATPase of Saccharomyces cerevisiae by octanoic acid. J Gen Microbiol 137:645–651. doi: 10.1099/00221287-137-3-645

114. Hosaka K, Nikawa J, Kodaki T, Yamashita S (1992) A dominant mutation that alters the regulation of INO1 expression in Saccharomyces cerevisiae. J Biochem 111:352–358.

Figures
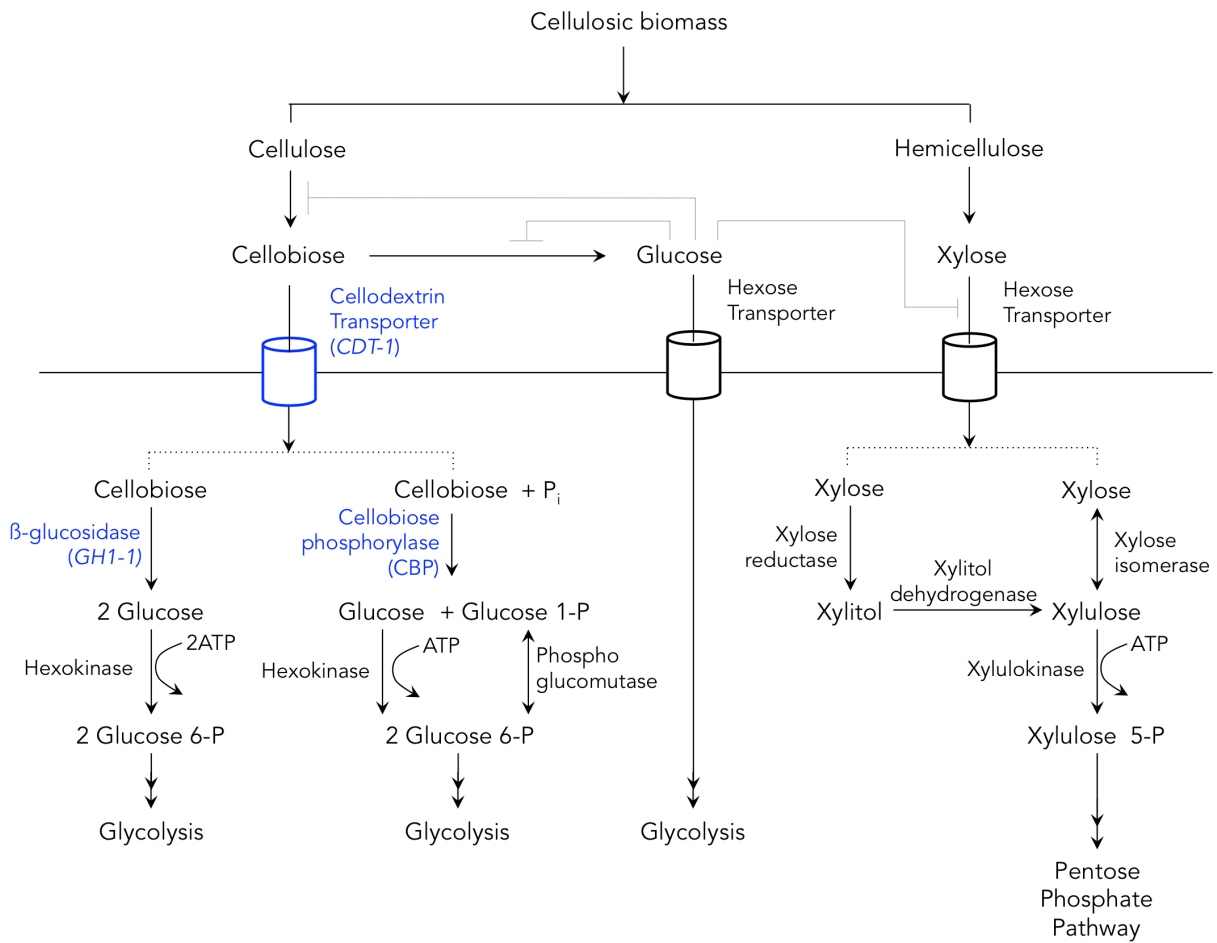
Fig. i-1. Simultaneous co-utilization of cellobiose and xylose. Cellobiose and xylose derived from cellulosic biomass can be co-utilized, bypassing glucose repression effect which causes sequential sugar utilization, increasing the overall processing time.
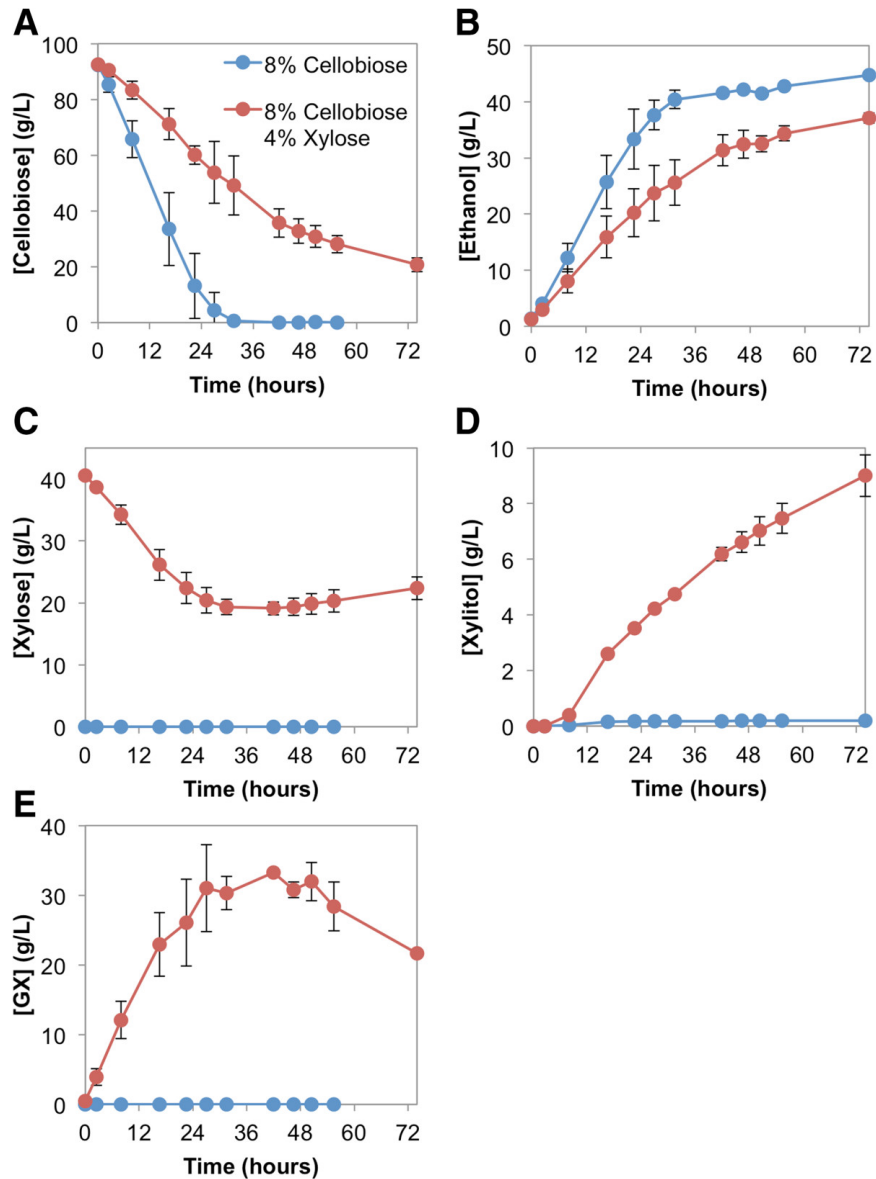
Fig. 1-1. Fermentation profile of engineered strain D452-2 in the presence and absence of xylose. *S. cerevisiae* strain D452-2 was transformed with the pCS plasmid, encoding cellodextrin transporter cdt1-F213L and SdCBP. Anaerobic fermentations were supplied with 80 g/L cellobiose in the presence (red dots) and absence (blue dots) of 40 g/L xylose. Extracellular concentrations of (A) cellobiose, (B) ethanol, (C) xylose, (D) xylitol and (E) glucopyranosyl-xylose are shown. Values and error bars represent the means and standard deviations of two independent biological replicates.
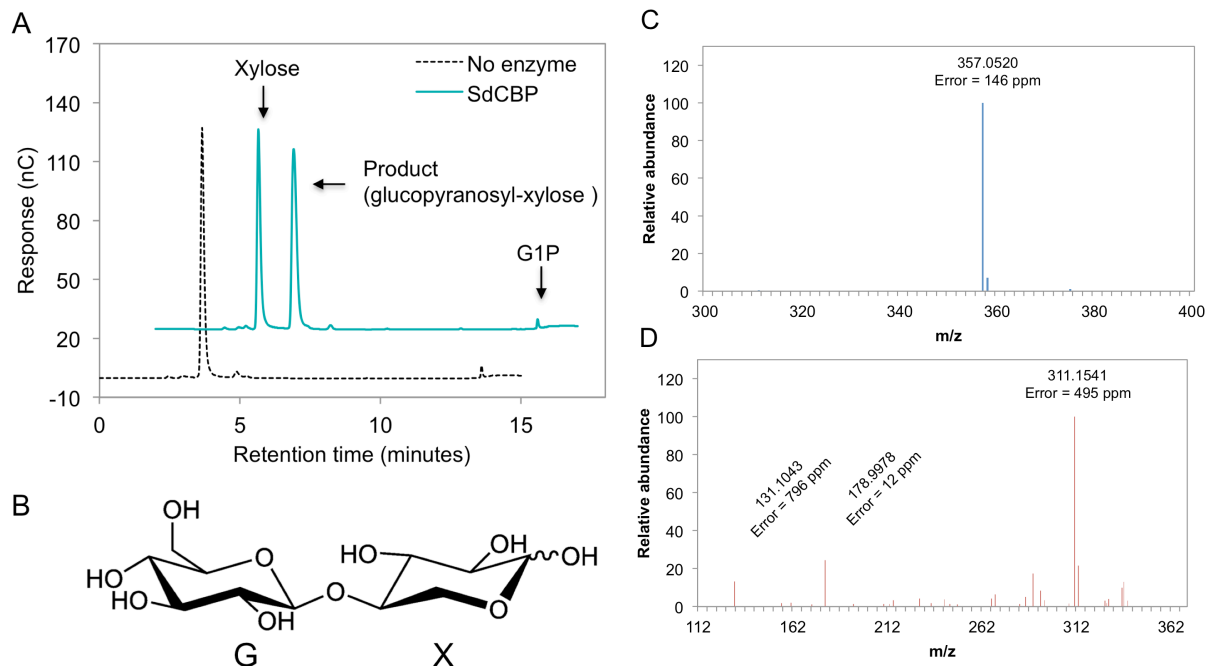
Fig. 1-2. *In vitro* **synthesis of glucopyranosyl-xylose catalyzed by purified SdCBP.**
(A) Reactions containing 10 mM xylose and 10 mM G1P, along with 20 nM purified
SdCBP in 20 mM MES, pH 6.0 solution were incubated at 37 °C for 12 hours. The
purified SdCBP was omitted from the negative control. A product signal (eluted at 4.9
minutes), along with decreases in xylose and G1P signals, were observed only when
SdCBP was provided in the reaction. Chromatograms are displayed with 2 minute-offset
between samples. (B) Structure of the glucopyranosyl-xylose dimer. Molecular mass of
the synthesized dimer was quantified using mass spectrometry (MS). The GX dimer is
expected to have a molecular mass of (312 g/mol). (C) Using a negative ionization
mode, a 357 m/z was detected. This is consistent with GX plus a formate adduct (312 +
46 – 1). (D) The 357 m/z species was further analyzed by tandem mass spectrometry
(MS-MS). The 311, 179 and 131 m/z signals correspond to m/z ratios expected for GX,
hexose and pentose sugars in the negative ionization mode, respectively.
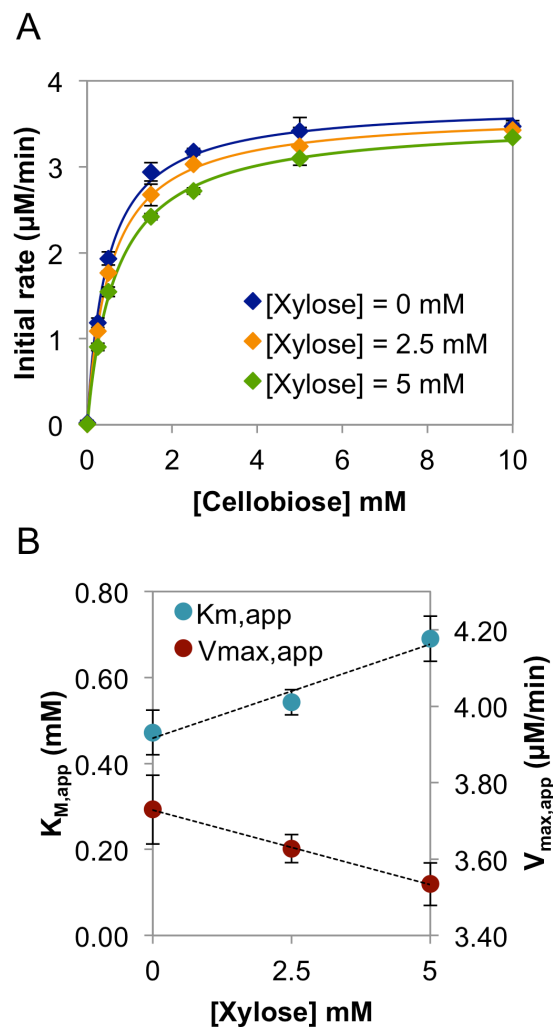
Fig.1-3. Xylose competition assay of SdCBP activity. The catalytic properties of *S. degradans* cellobiose phosphorylase were determined in the presence of 0, 2.5 and 5 mM of xylose. (A) Initial rates of cellobiose phosphorolysis were calculated from the amount of continuous G1P production at different cellobiose concentrations. All reactions were carried out in duplicate. (B) Apparent kinetic parameters of SdCBP supplemented with 0, 2.5 and 5 mM of xylose determined by non-linear curve fitting.
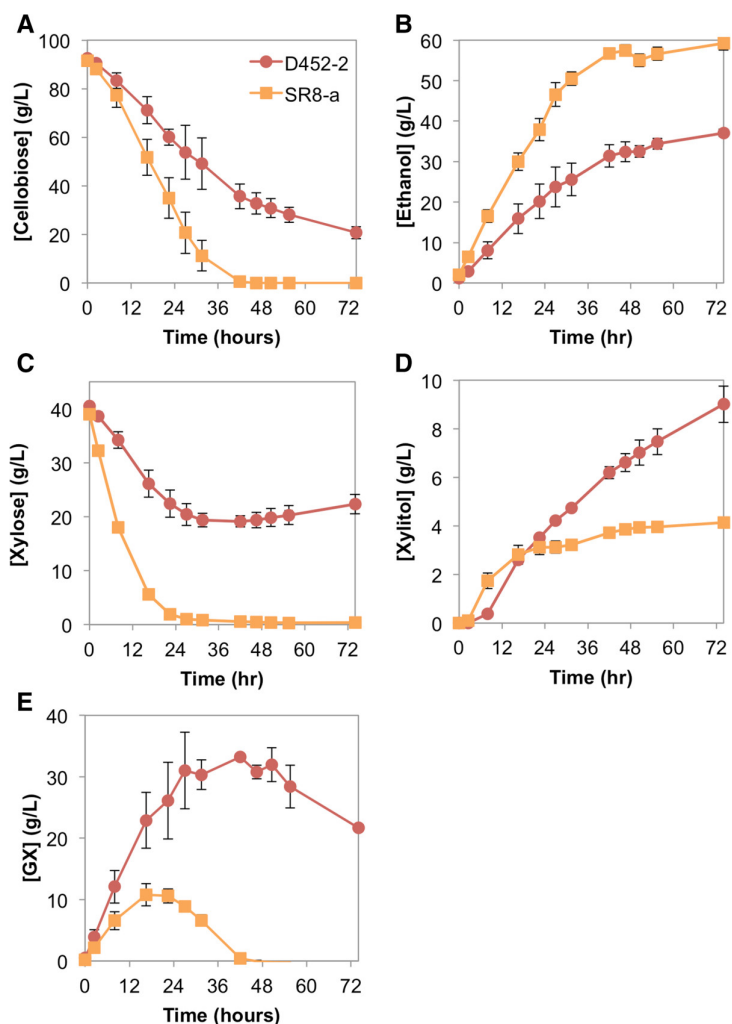
Fig.1-4. Fermentation profile of engineered D452-2 and SR8-a strains supplemented with cellobiose and xylose. *S. cerevisiae* D452-2 (red circle) and SR8-a (orange square) strains were transformed with the pCS plasmid. Anaerobic fermentations were supplied with 80 g/L cellobiose and 40 g/L xylose. Extracellular concentrations of (A) cellobiose, (B) ethanol, (C) xylose, (D) xylitol and (E) glucopyranosyl-xylose are shown. Values and error bars represent the means and standard deviations of two independent biological replicates.
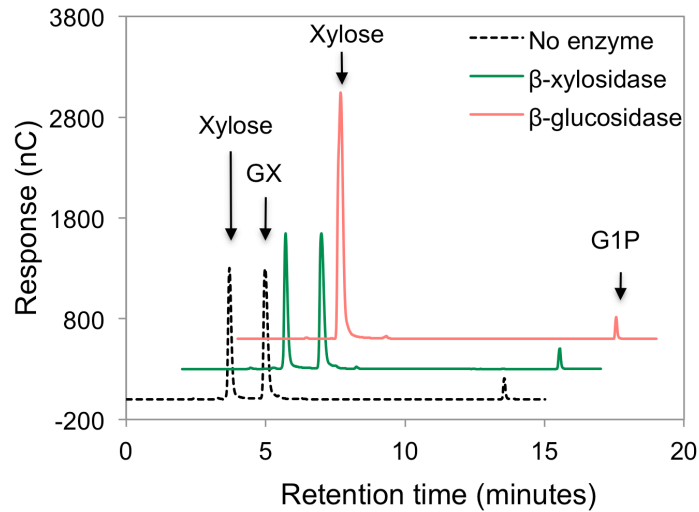
Fig.1-5. β-xylosidase (NCU01900) and β-glucosidase (NCU00130) activities on glucopyranosyl-xylose (GX). GX synthesized *in vitro* used as a substrate contained some traces xylose and G1P. Purified β-xylosidase and β-glucosidase were incubated with GX substrate mixture in 1X PBS, pH 7.4 buffer. The purified proteins were omitted in the control reaction. Chromatograms are displayed with 2 minute-offsets between samples.
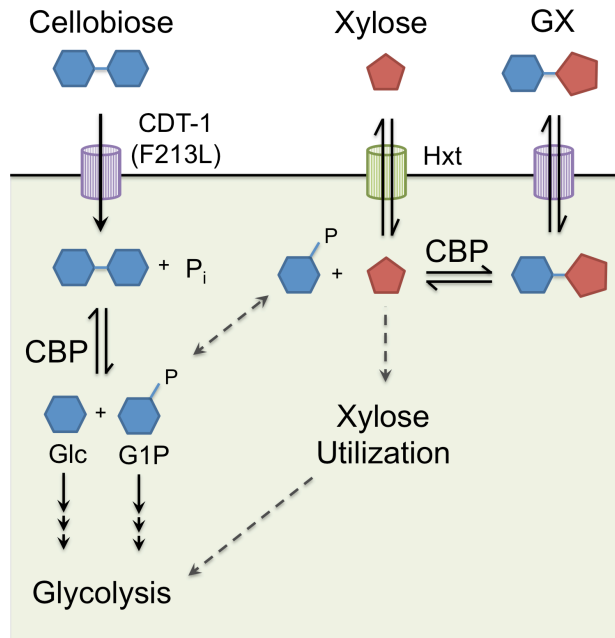
Fig.1-6. Model of CBP-mediated cellobiose consumption in the presence of xylose. Cellobiose and xylose are simultaneously imported via the cellodextrin transporter CDT-1 (F213L) and endogenous hexose transporters, respectively. Cellobiose undergoes phosphorolytic cleavage via CBP, generating glucose (denoted Glc) and G1P, both of which enter glycolysis. However, some of the G1P and imported xylose are condensed by CBP to produce GX in its thermodynamically-favorable reverse reaction. GX is then transported out of the cell and imported back into the cell by the cellodextrin transporter over the time course of fermentations. The intracellular GX is then cleaved to G1P and xylose by CBP when the intracellular cellobiose concentration drops in later times of the fermentation. Free xylose is then released back into the fermentation broth in the absence of the xylose consumption pathway.
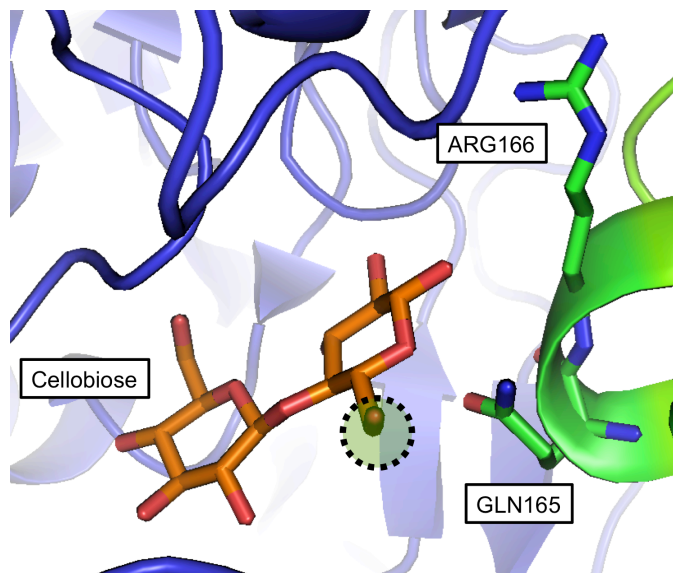
Fig. 1-7. Active site of *Cellulomonas uda* CBP in complex with cellobiose. The crystal structure of *C. uda* CBP is shown in complex with cellobiose [PDB:3S4A] (unpublished observations by Van Hoorebeke A *et al.*) . CBP is an asymmetric homodimer whose active sites are comprised of an (α/α)$_6$-barrel domain of one subunit (blue) and the helical extension from the N-terminal domain of the adjacent subunit (green). Cellobiose is bound in the active site with its reducing end pointing toward the N-terminal extension from the adjacent subunit (green). Arg166 and Gln165 on the adjacent subunit (green) might be in contact with cellobiose bound at the active site of the blue subunit. The 6-methoxy group that is present in cellobiose but absent in the GX molecule is circled. Xylose is expected to bind at the reducing end site, resulting in a possible interaction with the N-terminal extension of the adjacent subunit.
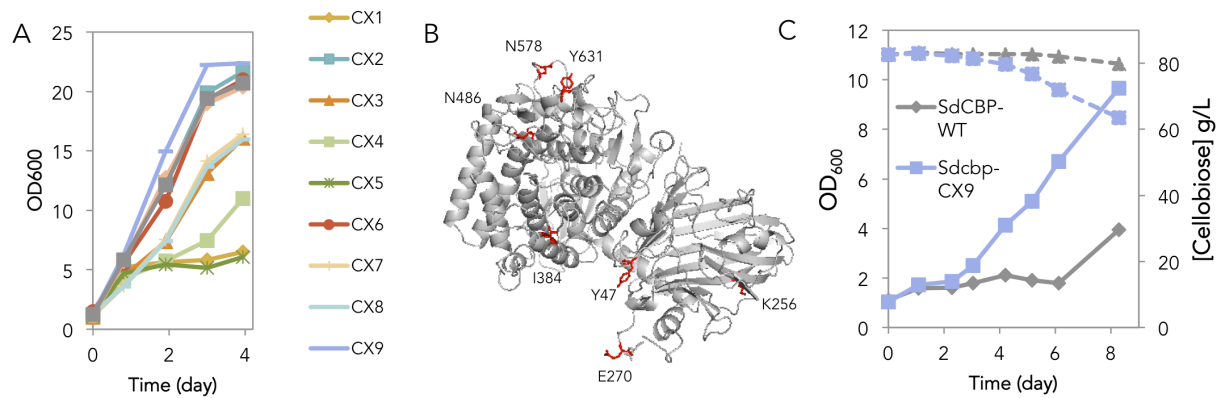
Fig. 2-1 SdCBP$_{CX9}$ and its aerobic growth and cellobiose consumption of original background strain expressing SdCBP$_{CX9}$. (A) Aerobic growth profile of strains from the 2% xylose 1% cellobiose selection. 10 larger-than-average colonies were picked from 2% xylose/ 1% cellobiose plates and subjected to aerobic growth in minimal media with 2% xylose and 1% cellobiose. Representative growth profiles are shown. (B) 7 mutations in SdCBP$_{CX9}$ allele are labeled in red on a SdCBP structure predicted by Phyre2 [43]. (C) OD600 and cellobiose consumption profile of strains expressing SdCBP-WT and SdCBP$_{CX9}$ re-introduced into a clean strain background, in 2% cellobiose plus 1% xylose. Shown is a representative experiment.

56

A

	Region 1	Region 2	Region 3	Rate g/(L·hour)
(---)	WT	WT	WT	0.17
(--m)	WT	WT	m	0.16
(-m-)	WT	m	WT	0.16
(-mm)	WT	m	m	0.18
(m--)	m	WT	WT	0.23
(m-m)	m	WT	m	0.20
(mm-)	m	m	WT	0.22
(mmm)	m	m	m	0.22
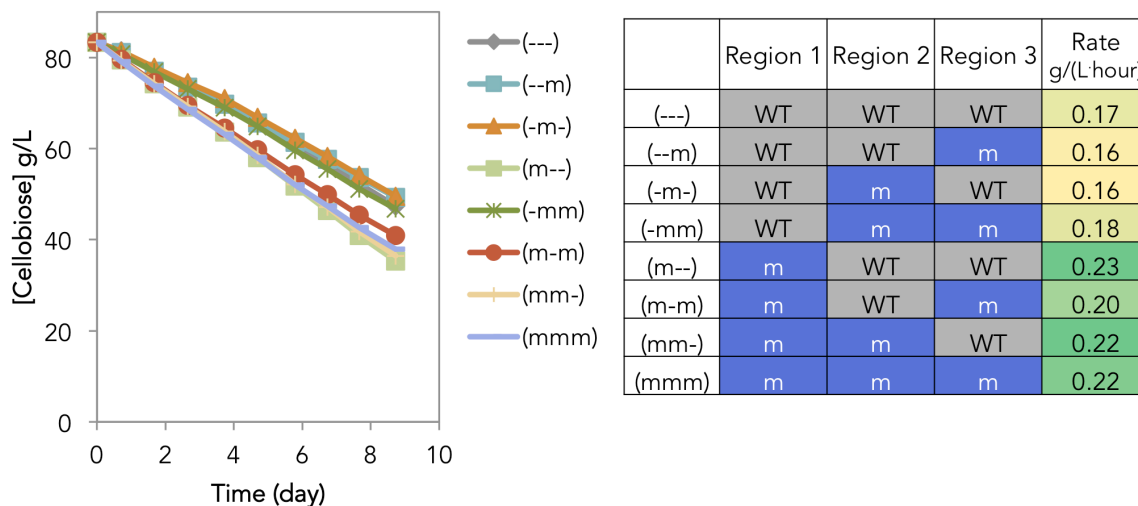
B
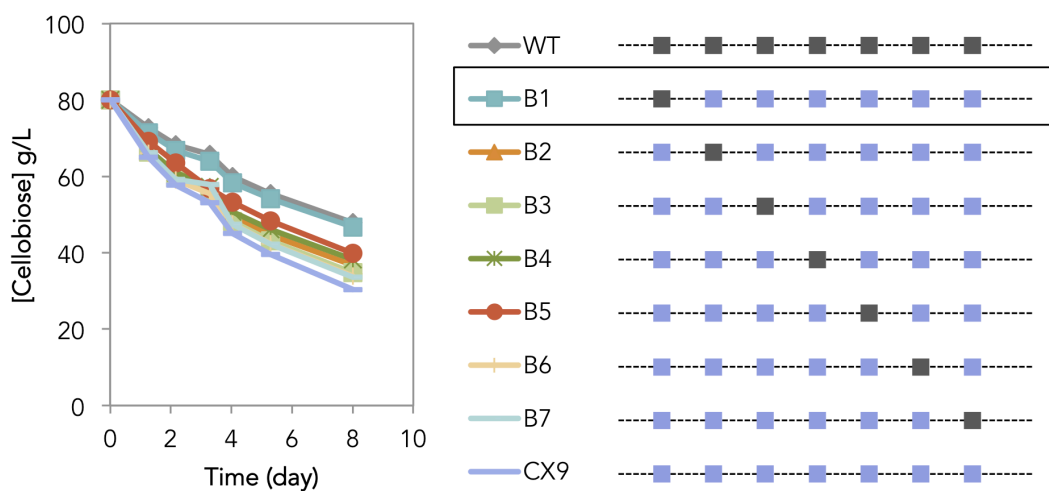
Fig. 2-2 Identification of the Y47H mutation in the SdCBP$_{CX9}$ allele. (A) Combinatorial chimera approach of SdCBP wildtype and SdCBP$_{CX9}$. Cellobiose consumption profiles and consumption rates (g/(L·hour)) are shown. (B) Cellobiose consumption profile of SdCBP$_{CX9}$ with each position reverted to that of wild-type SdCBP.
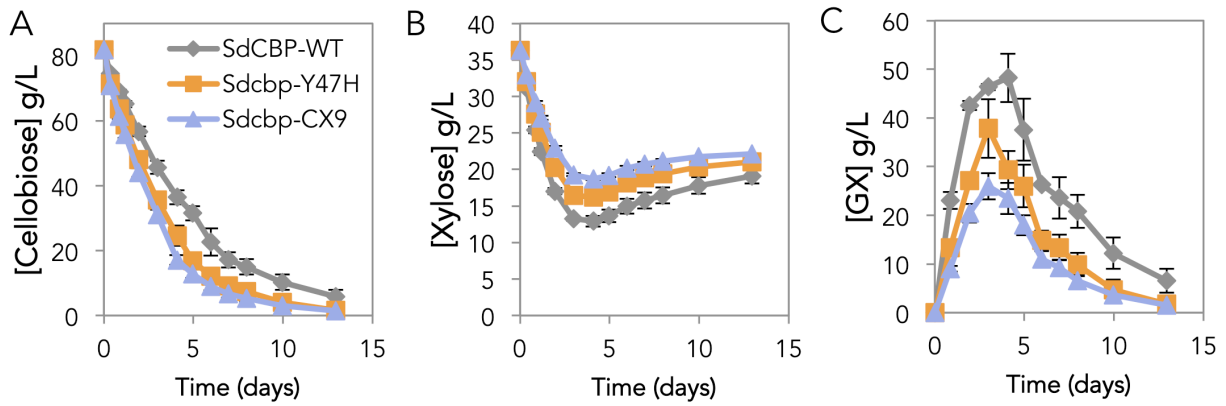
Fig. 2-3. In vivo analysis of _S. degradans_ CBP mutants. Extracellular concentrations of (A) cellobiose (B) xylose and (C) GX, using D452-2 strains expressing WT SdCBP or SdCBP mutants in anaerobic condition. Experiments were carried out in biological triplicate, and include standard deviations from the mean.
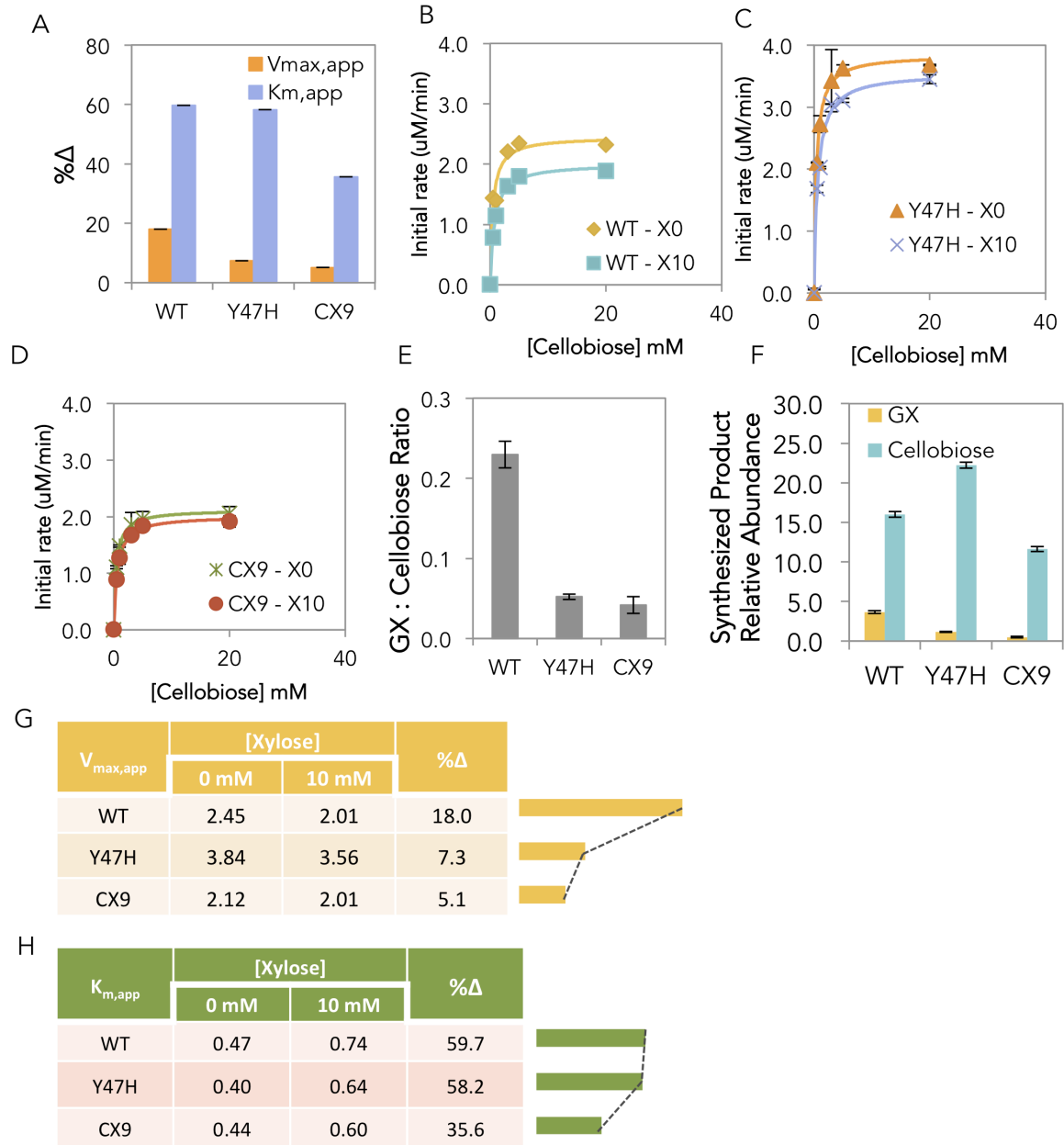
Fig. 2-4. *In vitro* **enzymology of *S. degradans* CBP mutants.** (A) Percentage difference in kinetic parameters, in the presence or absence of 10 mM xylose, of purified WT SdCBP and SdCBP mutants. Xylose competition assay of SdCBP phosphorylase activity of (B) wild-type SdCBP (C) SdCBP-Y47H and (D) SdCBP$_{CX9}$. (E) Ratio of GX to cellobiose produced in the end-point reverse reaction assays using purified WT SdCBP or SdCBP mutants. (F) End-point GX and cellobiose synthesis assay of WT SdCBP and SdCBP mutants. (G) $V_{max,app}$ and (H) $K_{m,app}$ values in the presence and absence of xylose of the two Sd*cbp* mutants in comparison to SdCBP WT. All experiments in A and B were carried out in triplicate, and are shown with standard deviations from the mean.
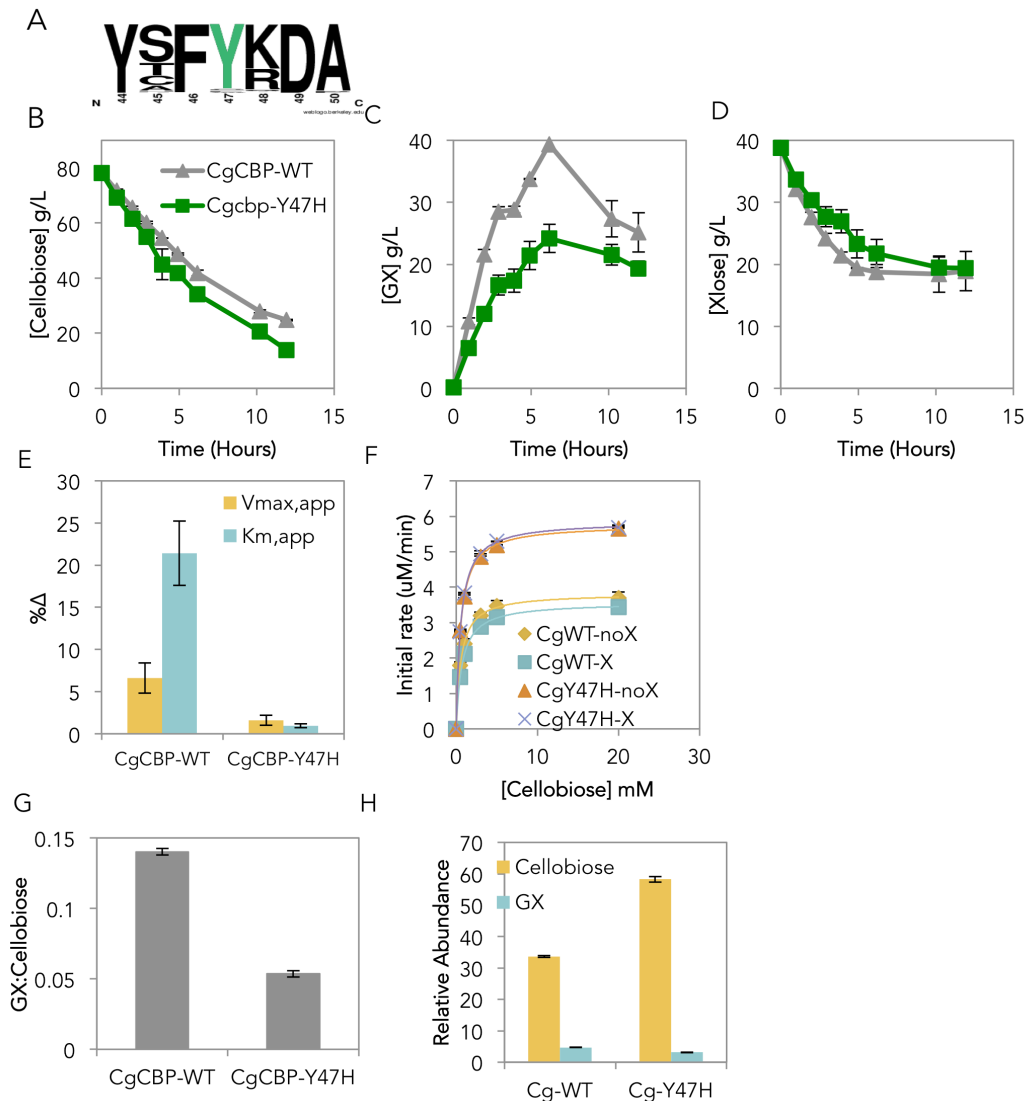
Fig. 2-5. Conservation of Y47H mutant phenotype in *C. gilvus* CBP. (A) Amino acid conservation among CBP homologs, near the protein N-terminus surrounding position 47. (B) Anaerobic cellobiose consumption, (C) GX production and (D) xylose concentrations of strains expressing WT CgCBP or the Cgcbp Y47H mutant. The starting OD600 was 20 (E) Percentage difference in kinetic parameters, in the presence or absence of 10 mM xylose, of purified WT CgCBP or the Cgcbp Y47H mutant. (F) xylose competition assay of CgCBP phosphorylase activity with and without 10 mM xylose (G) Ratio of GX to cellobiose produced in the end-point reverse reaction assays, using purified WT CgCBP or the Cgcbp Y47H mutant. (H) End-point GX and cellobiose synthesis assay of WT CgCBP and CgCBP Y47H. Experiments were carried out in triplicate, with standard deviations from the mean shown.
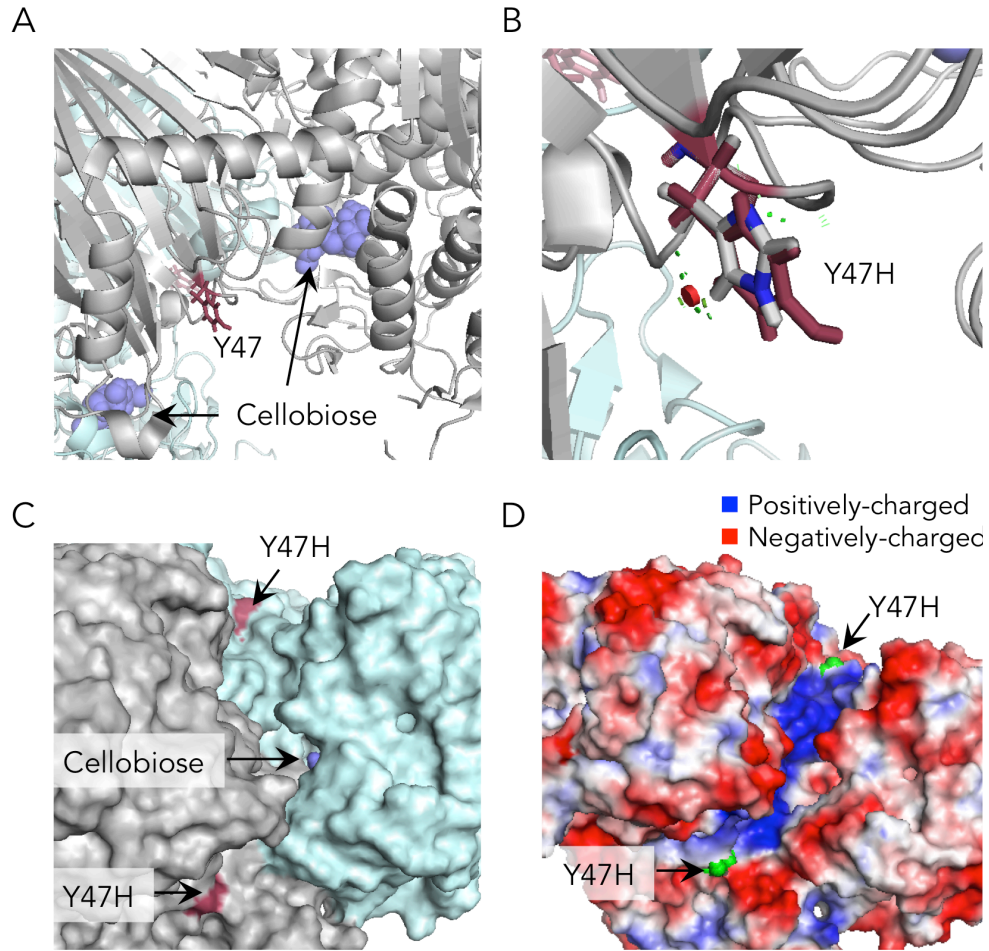
Fig. 2-6. In silico analysis of Y47H mutation in CBP structure. (A) Overview of *Cellulomonas uda* CBP structure in complex with cellobiose (denoted in blue). Tyrosine 47 is shown in red. (B) Computational replacement of Y47H. (C) Surface view of the CBP structure with the Y47H mutation denoted in red. (D) Electrostatic map representation of the CBP structure. Blue represents positive electrostatic potential, whereas red represents negative potential. Green indicates the positions of Y47 at the dimer interface.
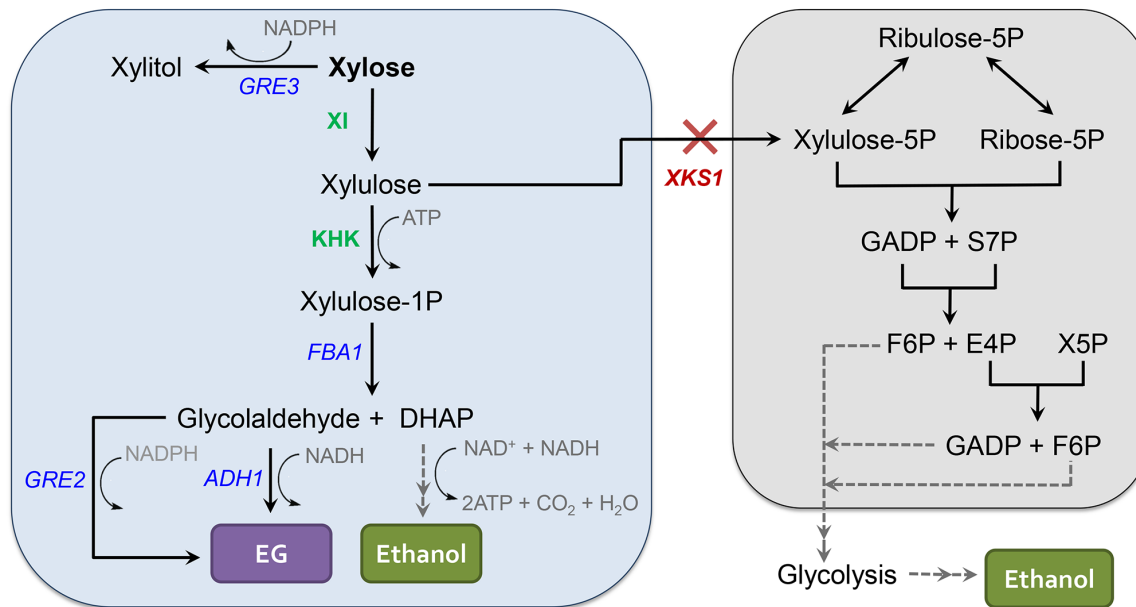
Fig 3-1. An alternative pentose sugar utilization in *S. cerevisiae*.
The system consists of two exogenous components, XI and KHK, which convert D-xylose to D-xylulose and X1P, respectively. X1P is then metabolized by *S. cerevisiae* endogenous enzymes—*FBA1*, *GRE2* and/or *ADH1*—producing glycolaldehyde and DHAP as intermediates and EG and ethanol as final products. *XKS1* deletion allows the metabolic flux to be directed to the synthetic pathway via X1P by eliminating a possible route of xylulose utilization via X5P through the PPP. Abbreviations in the figure are: PPP, pentose phosphate pathway; XI, xylose isomerase; KHK, ketohexokinase; *FBA1*, fructose 1,6-bisphosphate aldolase; *GRE2*, 3-methylbutanal reductase; *ADH1*, alcohol dehydrogenase; *XKS1*, xylulokinase; *GRE3*, aldose reductase; EG, ethylene glycol; Xylulose-1P, xylulose 1-phosphate; Xylulose-5P/X5P, xylulose 5-phosphate; DHAP, dihydroxyacetone phosphate; GADP, glyceraldehyde 3-phosphate; S7P, sedoheptulose 7-phosphate; F6P, fructose 6-phosphate; E4P, erythrose 4-phosphate.
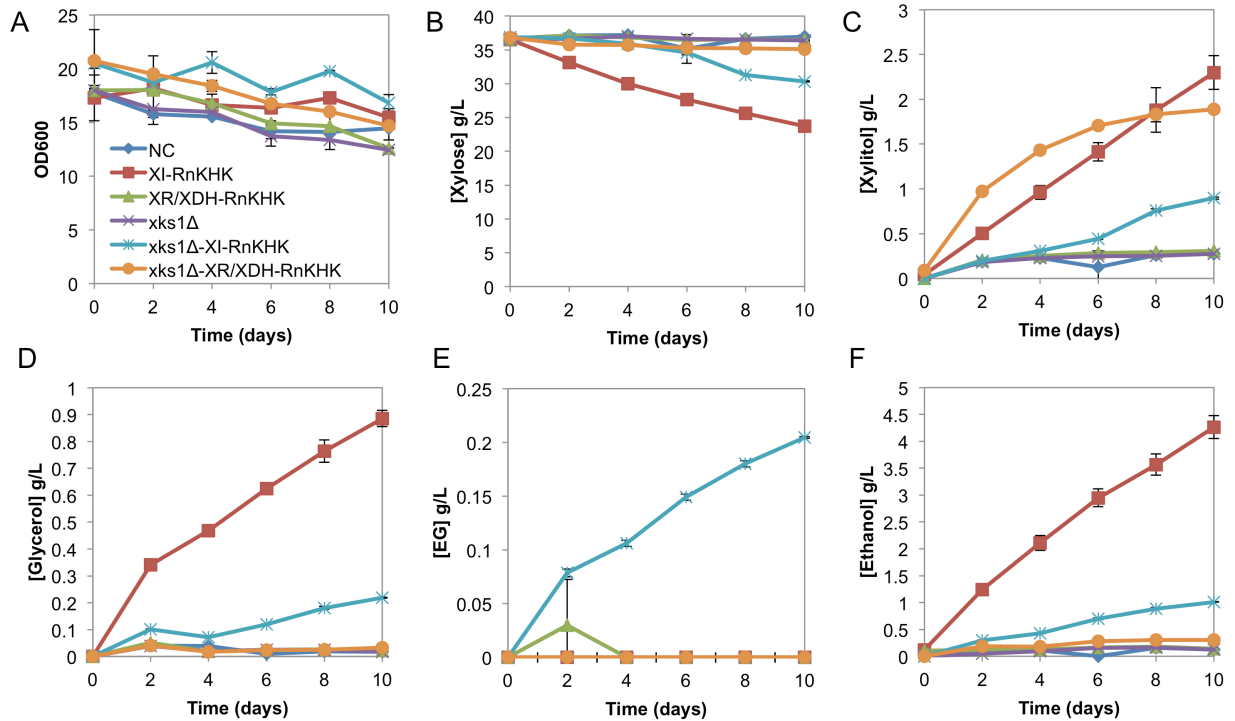
Fig 3-2. *In vivo* comparison of xylose isomerase (XI) and xylose reductase(XR)/xylitol dehydrogenase (XDH) conversions of xylose to xylulose in wild-type *XKS1* and *xks1Δ* strains expressing RnKHK. Strains were provided 40 g/L xylose as a sole carbon source under anaerobic conditions. (A) OD600 values, concentrations of (B) xylose (C) xylitol, (D) glycerol (E) ethylene glycol and (F) ethanol are shown. Error bars indicated standard errors, N = 2. NC and EG denote negative control and ethylene glycol, respectively.
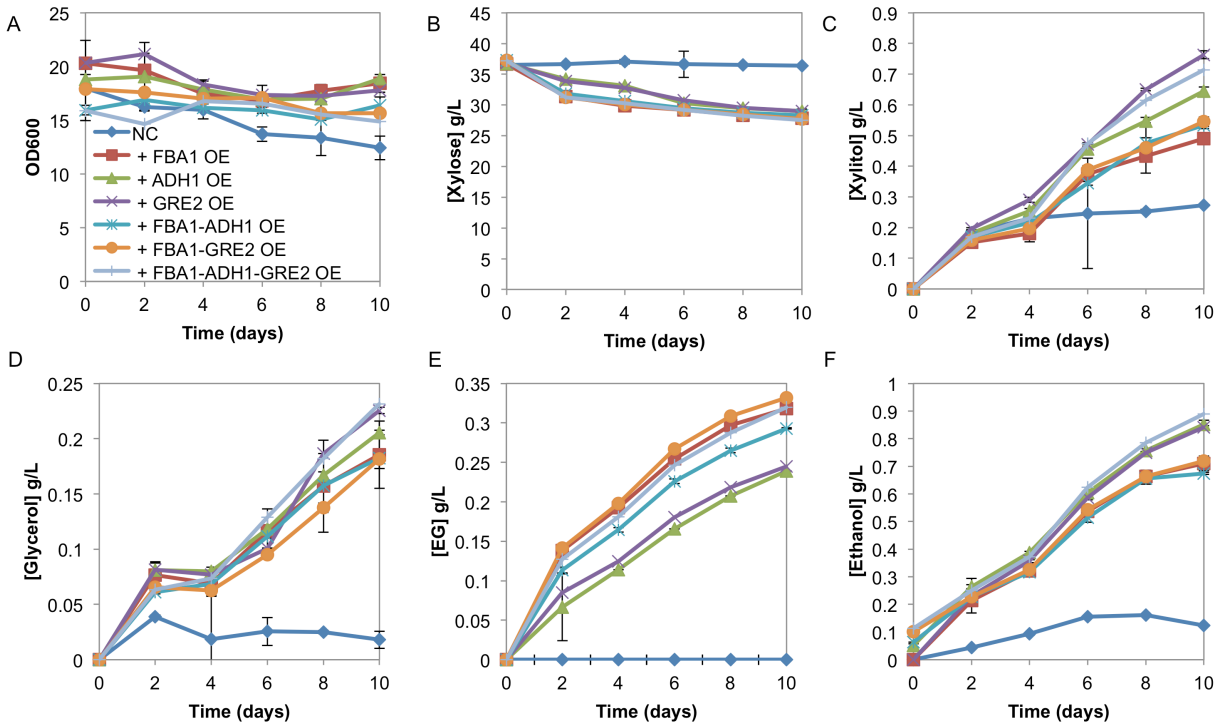
Fig 3-3. Effects of overexpression of endogenous enzymes in the alternative xylose utilization pathway. *xks1Δ* XI-RnKHK was used as the background strain for the overexpression comparisons. (A) OD600 values, concentrations of (B) xylose (C) xylitol, (D) glycerol (E) ethylene glycol and (F) ethanol are shown. Error bars indicated standard errors, N = 2. NC and EG denote negative control and ethylene glycol, respectively.
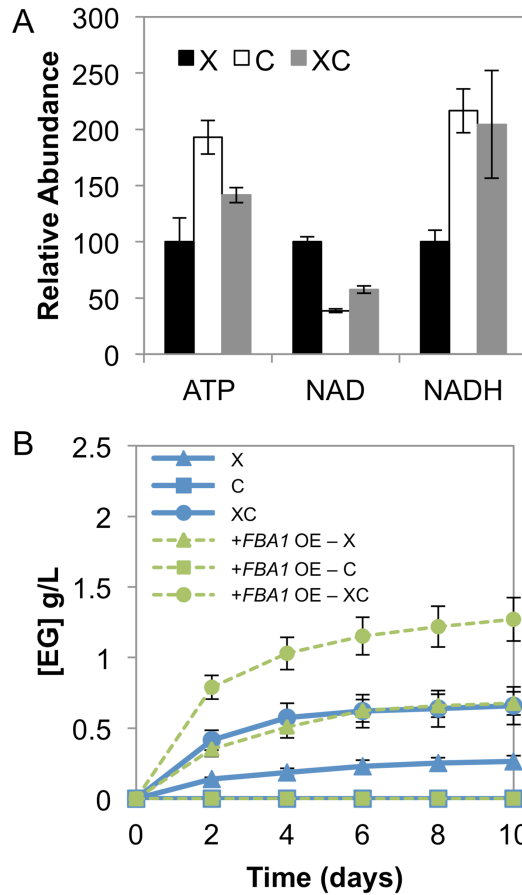
Fig 3-4. Synergistic effects of cellobiose and xylose co-utilization. (A) Intracellular concentrations of ATP, NAD+ and NADH are shown for fermentations with xylose, cellobiose and its mixture (denoted, X, C and XC respectively) provided to the *xks1Δ* XI-RnKHK-FBA1-CD strain. (B) *xks1Δ* XI-RnKHK-CD (denoted in blue) and *xks1Δ* XI-RnKHK-FBA1-CD (denoted in green) strains were provided with xylose in the presence and absence of cellobiose. Concentrations of ethylene glycol (EG) are shown. X, xylose; C, cellobiose; XC, mixture of xylose and cellobiose; OE, overexpression. Error bars indicated standard errors, N = 5.
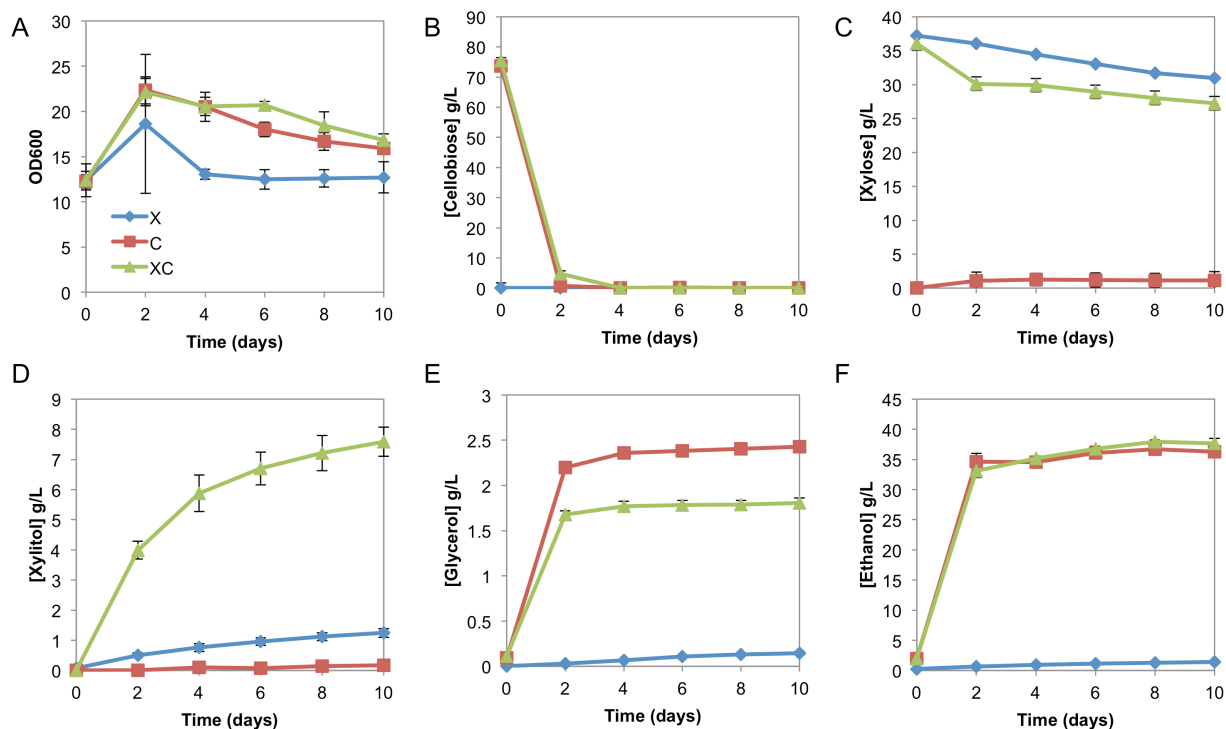
Fig. 3-5 Effect of cellobiose and xylose co-utilization. Strain *xks1Δ* XI-RnKHK-*FBA1*-CD was supplied with 80 g/L cellobiose, 40 g/L xylose or the mixture of 80 g/L cellobiose and 40 g/L xylose, denoted as C, X and XC, respectively. (A) OD600 values, concentrations of (B) cellobiose, (C) xylose (D) xylitol, (E) glycerol and (F) ethanol are shown. Error bars indicated standard errors, N = 5.
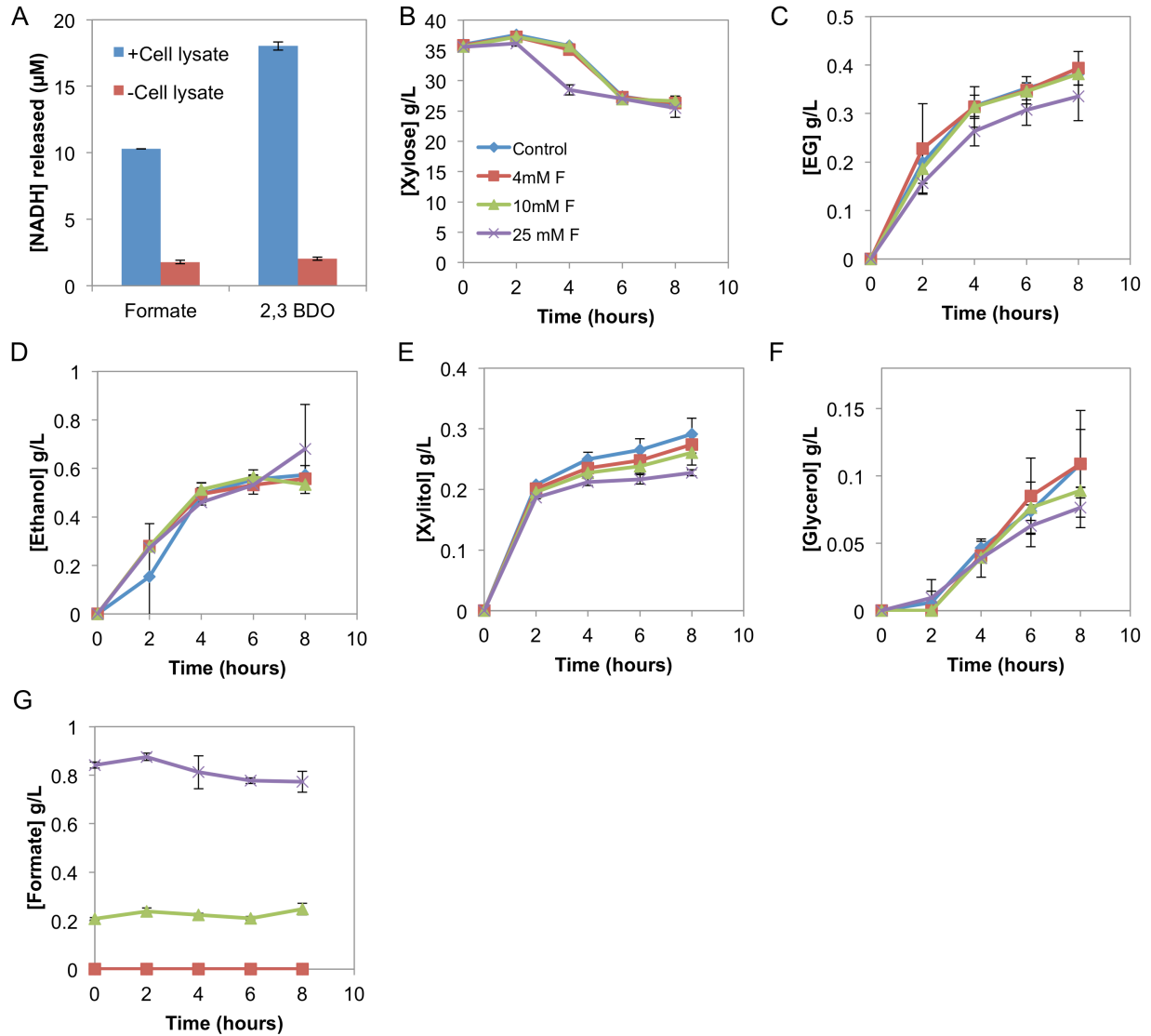
Fig. 3-6 Effect of formate addition to the fermentation broth. (A) Crude lysate activities of formate dehydrogenase (Fdh1p) and butanediol dehydrogenase (Bdh1p*).* 50 mM formate or 50 mM 2,3-BDO and 1 mM NAD+ were incubated at 30°C in 50 mM MES, pH 6.0 with or without cell lysates. NADH was measured spectrophotometrically using absorption at 340 nm and compared to the NADH calibration curve. (B) xylose (C) ethylene glycol (D) ethanol (E) xylitol (F) glycerol and (G) formate concentrations of anaerobic fermentation provided with xylose and varied concentrations of formate (denoted as F) are reported. Error bars indicated standard errors, N = 2.
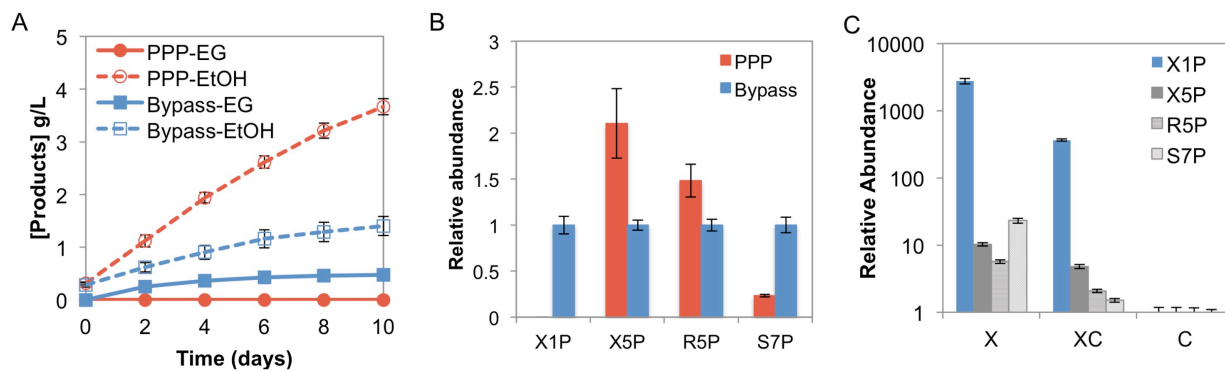
Fig. 3-7 Product titers and relative abundance of metabolites in fermentations with the alternative pathway. The traditional xylose isomerase pathway (denoted as "PPP") and the alternative xylose utilization pathway (*xks1Δ* XI-RnKHK-*FBA1*-CD denoted as "Bypass") were compared. (A) Ethanol and ethylene glycol (EG) production. (B) Relative abundance of intracellular d-xylulose-1-phosphate (X1P), d-xylulose-5-phosphate (X5P), d-ribose-5-phosphate (R5P) and d-sedoheptulose-7-phosphate (S7P), after 4 days of fermentation. Values are normalized to 1 for levels of each compound observed in the Bypass strain. (C) Abundance of metabolites in the Bypass strain provided with xylose (X), a mixture of xylose and cellobiose (XC) and cellobiose only (C) are shown. Samples taken after 4 days of fermentation, and values are normalized to 1 for the levels of each compound observed in the cellobiose-only fermentation. In all three panels, error bars indicated standard errors, N = 5.
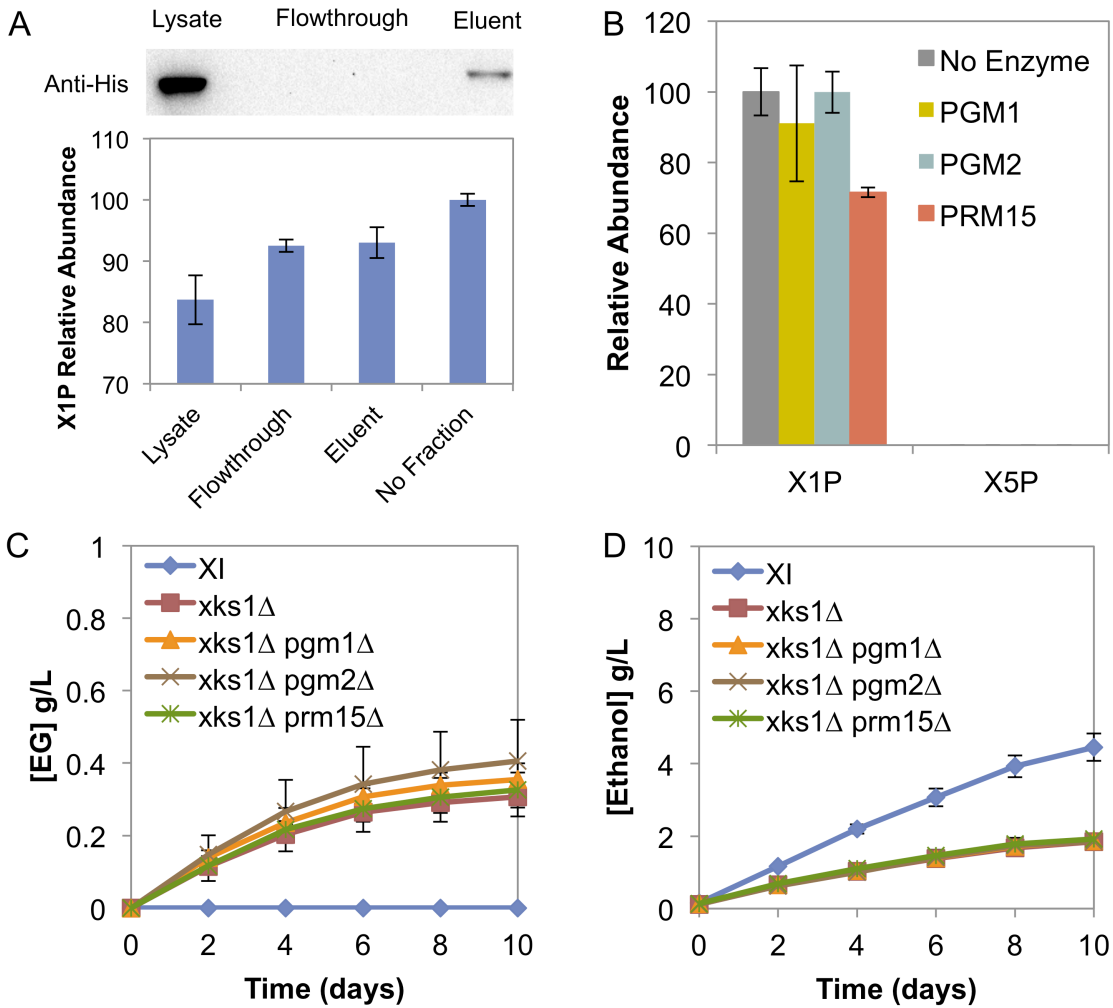
Fig. 3-8 Activities of crude lysates and purified enzymes on d-xylulose-1-phosphate. (A) Relative abundance of X1P and X5P of reactions catalyzed by crude lysates from the traditional xylose utilization pathway (denoted as PPP) and the alternative pathway (*xks1Δ* XI-RnKHK-*FBA1*-CD denoted as Bypass), providing X1P as a substrate incubated overnight. (B) Relative abundance of X1P of reactions catalyzed by purified Pgm1p, Pgm2p, Prm15p providing X1P as a substrate and incubated for 1 hour. (C) ethylene glycol (EG) and (D) ethanol concentrations of fermentation systems with *pgm1, pgm2* and *prm15* deletion backgrounds in addition to *xks1* deletion expressing XI-RnKHK-*FBA1*-CD. Error bars indicated standard errors, N = 2.
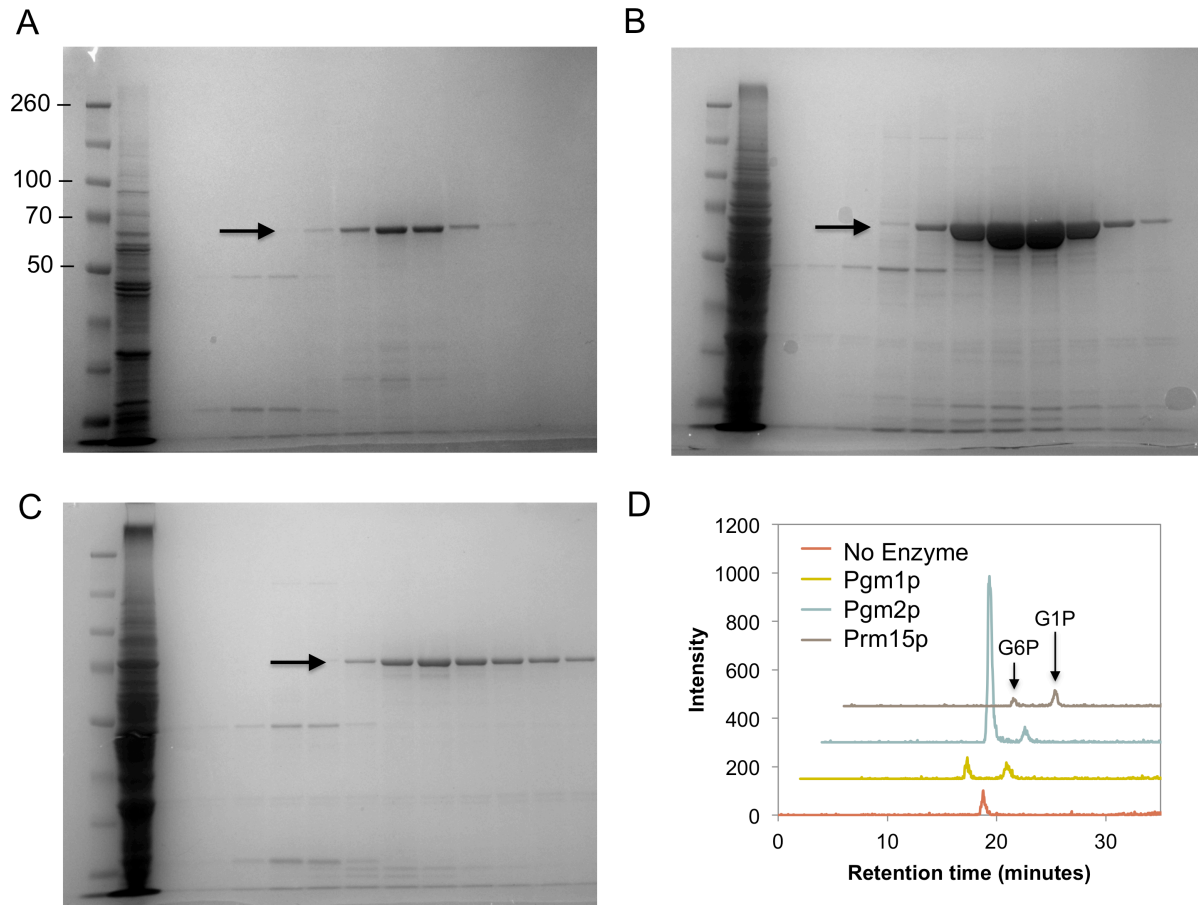
Fig. 3-9 Purification of the three mutases—Pgm1p, Pgm2p and Prm15p—and verification of their activities. Purified mutases (A) Pgm1p, (B) Pgm2p and (C) Prm15p were shown to have expected molecular weights of 64.1, 64.1 and 72.1 kDa, respectively (arrows). (D) Verification of activities of the purified mutases. Activities of purified Pgm1p, Pgm2p and Prm15p were tested by incubation with 1 mM glucose 1-phosphate (G1P) in 1X PBS, pH 7.4 buffer at 30°C. The reactions were stopped with 0.1 M NaOH after 1 hour. Glucose 6-phosphate (G6P) was detected when the purified mutases were included in the reactions. G6P was not detected in the control reaction with no enzyme present. Pgm1p, Pgm2p and Prm15p are known to catalyze G1P and G6P conversion. The chromatograms are shown with 2 minute offsets.
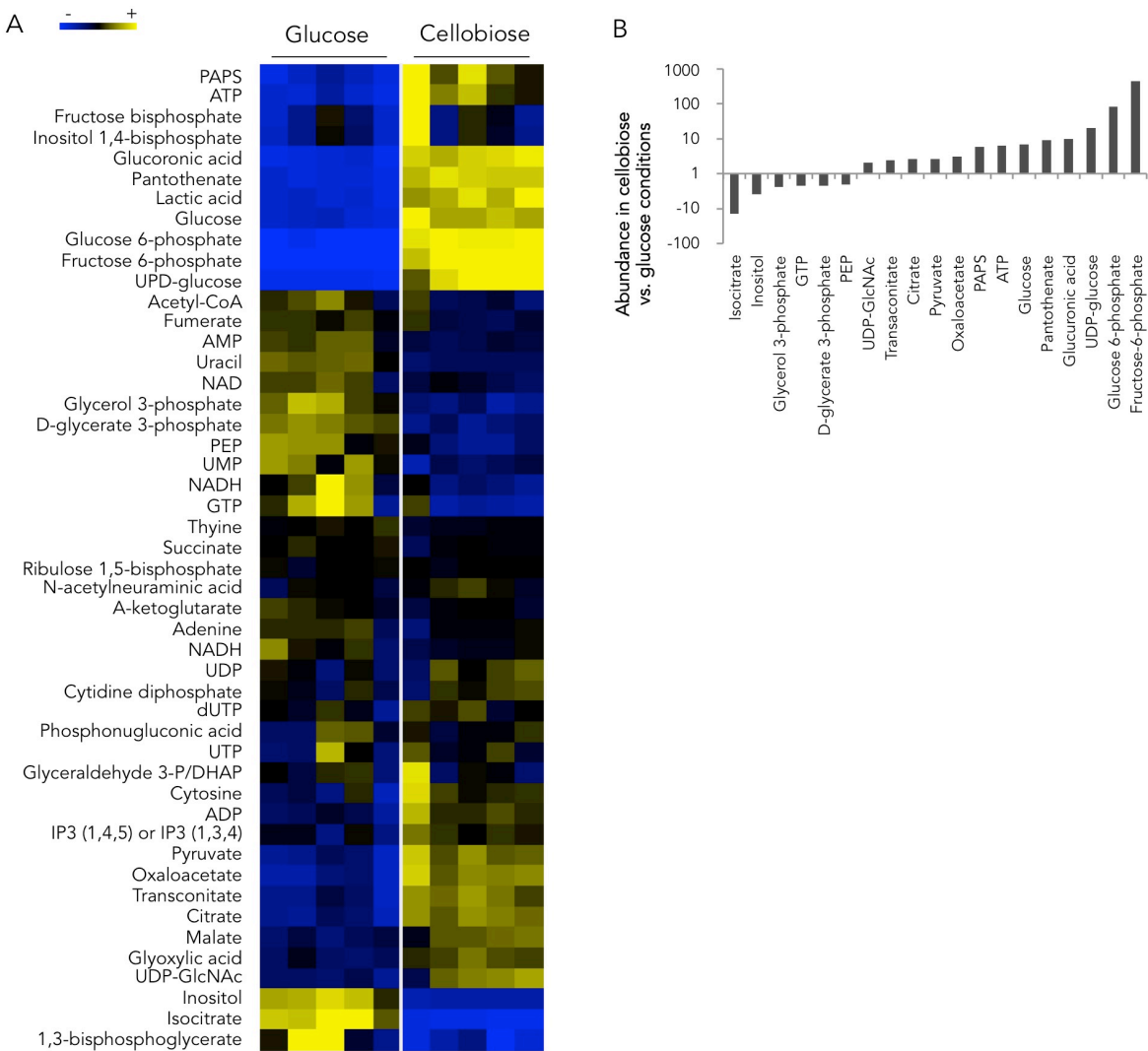
Fig. 4-1. Metabolite profile of cells provided with glucose or cellobiose. (A) Heatmap representation of steady state intracellular metabolite abundance of cells provided with glucose or cellobiose under anaerobic conditions. Shown are the results of 5 biological replicates. (B) Significant changes of intracellular metabolite levels in cells provided with cellobiose compared to cells provided glucose as a sole carbon source (p-value < 0.01 and fold-change >2, five biological replicates).
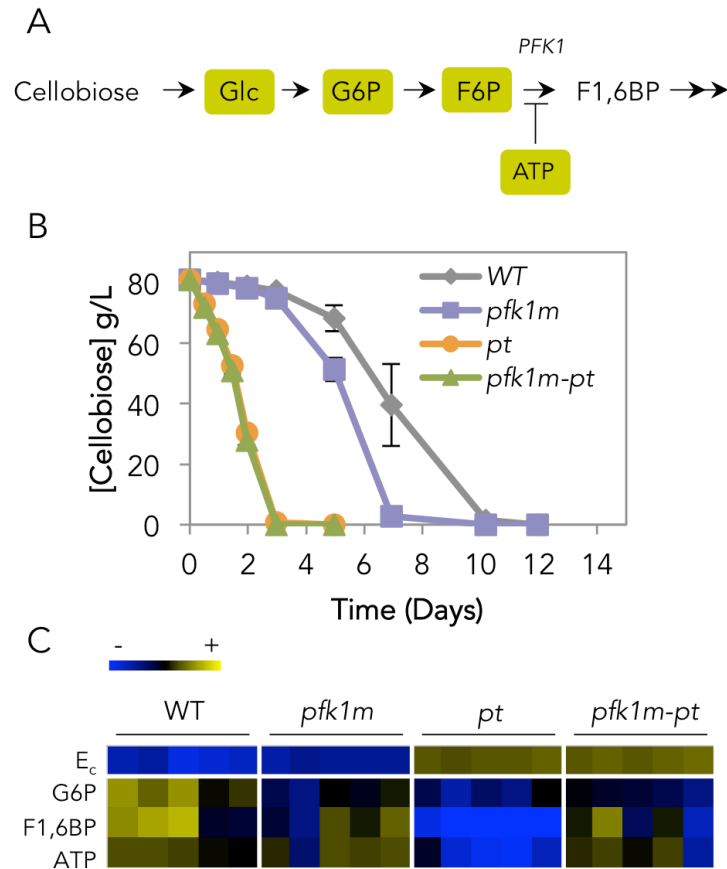
Fig. 4-2. Manipulation of phosphofructokinase (*PFK1*) and plasma membrane ATPase *(PMA1)*. (A) Schematic representation of cellobiose consumption route in the upper glycolytic pathway. Glc, G6P, F6P and ATP are highlighted, and were found in higher abundance when cellobiose was provided in comparison to glucose. (B) Cellobiose consumption profile of the strains with ATP-insensitive Pfk1 (*pfk1m*), constitutively active Pma1 (*pt*) and the combination of both mutations (*pfk1m-pt*) in comparison to the cellobiose pathway-only strain, here used as wild-type (WT). (C) Heatmap representation of the cellobiose consumption efficiency (E_c), G6P, F1,6BP and ATP levels of the NC, *pfk1m, pt* and *pfk1m-pt* strains, relative to the WT strain fermenting cellobiose. Shown are 5 biological replicates.
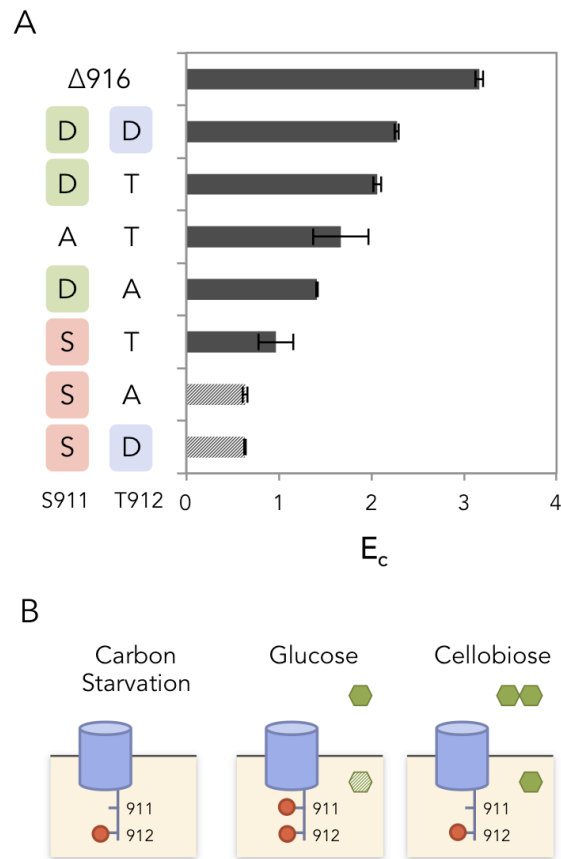
Fig. 4-3. Carbon starvation-like state of the plasma membrane ATPase (*PMA1*) in cellobiose-fermenting cells. (A) Cellobiose consumption efficiency (E_c) of cells expressing Pma1 with phosho-mimic or phosphorylation-preventing mutations at positions serine 911 (S911) and threonine 912 (T912). Shown are the mean and standard deviation for 3 biological replicates. (B) Phosphorylation states of Pma1 S911 and T912 under carbon starvation, glucose metabolizing and cellobiose metabolizing conditions.
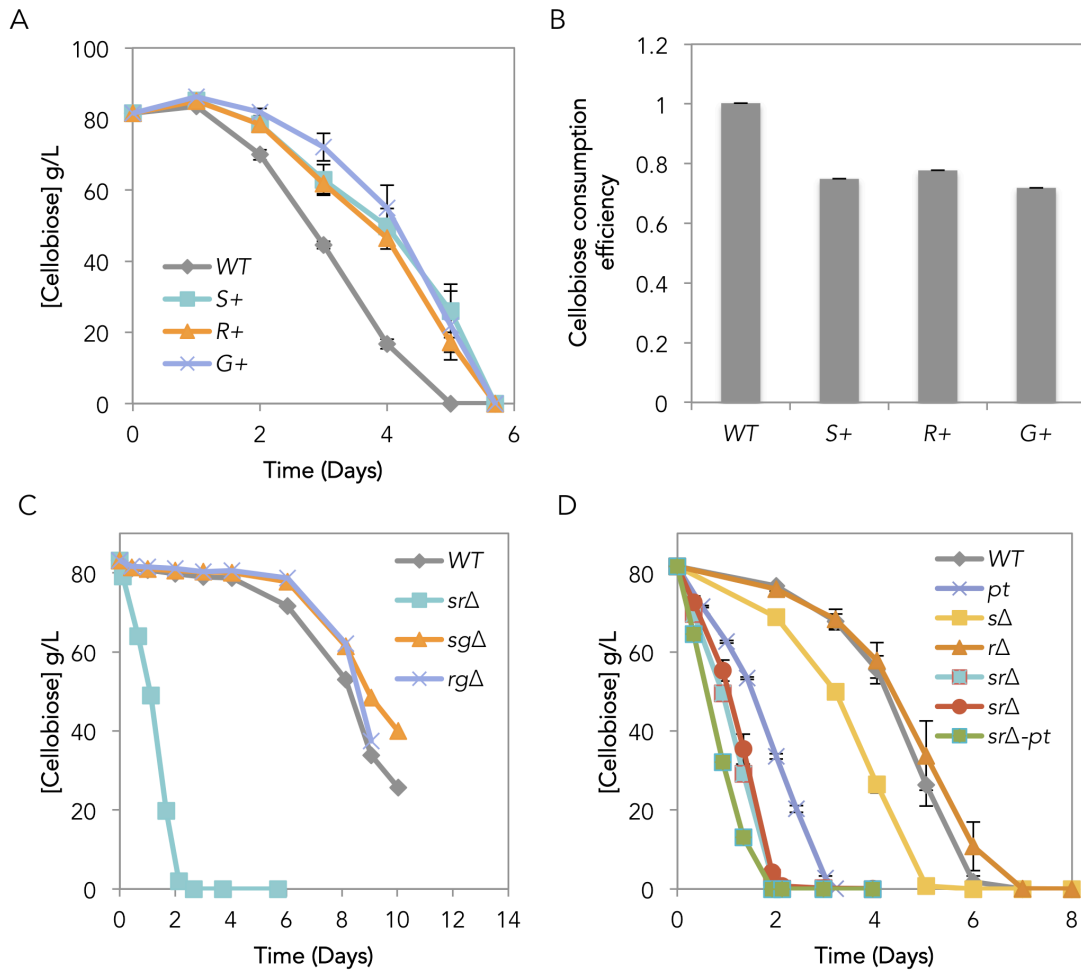
Fig. 4-4. Cellobiose consumption profiles and efficiency of Snf3, Rgt2 and Gpa2 mutants. (A) Cellobiose consumption profiles of strains with consitutively active Snf3 (R229K), Rgt2 (R231K) and Gpa2 (R273A). (B) Cellobiose consumption efficiency of the strains from panel A, with mean values and standard deviations of three biological reliplicates shown. (C) Cellobiose consumption profiles of Snf3, Rgt2, Gpa2 double deletion combinations. (D) Cellobiose consumption profiles of Snf3, Rgt2 and Gpa2 single deletion incomparison to the *srΔ, srgΔ and srΔ-pt* strains. In panels A, C, and D, the results of 3 biological replicates are shown.
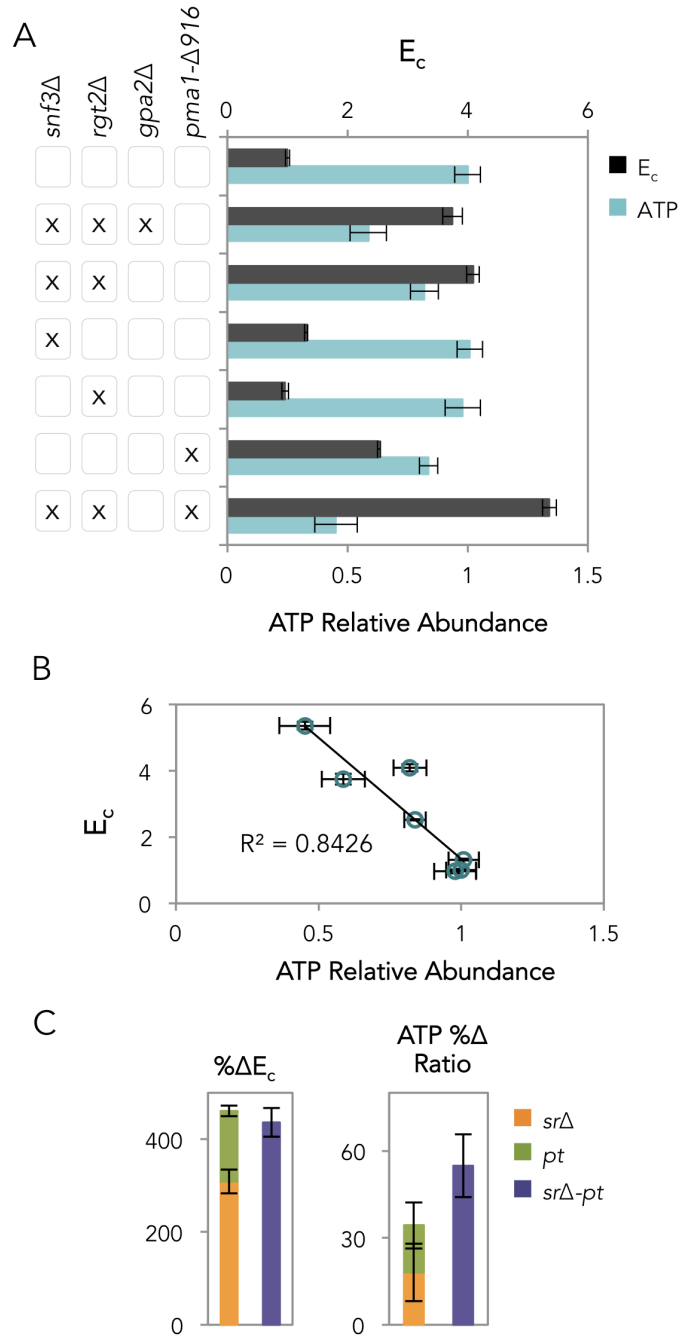
Fig. 4-5. Effect of glucose sensor deletions. (A) Cellobiose consumption efficiency (E_c) and cellular ATP levels of strains with different glucose sensor deletions and different combinations of constitutively-active Pma1 mutations. Shown are the averages and standard deviations of three biological replicates. (B) Correlation of E_c and cellular ATP. Standard deviations for three biological replicates are shown for each point. (C) Additive effect of the increase in E_c and the decrease in cellular ATP of $sr\Delta$ and pt in $sr\Delta$-pt strain. Three biological replicates and standard deviations are shown.
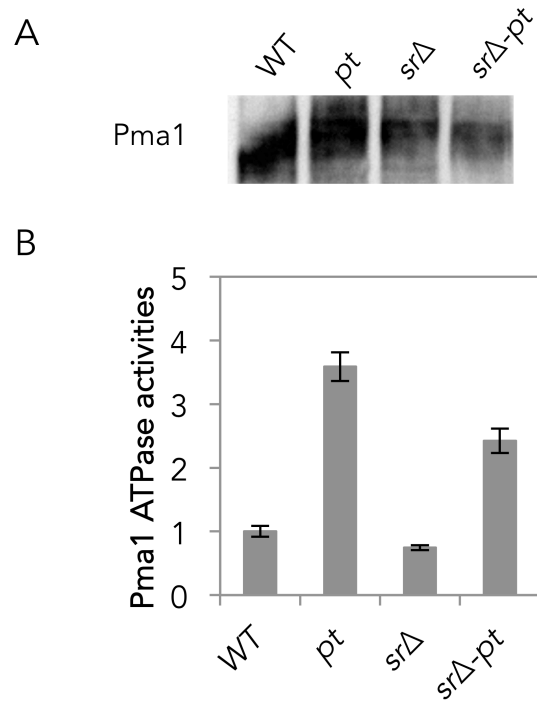
Fig. 4-6. Protein levels and activity assays of the plasma membrnae ATPase (Pma1). (A) Representative western blot against Pma1 in the plasma membrane fraction. (B) Raw Pma1 ATPase showing directly measured values.
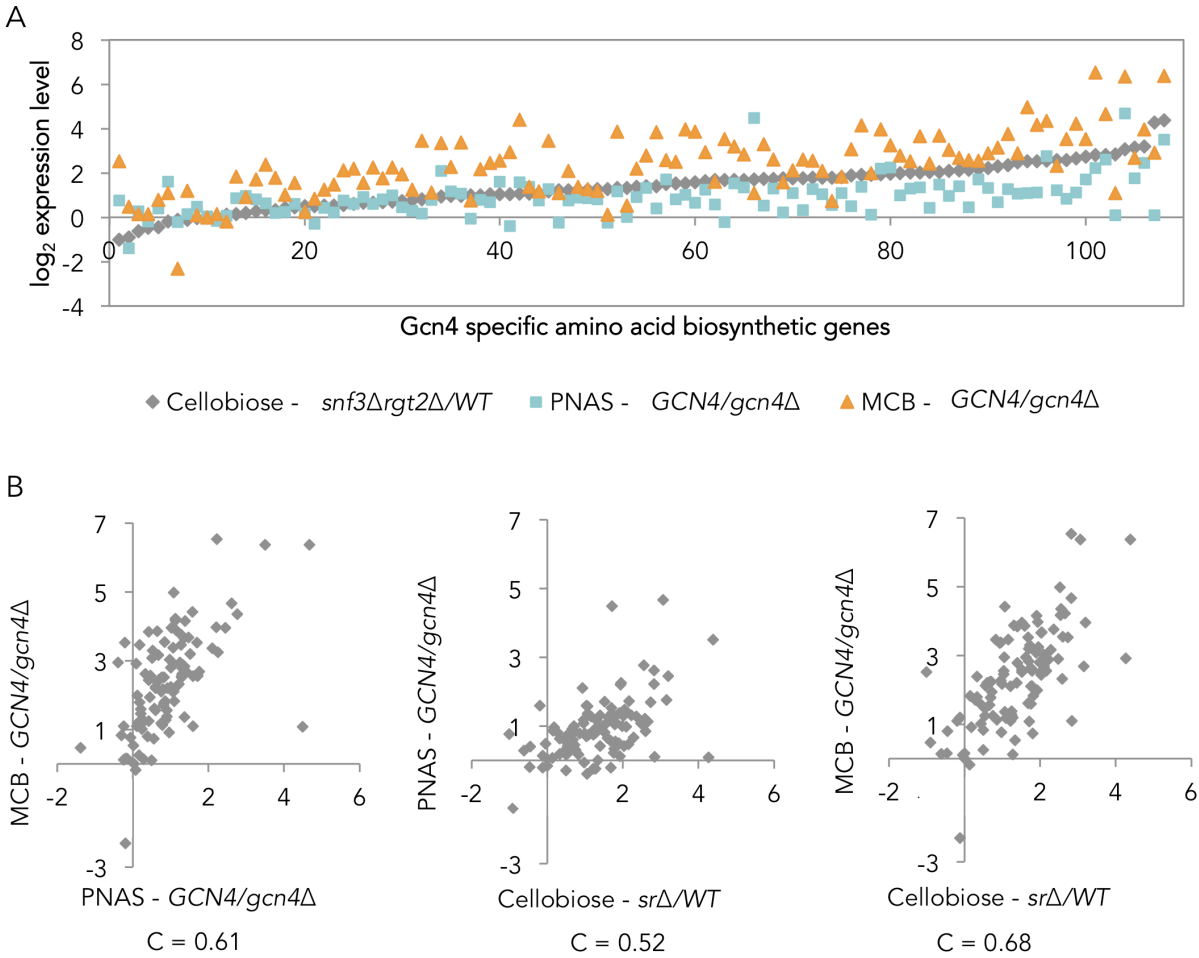
Fig. 4-7. Gcn4-specific amino acid biosynthetic gene comparison. (A) Differential expressional levels of strains from this study (*snf3Δrgt2Δ*/WT) in comparison to *GCN4/gcn4Δ* from Moxley *et al.,* 2009 (PNAS) [97] and Natarajan *et al.,* 2001 (MCB) [98] studies. (B) Pairwise plot of expression levels from three studies and their correlations.

Tables

Table 1-1 Strains and plasmids used in Chapter 1

Strains/plasmids	Characteristics	Reference
D452-2	*MATalpha, leu2, his3, ura3, and can1*	[114]
SR8	*ald6Δ* of the evolved strain D452-2 *leu2::LEU2* P_{TDH3}-*XYL1*-T_{TDH3}; *ura3::URA3* P_{TDH3}-*XYL1*-T_{TDH3} P_{PGK1}-*XYL2*-T_{PGK1} P_{TDH3}-*XYL3*-T_{TDH3}; *his1::HIS1* P_{PGK1}-*XYL2*-T_{PGK1} P_{TDH3}-*XYL3*-T_{TDH3}	[29]
SR8-a	SR8 *ura3*	Courtesy of Dr. Soo Rin Kim
pCT	pRS426- P_{PGK1}-*cdt*-1(F213L)-eGFP-t $_{CYC1}$	[8]
pSd	pRS425- P_{PGK1}-SdCBP-t $_{CYC1}$	[8]
pCS	pRS426-P_{PGK1}-*cdt-1*(F213L)-eGFP-t $_{CYC1}$-P_{PGK1}-SdCBP-t $_{CYC1}$	
pET-Sd	pET302-NT/6his-SdCBP	

Table 1-2 Fermentation paramters (Chapter 1)

Strain	Media	Cellobiose consumption rate (g/L · h)	Ethanol production rate (g/L · h)
D452-2	Cellobiose	3.6 ± 0.05	1.5 ± 0.03
D452-2	Cellobiose + xylose	1.4 ± 0.04	0.85 ± 0.02
SR8-a	Cellobiose	3.7 ± 0.09	1.5 ± 0.04
SR8-a	Cellobiose + xylose	2.9 ± 0.08	1.6 ± 0.04

Table 1-3 Kinetic parameters of β-glucosidase GH1-1 for glucopyranosyl-xylose and cellobiose

Kinetic parameters	Glucopyranosyl-xylose	Cellobiose
K_M (mM)	3.5 ± 1.4	0.49 ± 0.05
V_{max} ($\mu M \cdot min^{-1} \cdot nM^{-1}$)	0.48 ± 0.10	1.3 ± 0.04

Table 3-1 Plasmids and strains used in Chapter 3

Plasmids/ Strains	Characterization	Reference
pRS313	pRS313	ATCC® 77142
pRnKHK	pRS313-P$_{FBA1}$-RnKHKopt-T$_{CYC1}$	This study
pNT/his-RnKHK	pRS313-P$_{FBA1}$-NT/his-RnKHKopt-T$_{CYC1}$	This study
p1	pRS313-P$_{TDH3}$-RnKHKopt-T$_{CYC1}$	This study
pRnKHK-FBA1	pRS313-P$_{FBA1}$-RnKHKopt-T$_{CYC1}$-P$_{FBA1}$-*FBA1*-T$_{FBA1}$	This study
pSpKHK-FBA1	pRS313-P$_{FBA1}$-SpKHK-T$_{CYC1}$-P$_{FBA1}$-*FBA1*-T$_{FBA1}$	This study
pNcKHK-FBA1	pRS313-P$_{FBA1}$-NcKHK-T$_{CYC1}$-P$_{FBA1}$-*FBA1*-T$_{FBA1}$	This study
pRS315	pRS315	ATCC® 77144 Courtesy of Matthew Shurtleff
p2	pRS424-P$_{TEF1}$-BsXI-T$_{CYC1}$	
pXI	pRS315-P$_{TEF1}$-BsXI-T$_{CYC1}$	This study
pRS316	pRS316	ATCC® 77145
p3	pRS316-P$_{CCW12}$-T$_{CYC1}$	This study
pADH1	pRS316-P$_{CCW12}$-*ADH1*-T$_{CYC1}$	This study
pGRE2	pRS316-P$_{CCW12}$-*GRE2*-T$_{CYC1}$	This study
pADH1-GRE2	pRS316-P$_{CCW12}$-*ADH1*-T$_{CYC1}$-P$_{CCW12}$-*GRE2*-T$_{CYC1}$	This study
pET-xylB	pET302-NT/his-xylB	This study
pCD	pRS316-P$_{TDH3}$-CDT1-eGFP-T$_{CYC1}$-P$_{CCW12}$-gh1-1opt-T$_{CYC1}$	Unpublished data (Lin *et al.,* 2014)
pRS423-NT/his-PGM1	pRS423-NT/6xhis- P$_{TEF1}$-PGM1-T$_{CYC1}$	This study
pRS423-NT/his-PGM2	pRS423-NT/6xhis- P$_{TEF1}$-PGM2-T$_{CYC1}$	This study
pRS423-NT/his-PRM15	pRS423-NT/6xhis- P$_{TEF1}$-PRM15-T$_{CYC1}$	This study
S1	*S. cerevisiae* D452-2 *MATalpha, leu2, his3, ura3,* and *can1*)	
S2	S1 *xks1Δ*::KanMX	This study
NC	S1 pRS313, pRS315, pRS316	This study
XI-RnKHK	S1 pRnKHK, pXI, pRS316	This study
xks1Δ	S2 pRS313, pRS315, pRS316	This study
xks1Δ-XI-RnKHK	S2 pRnKHK, pXI, pRS316	This study
+ FBA1 OE	S2 pRnKHK-FBA1, pXI, pRS316	This study
+ ADH1 OE	S2 pRnKHK, pXI, pADH1	This study
+ GRE2 OE	S2 pRnKHK, pXI, pGRE2	This study
+ FBA1-ADH1 OE	S2 pRnKHK-FBA1, pXI, pADH1	This study

+ FBA1-GRE2 OE	S2 pRnKHK-FBA1, pXI, pGRE2	This study
+ FBA1-ADH1-GRE2 OE	S2 pRnKHK-FBA1, pXI, pADH1-GRE2	This study
S3	S2 pRnKHK, pXI, pCD	This study
Bypass	S2 pRnKHK-FBA1, pXI, pCD	This study
PPP	S1 pXI, pRS313, pCD	This study
S6	S2 pNT/his-RnKHK	This study
S7	*E.coli* BL21 (DE3) pET-xylB	This study
pgm1Δ	S2 *pgm1Δ::nat*MX pRnKHK-FBA1, pXI, pCD	This study
pgm2Δ	S2 *pgm2Δ::nat*MX pRnKHK-FBA1, pXI, pCD	This study
prm15Δ	S2 *prm15Δ::nat*MX pRnKHK-FBA1, pXI, pCD	This study